

Engineering the transport of signaling molecules in glycosaminoglycan-based hydrogels

D I S S E R T A T I O N

zur Erlangung des akademischen Grades

Doctor of Philosophy

(Ph.D.)

vorgelegt

der Fakultät Mathematik und Naturwissenschaften

der Technischen Universität Dresden

von

M.S., Yanuar Dwi Putra Limasale

(akadem. Grad, Vorname Name)

geboren am 06. January 1990 in Bayumas, Indonesien

Eingereicht am 02.09.2019

Die Dissertation wurde in der Zeit

von September 2015 bis August 2019

am Leibniz-Institut für Polymerforschung Dresden e.V. angefertigt

‘It is better to light a candle than to curse the darkness’

Eleanor Roosevelt

Abstract

Signaling molecules are critically important to regulate cellular processes. Therefore, their incorporation into engineered biomaterials is indispensable for the applications in tissue engineering and regenerative medicine. In particular, the functionalization of highly hydrated polymer networks, so-called hydrogels, with the signaling molecules, has been quite beneficial to provide multiple cell-instructive signals. Following this strategy, the incorporation of sulfated glycosaminoglycans (GAGs) into such polymer networks offers unprecedented options to control the administration of signaling molecules via electrostatic interactions. Moreover, mathematical models can be instrumental in designing materials to tune the transport and adjust the local concentration of the signaling molecules to precisely modulate cell fate decisions. Accordingly, this study aims to systematically investigate the impact of different binary poly(ethylene glycol)-glycosaminoglycan hydrogel networks on the transport of signaling molecules by developing and applying mathematical modeling in combination with experimental approaches. The gained knowledge was then applied to modulate the bioactivities of pro-angiogenic growth factor within the binary hydrogel and rationally design a new class of cytocompatible GAG-based materials for the controlled administration of pro-angiogenic growth factors.

Firstly, systematic studies on the mobility of signaling molecules within GAG-based polymer networks revealed differential effects of hydrogel network parameters such as mesh size, GAG content, and the sulfation pattern of the GAG building block on the transport of these signaling molecules.

Secondly, the effect of the GAG content of the hydrogel and the sulfation pattern of the GAG building block on the bioactivity of hydrogel administrated vascular endothelial growth factor (VEGF) have been analyzed. Since VEGF is a GAG-affine protein that plays a major role in angiogenesis, its ability to promote vascular morphogenesis has been investigated. The simulation and experimental results demonstrated the determining impact of the availability of free (unbound) VEGF as well as the presence of GAGs with a specific sulfation pattern within the

polymer network on the formation of the endothelial capillary network within the hydrogel.

Finally, a rational design strategy has been applied to extend a GAG-hydrogel platform to allow for a far-reaching control of its cell instructive properties. The resulting materials are independently tunable over a broad range for their mechanical properties and GAG content. The GAG content of the hydrogel matrices, in particular, was shown to modulate the transport of pro-angiogenic growth factors most. Moreover, the hydrogel also supports endothelial vascular morphogenesis.

In conclusion, the in here followed approach of combining experimental results and mathematical modeling for predicting the transport of signaling molecules and the rational design concept for customizing GAG-based hydrogel networks provide the fundamentals to precisely modulate cell fate decisions within GAG-based biohybrid polymer networks rationalizing their application for tissue engineering and regenerative medicine.

Acknowledgment

I would like to express my sincere gratitude to all the people who supported me throughout the completion of my thesis work. Firstly, I would like to thank my advisor Prof. Dr. Carsten Werner, for allowing me to work in his group and provide me with all the support, scientific expertise and show me the big picture of my research. I would like to thank Prof. Dr. Tilo Pompe for agreeing and taking the time to review this thesis and Prof. Dr. Yixin Zhang and Prof. Dr. Martin Bornhäuser for being a member of my thesis advisory committee and giving me valuable feedback throughout my thesis study.

I would also like to acknowledge the support of the Dresden International Graduate School for Biomedicine and Bioengineering for organizing helpful training and predoc courses.

In particular, I would like to express my special gratitude to my direct supervisor Dr. Ralf Zimmermann for bringing me to a mathematical modeling world, his valuable feedbacks, and always finding the time to advise and encourage me to improve my thesis work. It was also a privilege to me for being co-advised by Dr. Uwe Freudenberg. I am incredibly grateful for his scientific advice and guidance for improving my presentation and writing skills with his attention to detail and willingness to give critical feedback.

I would like to thank Dr. Lars Renner for introducing me to FRAP techniques and sharing his scientific insights during my early Ph.D. life, and it really brought me to see the first positive results out of my Ph.D. project.

I want to thank my office mates Dr. Manfred Maitz, for always helping with everything from a broken robot, filling the tax declaration to choosing the right menu for lunch. Dr. Dominik Hahn for the fruitful discussion and sharing his life experience, and Tina Helmecke for helping me dealing with bureaucratic issues, and Marion Fischer for being so friendly.

I would like to thank my friends, especially Passant, for the fruitful discussion on almost every aspect of my Ph.D. work and being like my second family in

Germany who can give me a unique perspective on personal levels, Ruchika for being so understanding and sharing her ideas of life, Jana for always being helpful and informative, Valentina for spreading optimism, Felix for sharing insightful discussion, and Lucas for helping me with technical issues. I also want to thank my other international friends Sebastian, Melissa, Andre, Heather, and everyone who made the MBC a pleasant and lovely place to work.

I am very grateful to my highly motivated B.Sc. students Linda, Annika, Laura, and Ina and my M.Sc. student Nig-Hui and Sarkhan, for all their support. I also want to thank our technicians Dagmar, Julia, Nelly, and Mila, for all the assistance whenever I needed them.

Finally, I want to thank my Indonesian friends in Dresden: Aji, Ubed, Bobby, Didik for the support, movies together, cooking, and sharing wonderful adventures in Europe.

Contents

Abstract	iii
Acknowledgment	v
Contents	vii
1. Introduction	1
1.1 Motivation	1
1.2 State of the art of modulation of the transport of signaling molecules in GAG-based materials	2
1.3 Aim of the work	8
2. Fundamentals	11
2.1 Extracellular matrix and the cell signaling functions.....	11
2.1.1 The extracellular matrix (ECM) structure and functions	11
2.1.2 GAG as the regulator of signaling molecule activity in the ECM	14
2.2 Modelling the transport of signaling molecules in affinity-based systems.	17
2.3 GAG-based biomaterials control the administration of pro-angiogenic growth factors.....	20
2.3.1 GAG-based biomaterials as a controlled release system of pro-angiogenic growth factors	20
2.3.2 GAG-based biomaterials as a 3D cellular encapsulation matrix for vascular tissue engineering	22
2.4. Modular starPEG-GAG hydrogels platform	25
3. Materials and Methods	28
3.1 Preparation of hydrogels	28
3.1.1 Binary GAG hydrogel systems	28
3.1.2 Ternary GAG hydrogel systems.....	28
3.1.3 Synthesis of the starPEG-MMP cleavable peptide conjugate.....	29

3.2 Physical characterization of hydrogels	29
3.2.1 Rheological and volume swelling measurements	29
3.3 Protein diffusion studies in hydrogels	30
3.3.1 Fluorescent protein labeling and purifications	30
3.3.2 Fluorescence recovery after photobleaching (FRAP)	30
3.3.3 The formation of fluorescent protein gradient in microfluidic devices	33
3.5 Protein release studies from hydrogels	35
3.6 Cell cultures	36
3.7 <i>In vitro</i> assays	36
3.7.1 Endothelial cell vascular morphogenesis	36
3.7.2 Endothelial cell chemotaxis	37
3.8 COMSOL mathematical modeling and simulation	39
3.9 Microscopy techniques and image analysis	42
3.9.1 Fluorescence staining and immunocytochemistry	42
3.9.2 Image analysis	43
3.10 Statistical analysis	43
4. Results and discussion	44
4.1. Molecular transport of signaling molecules in the binary GAG-based hydrogel systems	44
4.1.1 Introduction	44
4.1.2 Protein mobility in GAG-based hydrogels	46
4.1.3 Protein release from GAG-based hydrogels	53
4.1.4 Modelling the transport of protein within GAG-based hydrogel systems	57
4.1.5 Sensitivity analysis of different COMSOL model parameters on the release characteristics of protein from hydrogel	58
4.1.6 Discussion and summary	62

4.2 Tuning the activity of pro-angiogenic growth factor within binary GAG-based hydrogels	70
4.2.1 Introduction	70
4.2.2 Physical properties of hydrogels	72
4.2.3 VEGF release from hydrogels with varied GAG content and GAG sulfation patterns	75
4.2.4 Effect of GAG concentration and sulfation pattern on the formation of vascular structures of endothelial cells within hydrogels	77
4.2.5 Spatial patterning of cellular activity within hydrogel matrices	84
4.2.6 Discussion and summary	88
4.3. Cell-instructive ternary hydrogel system with variable GAG content	95
4.3.1 Introduction	95
4.3.2 Physical properties of ternary hydrogels	98
4.3.3 Mobility of heparin affine proteins within- and the release out of ternary hydrogels	99
4.3.4 The gradient of signaling molecules within ternary hydrogels	102
4.3.5 Endothelial cell capillary morphogenesis within ternary hydrogels ..	106
4.3.6 Discussion and summary	107
5. General discussion	112
5.1 Summary and conclusion	112
5.1.1 Molecular transport and binding in the starPEG-GAG hydrogels	113
5.1.2 Modulation of the activity of pro-angiogenic growth factor within the starPEG-GAG hydrogels	115
5.1.3 Cell-instructive ternary hydrogels with variable GAG content	116
5.2 Future perspectives	118
5.2.1 Advanced modeling transport and binding of protein within the starPEG-GAG hydrogels	118

5.2.2 Signaling molecule gradients	119
5.2.3 Network properties and applications of ternary hydrogels.....	121
6. Appendix	123
6.1 Supplementary materials and methods	123
6.1.1 Determination of protein binding affinity to GAG and GAG derivatives	123
6.1.2 Estimation of biomolecule sizes	124
6.1.3 Estimation hydrogel mesh sizes	124
6.1.4 The diffusion of signaling proteins within an affinity-based system .	125
6.1.5 Mathematical model assumptions	126
6.1.6 COMSOL modeling	127
6.1.7 Vascular network analysis	133
6.1.8 Metabolic activity assays.....	133
6.1.9 Bioactivity of VEGF.....	134
6.2 Supplementary data	135
6.2.1 Protein binding to GAGs or- GAG-derivatives.....	135
6.2.2 Adaptation of FRAP technique to analyze protein mobility in the hydrogels	138
6.2.3 Estimation of hydrogel mesh size.....	142
Bibliography	147
List of figures	165
List of tables	168
Nomenclature.....	169

1. Introduction

1.1 Motivation

Soluble signaling molecules are critically important to regulate cellular processes such as cell survival, migration, differentiation, and proliferation, which orchestrate physiological phenomena including tissue repair and regeneration [1, 2], angiogenesis [3-6], and immunomodulation [7, 8]. Therefore, incorporating such cell-instructive signals into hydrated polymer networks, so-called hydrogels, is highly indispensable for their applications in tissue engineering and regenerative medicines. The mobility of bioactive proteins within- and the subsequent release from the hydrogel may not only affect the activity of cells within the scaffold but may also determine the host responses at the site of implantation [9-13]. Despite the significant roles of signaling molecules in cell fate decisions, controlling their retention and activity within the tissue-engineered construct remains a significant challenge primarily because of their short half-lives [14, 15] and narrow therapeutic windows [16, 17]. Therefore, engineering delivery strategies for soluble signaling molecules that could modulate the release and prolong their bioactivity are essential to precisely control cell fate decisions.

Several studies have examined the development of delivery systems based on polymeric biomaterials to achieve tunable and sustainable delivery of the growth factors [4-6, 16, 18, 19] while minimizing the side effects of improper dosing [20]. Growth factors, a particular class of soluble signaling molecules, can be physically entrapped within the polymeric network to control their release rate from the polymer matrix. However, the extended-release of growth factors resulting from this approach will only last for a few hours to a day, depending on the thickness of hydrogel [126]. To overcome this, the covalent immobilization and engineering of growth factors with higher affinity for the matrix may be applied to prolong the retention within the polymer network. Their applications have been successfully reported [21-24]. Nevertheless, both approaches may alter the growth factor functionalities and require complicated procedures. Alternatively, the incorporation of sulfated glycosaminoglycans (GAGs) into

engineered biomaterials can be explored to modulate the release kinetics and preserve the bioactivity of growth factors within engineered biomaterials [25]. Due to the presence of a heparin-binding domain, positively charged surface patches of the growth factors can reversibly interact with negatively charged GAGs through electrostatic interaction, thereby increasing their retention and stability [26]. Besides, the GAGs were also known to facilitate various growth factors binding to their receptor and potentiate the receptor activation, therefore, enhancing their overall bioactivity [27-29].

1.2 State of the art of modulation of the transport of signaling molecules in GAG-based materials

The high-affinity interaction between GAGs and various soluble signaling molecules have inspired the utilization of GAGs as an affinity ligand for delivery systems of growth factors for various applications, including BMP-2 for bone regeneration [30], VEGF and FGF-2 for tissue vascularization [4-6], SDF1 α for endogenous cells recruitment [19, 31], neurotrophin-3, NGF, and GDNF for nerve regeneration [32-34], and TGF- β for wound healing [35]. In order to achieve a desired cellular response upon the *in vitro* or *in vivo* applications of the GAG-based-affinity system, several features of the materials can be tuned to control the mobility of encapsulated proteins and the subsequent release from the matrices (**Figure 1.1**).

The chain lengths and the sulfation pattern of the GAG are essential for the growth factor binding and the ability of GAGs to enhance the stability of signaling molecules [36]. In particular, controlling the degree of sulfation of the GAG has been exploited to modulate the local affinity interaction between signaling molecules and GAG-based polymer matrices [37, 38]. For example, Attallah et al. have developed a starPEG-heparin hydrogel system with varied sulfation patterns through a cytocompatible Michael type addition crosslinking scheme between the thiol functionalized starPEG and maleimide-functionalized heparin [38]. Heparin derivatives with variable sulfation degree (N-, 6O-, and 6ON-desulfated heparins) were generated and incorporated into the hydrogel to create hydrogels with variable GAG sulfation patterns, allowing the modulation of

gradient and release of platelet-derived growth factor (PDGF) from hydrogel matrices. Moreover, similar strategies have also been applied to control the release kinetics of FGF2 and VEGF from the starPEG-heparin hydrogel constructs using different crosslinking chemistry for network formation [6, 39]. Both overall and local sulfate density of the hydrogel was shown to modulate the rate of VEGF release *in vitro*. Moreover, the hydrogels with the lowest sulfate content were superior in promoting angiogenesis [6].

Besides the local affinity, the overall affinity of GAG-hydrogels can also be tuned by adjusting the density of signaling molecule binding sites in the system. Depending on the structure and molecular weight of a particular protein and heparin, heparin may simultaneously bind several protein molecules [40]. However, as simplification, it is often assumed that one soluble signaling molecule bind to one heparin, i. e. in a 1:1 binding stoichiometry. This implies that the total heparin content of the hydrogel is directly proportional to the number of total protein binding sites in the gel.

The strategy to adjust the heparin content of GAG-based materials has been successfully applied to modulate the release kinetics of many heparin-binding proteins [41-46] and enhanced the bioactivity of the molecules within engineered matrices. For example, Jha and coworkers developed bioinspired hyaluronic acid-based hydrogels to aid stem cell transplantation therapy [42]. The incorporation of the heparin within the matrix enhanced the retention of the exogenously supplemented TGF- β 1 over 20 days. Besides, a tunable release could be achieved by modulating the concentration and molecular weight of heparin [43]. Similarly, the sustained release of bone morphogenetic protein-2 (BMP-2) from heparin containing hyaluronic acid microgels can also be achieved by varying the heparin content of the microgel from 1-10% (w/w) [41]. In a related study, heparin functionalization has been exploited to enhance the binding and retention of VEGF in polycaprolactone/ alginate scaffolds [45]. Heparin immobilization on the construct could modulate the VEGF binding and release and promote a more robust de novo vessel formation than the non-functionalized scaffold.

Adjusting the GAG content within a GAG based hydrogel is not always possible, especially within a system where the GAG is utilized as the major building block of the material [47, 48]. Incorporating small quantities of the GAG into such a kind of hydrogel is limited by the minimum solid content requirement that allows for the hydrogel formation. As a result, modulating the availability of free binding sites of the protein within the hydrogel network by merely changing the ratio of the protein loading to the GAG content can be used as an alternative strategy to modulate the release kinetics of proteins. This strategy has been previously applied to modulate the overall release of VEGF, FGF-2, PDGF-BB, TGF- β , and IL-4 from heparin-based hydrogels [4, 6, 26, 35, 38, 39]. In general, more protein release could be observed as the loading concentration increases. However, this approach did not change the overall release efficiency of the system, as in the case of tuning the hydrogel intrinsic binding properties.

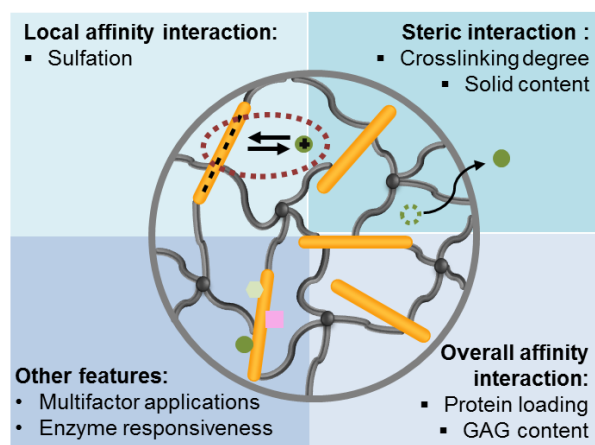


Figure 1.1. Different strategies to modulate the transport of signaling molecules within GAG-based materials. Modified from [25].

In addition to modulating the affinity of signaling molecules to GAG, the mobility of proteins embedded within the GAG-based hydrogels can also be tailored by tuning the mesh size of hydrogels. In this approach, the extent of protein diffusion is governed by the steric interaction between the protein and polymer network. If the mesh size of the hydrogel is larger than the protein size, the protein diffusion is inversely proportional to the molecular size of the protein, similar to the protein diffusion profile in the solution [49]. The incorporation of enzymatically cleavable peptide sequence into the GAG hydrogel network allows for the

remodeling of polymer network by cell-secreted matrix metalloproteinases (MMPs) that enlarge the mesh size and subsequently induce a higher release of encapsulated molecular cargos. For example, Prokoph et al. have utilized this concept to modulate the release of SDF1 α from starPEG-heparin hydrogel matrices to induce the recruitment of early endothelial progenitor cells (eEPC) into an ischemic tissue [19]. *In vitro* release studies of the SDF1 α from the hydrogel have shown that the addition of the MMPs into the cleavable hydrogel could enhance the SDF1 α release, especially within the first 24 H of the release studies. Moreover, tuning the degradability of the polymer network can further be applied by incorporating MMP-cleavable peptides along with the linkers of differing hydrolytic sensitivity to tailor the release of protein from the scaffold [50].

Many studies have shown that the incorporation of GAG within a synthetic polymer network enhances the retention of many therapeutically relevant growth factors [5, 19, 39]. However, maintaining a subtle balance between the retention and delivery of signaling molecules to the surrounding tissues or encapsulated cells can be crucial in determining cell fate decisions. As an affinity ligand, GAG determines the relative concentration of the matrix-bound and freely diffusing factor [32, 51-53], which can have different bioactivity [22, 54]. Combining all the GAG hydrogel network parameters into a mathematical model could be instrumental in designing materials that achieve the desired rate of morphogen transport [32, 55], to precisely modulate cellular responses [30, 56]. Besides, the model will also potentially speed up the discovery of biomaterials with tailored signaling molecule transport properties by testing different combinations of parameters *in silico* before experimental evaluation.

The application of mathematical models to predict the transport of signaling molecules within GAG-based materials in the presence or absence of matrix degradation has been previously described [33, 53, 55, 57]. For example, Sakiyama-Elbert and Hubbell developed a mathematical model to describe the release of fibroblast growth factor 2 (FGF-2) from a fibrin matrix functionalized with the heparin [53]. Simulation results using the model allowed the determination of the optimal ratio of heparin to the growth factor that could

minimize the passive release of the factor from the matrix. In a related study using the same delivery system, the effect of heparin content of the fibrin matrix to modulate the release of neurotrophin-3 (NT-3) for spinal cord injury was investigated [33]. The mathematical model suggested the optimal ratio between the heparin and the heparin-binding peptide that shifted the balance of the growth factor toward a matrix-bound state rather than a free heparin-bound state. In the study, the experimental release also confirmed the impact of heparin content on the overall release of NT-3. However, a direct comparison between the resulting experimental release and theoretical release was not presented.

Similarly, Hettiaratchi et al. developed a computational model to predict the BMP-2 release from alginate-based hydrogels containing heparin microparticles (HMPs) *in vivo* [55]. The mathematical model suggested that the incorporation of HMPs lowered the BMP-2 released into surrounding tissues, and the release of the BMP-2 can be tailored by modulating the amount of HMPs in the construct. Nevertheless, the enhancement in the retention of growth factors through the incorporation of HMPs did not improve the materials' *in vivo* performance. The results of the studies also pointed out that additional parameters such as the competitive binding of the serum-borne proteins to the affinity ligands need to be considered when applying the engineered materials *in vivo* to achieve more predictable biological outcomes [58].

More recently, a mathematical model has also been applied to predict the release kinetics and short-range gradient of SDF1 α from microparticles containing GAG that mimic cytokine releasing cells within a three-dimensional extracellular matrix [59]. The gradient of proteins developed from the particles was shown to be dependent on the concentration and affinity interaction facilitated by the GAG. Moreover, the functionality of the gradient to modulate cellular responses was demonstrated by a directed migration of hematopoietic cell line and primary murine hematopoietic stem and progenitor cells (Sca-1+CD150+CD48-) toward the SDF1 α containing microparticles over periods of several hours. In a related study, the same approach has also been adapted to emulate paracrine signaling of TGF β 1 during wound healing [60]. The slow and sustained delivery of TGF β 1 from the microparticles was shown to induce the differentiation of dermal

fibroblasts into myofibroblasts at a significantly lower concentration than the systemic delivery of signaling molecules.

Mathematical models have been previously applied to guide the design of GAG-based biomaterials for bone and neural tissue engineering [55, 57, 61]. However, their applications in vascular tissue engineering have not been reported. The vascular network is essential to supply the cells with the nutrients and oxygen as well as for the removal of metabolic waste to maintain the cell survival and functions beyond their diffusion limit in tissues ($< 200\ \mu\text{m}$) [62-64]. As such, the ability to engineer functional microvasculatures is essential for the success of therapeutic vascularization and tissue engineering [65]. Within this context, pro-angiogenic growth factors, including the vascular endothelial growth factor (VEGF), plays a pivotal role in regulating vascular functions and development by stimulating proliferation, migration, survival, and differentiation of endothelial cells [66-72]. Previous studies on the VEGF gene therapy revealed that the newly generated vessel could be therapeutically beneficial only when they were stable indefinitely [73]. Accordingly, this could be achieved when the VEGF stimulation was provided for at least four weeks [74-76]. The GAG-based materials could offer powerful options to enhance the stability of pro-angiogenic growth factors and modulate their sustained administration [6, 77]. Thus, rational design strategies using the mathematical model that described the influence of each GAG hydrogel network parameters on the transport of the signaling molecules will potentially enhance the cell-instructive properties of the material to promote strong angiogenesis responses.

GAGs can bind to a broad spectrum of proteins with different properties [7, 78]. Therefore, a systematic study on the transport of signaling molecules with various physicochemical properties in a fully defined and tunable GAG-based hydrogel platform would allow us to dissect the influence of each hydrogel network parameter on the transport of the growth factors. Previously, we have developed the cell-instructive binary GAG-based-hydrogel system based on heparin and 4-arm poly(ethylene glycol)-(starPEG) peptide conjugates [47]. The theory-driven material design concept has enabled the formation of hydrogels with different mechanical properties at an invariant heparin content [79]. This strategy has also

been extended to generate hydrogels with similar mechanical properties of varying sulfation patterns [110, 309]. The overall GAG content and the GAG sulfation pattern of the system can be varied to tailor the binding of various cytokines and growth factors of different physicochemical properties [38, 78]. Besides, the system is compatible with a direct encapsulation of human umbilical veins endothelial cells (HUVECs) and has been adapted as a 3D *in vitro* model of angiogenesis [3].

1.3 Aim of the work

The thesis study aimed to systematically investigate the impact of different starPEG-GAG hydrogel network parameters on the transport of signaling molecules of different physicochemical properties by developing and applying mathematical modeling and combine it with experimental approaches. The gained knowledge should then be applied to control the vascular endothelial cell morphogenesis within already established starPEG-GAG-hydrogels and as an extension to rationally design a set of GAG-based hydrogels with well-adjusted network properties that significantly extend the current state of the art for the control of transport and biological activity of pro-angiogenic growth factors.

To accomplish these goals, the project should be divided into three sections:

- 1. Understanding of the transport and binding of signaling molecules within the existing binary starPEG-GAG hydrogel system**
- 2. Modulation of the bioactivity of pro-angiogenic growth factors to control the vascular endothelial cell morphogenesis within the binary starPEG-GAG hydrogel system**
- 3. Development of a ternary starPEG-GAG hydrogel system allowing for a far-reaching control of the GAG content to enhance the administration of pro-angiogenic growth factors**

In this thesis, the impact of different network parameters of the binary starPEG-GAG hydrogels, including the mesh size, GAG content, and GAG sulfation

pattern on the mobility and release kinetics of model proteins with different sizes and affinity to GAGs, will be first analyzed. Following the development of a mathematical model to analyze the diffusion and binding of signaling molecules within the polymer network, the impact of tuning the GAG content and GAG sulfation pattern of the hydrogel on the vascular endothelial growth factor (VEGF)-mediated endothelial cell vascular morphogenesis will be examined. Lastly, a ternary GAG-based hydrogel system will be developed to control the administration of pro-angiogenic growth factors by extending our previously established binary hydrogel system synthesis protocol [47]. The network characteristics, transport properties, as well as the applicability of the materials to support endothelial cell morphogenesis, should be evaluated.

Taken together, this thesis project aimed to combine experimental and computational modeling approaches to systematically evaluate the influence of network properties of the GAG-based biohybrid hydrogels on the mobility of various signaling molecules with different properties, allowing for the rational design of hydrogels. This insight gained here may be applied to the design and translation of GAG-based biohybrid hydrogels for tissue engineering and regenerative medicine applications.

2. Fundamentals

2.1 Extracellular matrix and the cell signaling functions

2.1.1 The extracellular matrix (ECM) structure and functions

The extracellular matrix (ECM) is a dynamic structure around the animal cells providing the structural support, anchoring site, and biochemical signaling (**Figure 2.1**). Besides providing the mechanical cues to the cells, the ECM also controls the development, cellular morphogenesis, homeostasis, and differentiation of stem cells by regulating the availability of biomolecular signals and their receptors and the local physicochemical properties (pH and hydration) of the cellular microenvironment [80-83]. The ECM continuously undergoes remodeling due to a dynamic interplay between the cells and their environment, creating diversity in the structural and compositional of the ECM of different types of tissues [83, 84]. Several pathological conditions, such as cancer and abnormal scarring, are even characterized by their unique ECM composition and microarchitectures [83, 85].

2.1.1.1 The components of the ECM

The ECM consists of a complex and organized cell-secreted meshwork of glycoprotein, polysaccharides/ glycosaminoglycans (GAGs), and proteoglycans. Collagen is the most abundant glycoprotein in the ECM, and it constitutes about more than 40% of the protein in the human body. Naturally, it forms a strong fibrous structure that provides mechanical support or attachment site to the cells. Twenty-eight different types of collagen have been identified. Each variant comprises an intertwined triple helix of polypeptide chains that exist as homotrimers or heterotrimers [86]. This triple helix structure particularly allows the collagen fiber to engage in different functions, including self-association, binding to the other ECM proteins, glycosaminoglycans (GAGs), and nucleic acids [82].

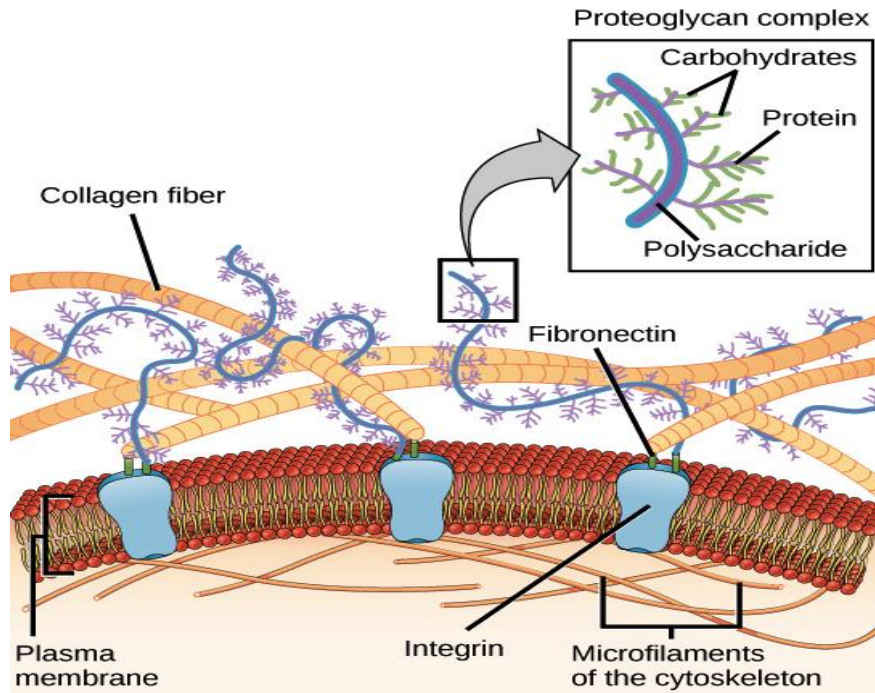


Figure 2.1. The extracellular matrix (ECM). The ECM is a complex meshwork containing structural and adhesion proteins, as well as highly hydrated proteoglycans. Adapted from [87]

In the ECM, a collagen fiber is embedded within woven hydrated proteoglycan complexes. Proteoglycan distribution is varied within the tissues. Large proteoglycans, including aggrecan and versican, are secreted into the extracellular space; small proteoglycans such as decorin and lumican are located within the basement membrane, whereas proteoglycans like syndecans and serglycin are found on the cell surface and inside the cells, respectively [82]. The structure of proteoglycans composed of a core protein that is covalently linked to GAGs, long and linear negatively charged polysaccharides with disaccharide units. The hydrophilic nature of the GAG component of proteoglycans correlates well with its function to provide hydration and mechanical resistance to the tissues.

GAGs can be classified into several main groups that differ in their degree of sulfation, chain length, and sugar composition of the disaccharides unit. These groups include hyaluronic acid (HA), chondroitin sulfate (CS), dermatan sulfate (DS), keratan sulfate (KS), heparan sulfate (HS), and the closely related family, heparin (Hep). Except for HA, all GAGs are sulfated. The degree of GAG sulfation and spacing along the protein core determine the proteoglycan binding

affinities for different molecules within the ECM, such as the growth factors, chemokines, and other ECM proteins like laminin and fibronectin, and cell surface receptors; suggesting their role in various cellular processes [88-92].

Apart from the structural components, the ECM contains connector proteins, such as laminin and fibronectin, that facilitate the interactions between the structural elements and other components of the ECM or cells. Typically, the connector proteins are composed of multidomain of glycoprotein that serves as a binding site of other ECM proteins, signaling molecules such as vascular endothelial growth factors (VEGFs) [93] and the transforming growth factor- β 1 (TGF- β 1) [94], and the cell surface receptors [82]. Notably, the adhesive RGD sequence of fibronectin can be incorporated into cell-instructive materials to mediate the cell attachment on the surface- or within 3D polymeric networks.

2.1.1.2 The functions of the ECM

Cells respond to mechanical signals that originate from the external forces, cell-cell, and cell-matrix interactions in a process called mechanotransduction [95, 96]. As described before, the cell perceives biomechanical signals in the ECM through integrin proteins. The binding of integrin to the ECM proteins triggers the activation of intracellular signaling pathways that induce the expression of genes involved in the regulation of cell proliferation, differentiation, and apoptosis [81] (**Figure 2.2**). Equally, the resident cells also constantly renew and remodel the ECM through synthesis, modification, reassembly, and degradation of surrounding ECM components and the release of biomolecular signals that are immobilized in the matrix [97]. Subsequently, the released signaling molecules affect the nearby cells in an autocrine or paracrine manner, leading to diverse cellular functions. Overall, this suggests that the cross-talk between the biochemical and mechanical signaling allows integrating local signals that orchestrate complex cellular responses.

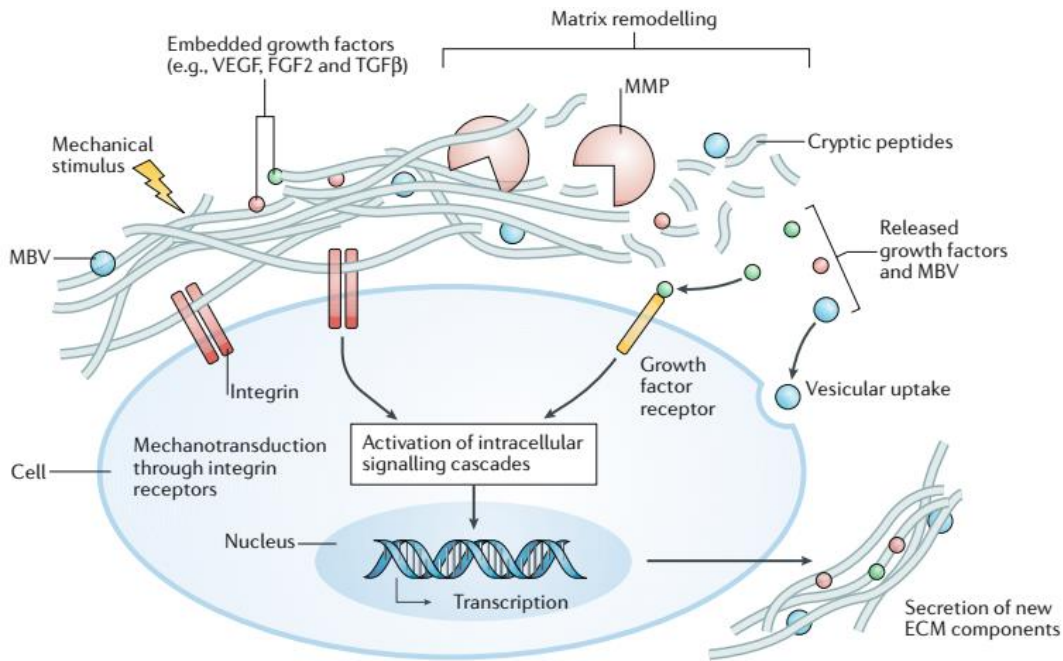


Figure 2.2. Cells respond to biophysical and biomolecular signals from the ECM and actively remodel their microenvironment. Physical and biochemical cues from the ECM are perceived by the cells by activating intracellular signaling pathways that trigger the gene expression, synthesis, and secretion of ECM components. Matrix remodeling initiated by the resident cells through the secretion of matrix metalloproteases (MMP) degrades the ECM and allows the release of growth factors that activate diverse cellular functions. Adapted from [97]

2.1.2 GAG as the regulator of signaling molecule activity in the ECM

2.1.2.1 Signaling function of GAGs

Glycosaminoglycans have a profound effect on potentiating the growth-factor mediated cellular signalings. In particular, heparan sulfate (HS) has long been recognized as a co-receptor of growth factors that facilitate the binding to the receptor tyrosine kinases and the resulting cellular responses. As an example, the complex formation between the HS, FGF-2, and the FGF2 receptor (**Figure 2.3A**) could promote the dimerization of FGF/FGFR and, subsequently, activate the tyrosine kinase domain and downstream signaling pathways that modulate the cell motility, survival, and proliferation [98]. Besides, glycosaminoglycan is known to interact with the integrin on the cell surface [99]. Such interaction could eventually convey the signaling from the integrin to the growth factor receptor

through the association between integrin cytoplasmic tail and adaptor proteins such as focal adhesion kinase and Src [100, 101] (**Figure 2.3B**).

2.1.2.2 Protection and stabilization of growth factors

Protecting the growth factors from thermal denaturation and degradation by proteases is another mechanism by which the GAGs enhance the bioactivity of proteins over time (**Figure 2.3C**). The stabilizing effects of polyanions, including the heparin or heparan sulfate against physical or enzymatic degradation has been previously documented on cytokines [102-104], and growth factors such as fibroblast growth factor (FGF-1) and FGF-2 [103, 105]. While the thermal denaturation can happen anytime, especially at a high temperature, the degradation of growth factors within the tissues may be elevated under certain physiological conditions such as the inflammation stage of the wound healing process. In this case, the GAG-based biomaterials could be instrumental in promoting tissue regeneration by protecting pro-regenerative cytokines from cell-secreted proteases. In a recent study, Schirmer and co-workers have demonstrated that the heparin-based hydrogel could protect the encapsulated IL-4 against thermal denaturation and cleavage by protease's model [26]. Moreover, the hydrogel also sustainability released the cytokine over two weeks, and as indicated by the ability to promote the activation of macrophages, the released protein also still maintained the bioactivity.

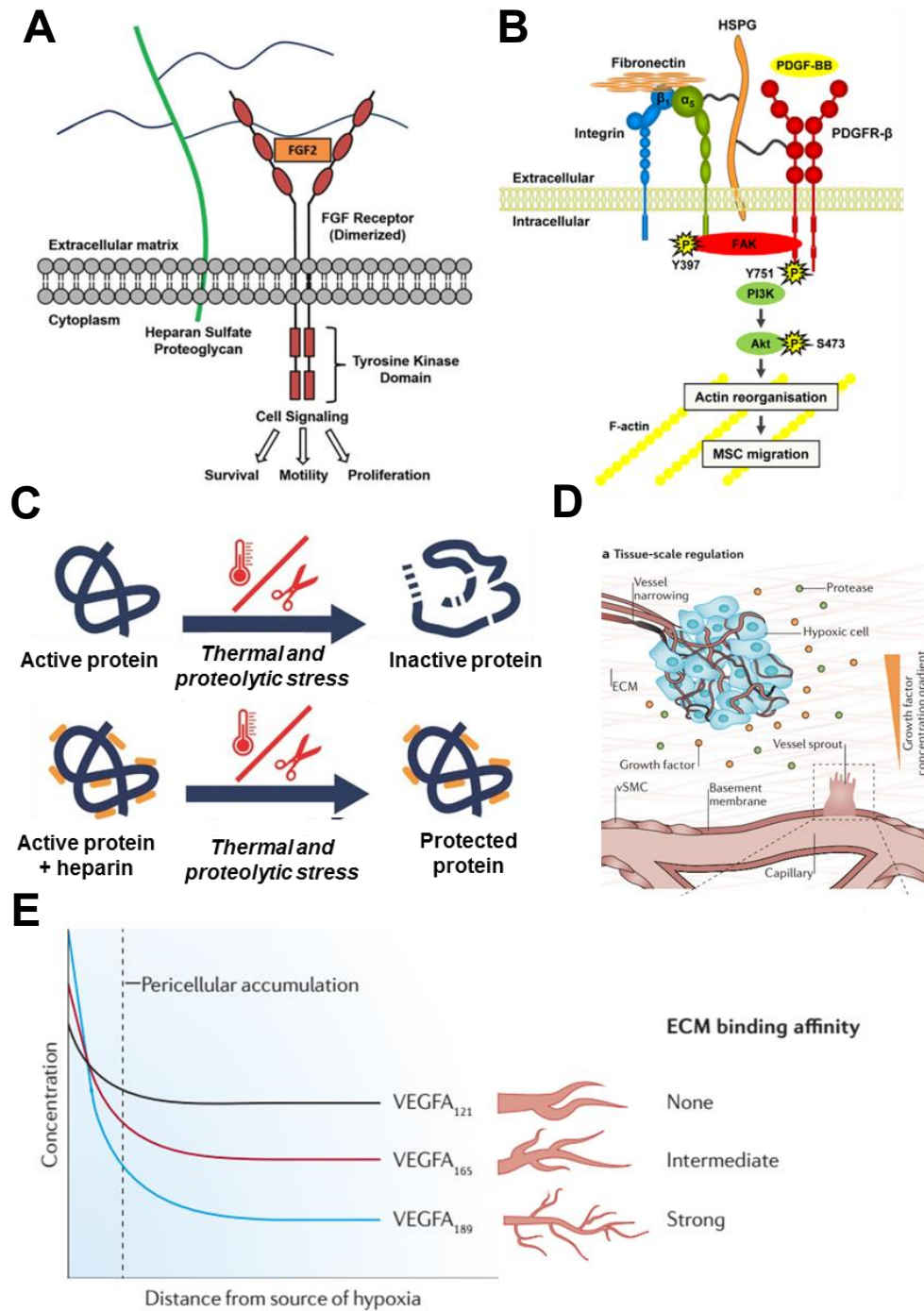


Figure 2.3. GAG regulates the activity of soluble signaling molecules. (A) GAG enhances the FGF-2 binding to the receptor. (B) GAG mediates the association between the extracellular domains of the receptor of PDGF-BB to the integrin. (C) GAG protects the growth factors from thermal and proteolytic degradation. (D) During the angiogenesis, GAG maintains the formation of the VEGF gradient. (E) The affinity of VEGF isoforms to the GAG determine their gradient profiles within the ECM, which eventually shapes different vascular morphologies. Figure A, B, C, and D-E are adapted from [98], [101], [26], and [106], respectively.

2.1.2.3 Formation of growth factor gradient

The glycosaminoglycan controls the spatiotemporal presentation of soluble signaling molecules within the ECM. This mechanism can be illustrated, for example, during the angiogenesis process. Angiogenesis involved the secretion of proteases that degrade the basement membrane, allowing the endothelial cells to migrate into the tissue and forming sprouting vasculatures. Subsequently, VEGF's gradient guides the migration of endothelial cells, controls their proliferation rates and initiates the vascular morphogenesis events (**Figure 2.3D**). Moreover, VEGF can be synthesized either as a longer isoform (VEGF189 and VEGF165) or shorter isoform (VEGF121) [106-108], which influence their ECM binding properties. The binding affinity of VEGF to the GAG not only guides the migration of endothelial cells but also shapes the overall morphologies of vasculatures (**Figure 2.3E**). VEGF165 and VEGF 189 have very restricted mobility and form a steep VEGF gradient that orchestrates the formation of a large density of thin and highly branched vessels [108, 109]. On the other hand, the VEGF121 creates a shallow VEGF gradient in the ECM that lead to the formation of short, a small number of leaky vessels with a wide diameter [106, 109-112].

2.2 Modelling the transport of signaling molecules in affinity-based systems

Affinity-based growth factor delivery system modulates the release kinetics of embedded growth factors through the affinity interactions between the binding ligand and growth factor of interest. The binding ligand can be a protein, peptide, DNA, or glycosaminoglycans (GAGs), and typically linked to the hydrogel network through a covalent linkage [52, 113, 114]. Selecting the right binding ligand with a specific strength of interactions is essential to control the administration of bioactive molecules at a desired rate and dosage. For that, several methods, including isothermal titration calorimetry (ITC) [115], Surface plasmon resonance (SPR) [116], biolayer interferometry (BLI) [117], and microscale thermophoresis [118], have been developed to measure the strength of interactions (K_D) between the binding ligand and proteins (**Table 2.1**).

2. FUNDAMENTALS

Table 2.1. Different methods used to quantify binding interactions. Data are from [115, 116, 119-127]. ΔH , and ΔS are enthalpy and entropy of binding, respectively.

Method	ITC	SPR	BLI	MST
K_D range	10^{-6} to 10^{-9} M	10^{-3} to 10^{-12} M	10^{-6} to 10^{-9} M	10^{-3} to 10^{-12} M
Thermodynamic data (ΔH , ΔG , ΔS)?	Yes	Yes	Limited	Yes
Kinetics data (k_a/k_d)?	No	Yes	Yes	No
Immobilization?	No	Yes	Yes	No
Modifications (e.g. fluorescent tag)?	No	No	No	Yes
Concentration analysis	No	Yes	Yes	No
Sample consumption	High	Low	Low	Very low
Sensitivity	Medium	High	Medium	Low

The affinity-based growth factor delivery system controls the release kinetics of encapsulated proteins by harnessing the reversible interaction between protein and ligand (**Figure 2.4**). A combination of intermolecular forces such as ionic interaction, hydrophobic or van der Waals interaction, and hydrogen bonding usually facilitates binding a protein to the immobilized affinity-ligand. The rate formation and dissociation of the protein-ligand complex collectively are governed by the association and dissociation rate constant, respectively. The ratio between these values ($K_D = k_d/k_a$) determines the strength of affinity interactions (K_D). The K_D value is also determined by the equilibrium concentration of free ligand, protein, the ligand-protein complex. Overall, the changes in the concentration of protein within the polymer matrix can be modeled using the reaction-diffusion model [51, 52]. Accordingly, the transport of signaling molecules within an affinity-based system can be tuned primarily through adjusting the strength of affinity interactions, the concentration of binding ligand, the rate dissociation of the complex, initial protein loading concentration as well, as the size and geometry of hydrogel constructs.

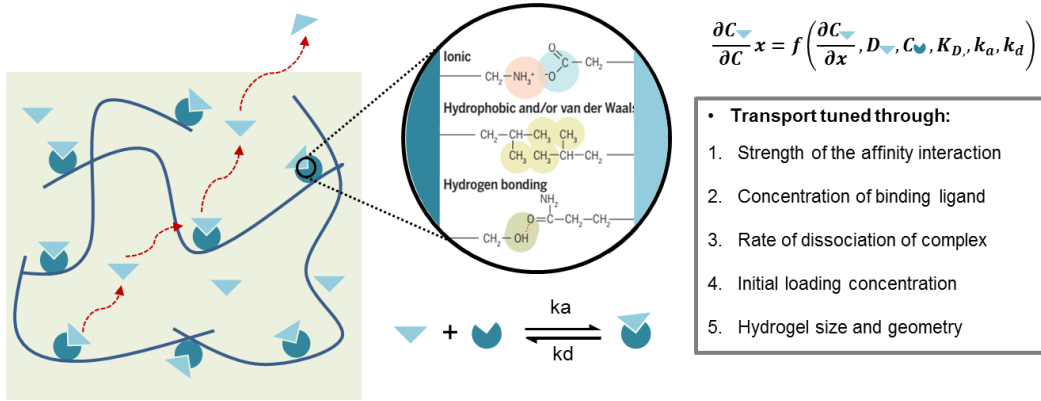


Figure 2.4. Affinity-based growth factor delivery system. The binding ligand is immobilized within the polymer network allowing the reversible interaction with the encapsulated proteins — various intermolecular forces, including the ionic, hydrophobic, Van der Waals interactions, and hydrogen bonding, contribute to the formation of protein-binding ligand complex. The extent of complex formation is governed by their kinetics rate constants. The binding interactions, along with the diffusion process, can be modeled using the reaction-diffusion model. Multiple parameters that governed the transport of signaling molecules within the matrix are summarized. Figure modified from [119]

The application of a mathematical model to predict the transport of growth factors within affinity-based systems has been previously described [33, 53, 55, 57]. For example, Sakiyama-Elbert and co-workers developed a mathematical model to describe the release of heparin-binding protein (FGF-2) from a fibrin matrix functionalized with the heparin [53]. In another study, Lin and Metters developed metal-chelating affinity hydrogels for the sustained delivery of recombinant protein containing Histidine tag [18, 128, 129]. Overall, their study emphasized that the protein release from the polymer matrices can be systematically controlled using ligands with a defined binding and rate constant. As such, metal ion-mediated sustained protein release from these affinity hydrogels is governed by equilibrium protein-ligand binding affinity (dissociation constant, K_D) as well as by the protein-ligand dissociation kinetics (dissociation rate constant, k_d) [129]. In this case, while the equilibrium dissociation constant determined the initial rate of the protein release, the dissociation rate constant controlled the long-term release behavior.

More recently, the Shoichet group has developed an affinity-based delivery system for the fusion protein containing Src homology 3 (SH3) domains [52, 130-132]. Computational [52], and experimental studies on the release of SH3 fusion proteins including FGF-2 [132], insulin-like growth factor (IGF-1) [133], chondroitinase ABC [130], and ciliary neurotrophic factor (CNTF) [131], from methylcellulose- and hyaluronic acid/ methylcellulose hydrogels revealed that the release of these proteins could be precisely modulated over several days through adjusting the peptide affinities to the SH3 domain. Besides, simulation based on the reaction-diffusion model has also confirmed that the ratio of ligand to protein and hydrogel geometry could affect the protein release characteristics [52].

2.3 GAG-based biomaterials control the administration of pro-angiogenic growth factors

2.3.1 GAG-based biomaterials as a controlled release system of pro-angiogenic growth factors

Pro-angiogenic growth factor administrations using GAG-based materials have been shown to promote pro-angiogenic effects *in vitro* and tissue vascularization *in vivo* (**Figure 2.5A**). For example, Peattie et al. developed PEG-based hyaluronic (HA) hydrogels to deliver FGF and VEGF [134]. *In vivo*, the hydrogel functionalized with VEGF was shown to induce a higher vessel density and neovascularization than the hydrogel containing no growth factors, hydrogel functionalized with the FGF alone, or soluble growth factor treatments. Moreover, functionalization of the PEG-based matrices with heparin could also sustain the delivery of VEGF and maintain its bioactivity for a longer time [135]. The implantation of the VEGF-loaded gel in mice was shown to enhance a higher vascularization in the tissue surrounding the scaffold as compared to the unloaded hydrogels. A similar improvement over the tissue vascularization was also observed upon FGF delivery using a hybrid of chitosan-heparin hydrogel [136]. In a related study, HA-PEG hydrogel was modified with gelatin and heparin to control the release of various pro-angiogenic growth factors, including the Ang and VEGF [137]. The gels functionalized with either VEGF or Ang-1 induced

remarkable vascularization responses *in vivo* compared to the gels containing no growth factor. Overall, these studies suggest that the functionalization of engineered biomaterials with pro-angiogenic growth factors enhances tissue vascularization.

The release of pro-angiogenic factors can be tuned by adjusting the GAG content and the GAG sulfation pattern of the hydrogel. As an example, Pike and coworkers modulate the release of FGF and VEGF from PEG-hyaluronic acid hydrogel matrices by varying the amount of incorporated heparin [77]. The growth factors can be sustainably released *in vitro* over 42 days by incorporating only less than 1% (w/w) of heparin, and the total amount of growth factor release decreased monotonically with increasing heparin concentration. Remarkably, the highest vascularization index was only observed when the hydrogels were functionalized with both heparin and growth factors. In a related study, the sulfation pattern of heparin could be selectively varied to tailor the binding and release of VEGF from starPEG-heparin hydrogels [6]. Both overall and local sulfate density of the hydrogel was shown to modulate the rate of VEGF release *in vitro*. However, in general, 6O- and N- sulfate groups are more pronounced in determining the amount of VEGF released from the system.

Simultaneous multifactorial administration of angiogenic growth factors from the GAG-based polymeric matrices can be explored to synergistically enhance the bioactivity of the factors *in vitro* or *in vivo*. PEG-hyaluronic acid hydrogels have been previously applied to control the delivery of keratinocyte growth factor (KGF) and VEGF [138]. Combined delivery of both factors into ear pinnae of a mice model using the hydrogel could additively induce a greater extent of neovascularization than single growth factor delivery with the hydrogel or simultaneous bolus delivery of both factors. Similarly, Zieris et al. utilized the starPEG-heparin hydrogel system for the dual independent delivery of VEGF and FGF [5]. More recently, co-delivery of a chemokine, SDF1 α , and lipid-based pro-angiogenic factors, sphingosine-1-phosphate analog (FTY720), has also been explored to modulate the pro-regenerative potential of immune cells. PEG-hydrogel functionalized with heparin and lipid chaperon of albumin allowed for the controlled delivery of FTY720 and SDF1 α [139].

2.3.2 GAG-based biomaterials as a 3D cellular encapsulation matrix for vascular tissue engineering

The capacity of GAGs to regulate the activity of signaling molecules in the ECM has inspired their incorporation into vascular tissue engineering matrices (**Figure 2.5B**). Typically, the GAGs also blend with the naturally derived biopolymer or fully synthetic polymer to enhance the cell-instructive and mechanical properties of the constructs [140, 141]. Several cell types, such as fully differentiated HUVECs [3, 141, 142], EPCs [143], and tissue-specific progenitor cells [42, 43, 144, 145], have been reported to display their vasculogenic potential within the GAG-based materials. Their ability to form stable and lumenized vascular structures were also controlled by the presence of supporting cells, such as fibroblast, and smooth muscle cells, and mesenchymal stem cells [3]. For initiating the vascular morphogenesis, functionalization of the matrix with pro-angiogenic growth factors such as VEGF, TGF β , FGF-2, SDF1 α , either individually or in combinations, is often required. In addition to the biomolecular characteristics of the scaffold, the network properties of GAG hydrogels, such as matrix degradability, cell adhesiveness, and stiffness, were also shown to determine the extent of vascular network formation. The robust capillary-like structures developed within well-defined GAG-based materials will allow its further applications for drug discovery, tissue engineering, and studying vascular biology (**Figure 2.5C**).

Heparin might be combined with the hyaluronic acid within a tissue engineering construct to synergistically harness the angiogenic properties of both materials. For example, Jha et al. utilized hyaluronic acid-based hydrogel supplemented with a low amount of heparin to aid cardiac progenitor cells (CPCs) transplantation therapies [42]. The adhesion peptide and stiffness of the hydrogel and the growth factor sequestering capacity were shown to affect the survival and engraftment of stem cells [42, 145]. The inclusion of heparin within the system also enhanced the function of CPCs *in vivo* to promote vascularization by coordinating the presentation of the encapsulated TGF β and sequestration of various cell-secreted factors. The follow-up study also determined that the growth factor sequestration capacity of the hydrogel can be tuned by changing the content or molecular

2. FUNDAMENTALS

weight of the heparin [43]. The hydrogel with the highest affinity to the growth factors (with the highest heparin content and the largest molecular weight of heparin) supported a more robust stem cell differentiation and vessel formation.

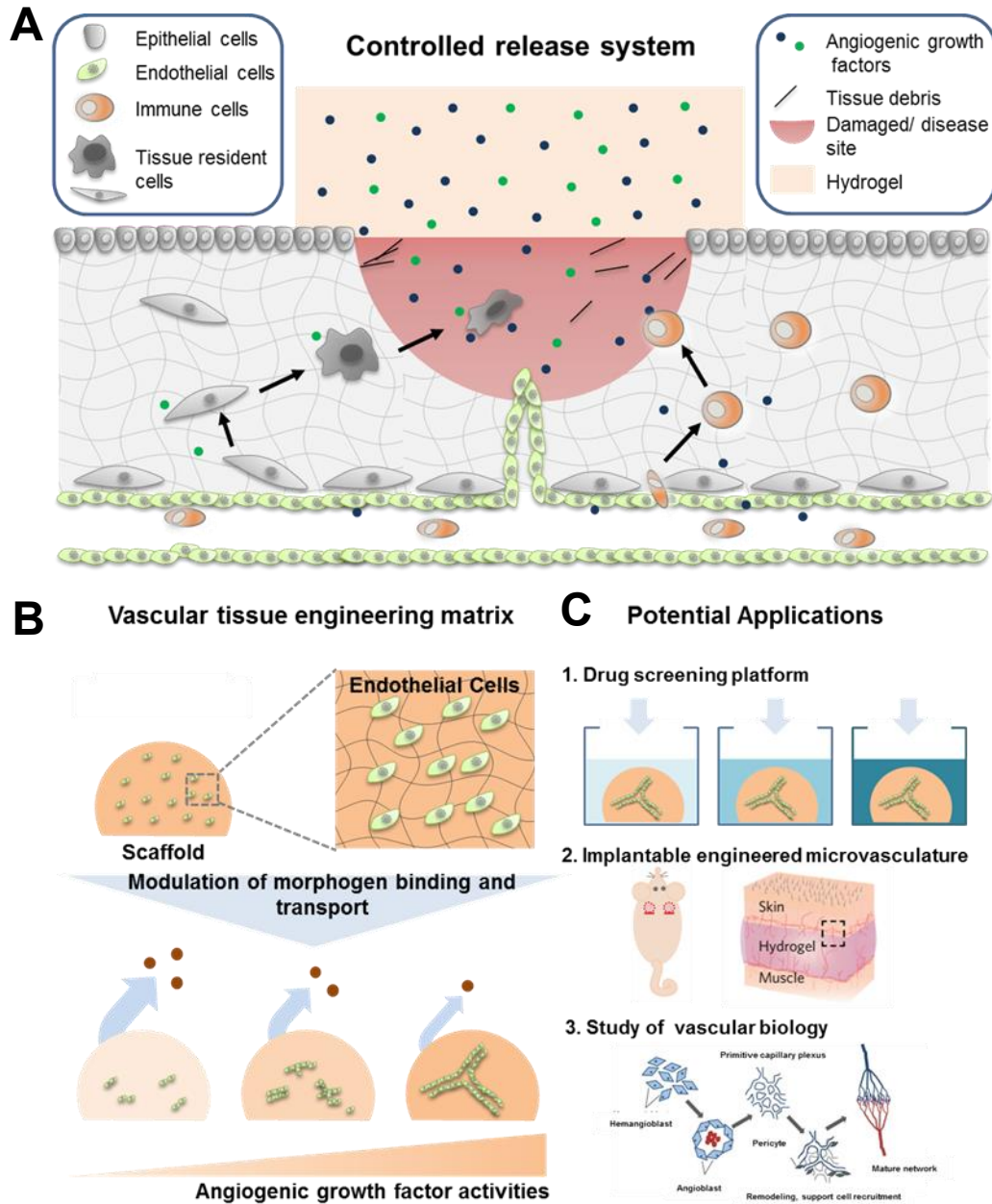


Figure 2.5. The application of GAG-based materials to control the activity of pro-angiogenic growth factors. (A) GAG-based material sustainably delivers pro-angiogenic growth factors to promote angiogenesis in the damaged/ diseased tissues. (B) GAG-based materials can be applied as a cell instructive scaffold to generate robust microvasculature *in vitro*. (C) The microvascular network within the hydrogel can further be utilized as an anti-angiogenesis drug screening platform, implantable microvasculature for tissue engineering applications, or an *in vitro* culture model of vascular biology. Figure C-2 and C-3 are adapted from [146] and [17], respectively.

2.4. Modular starPEG-GAG hydrogels platform

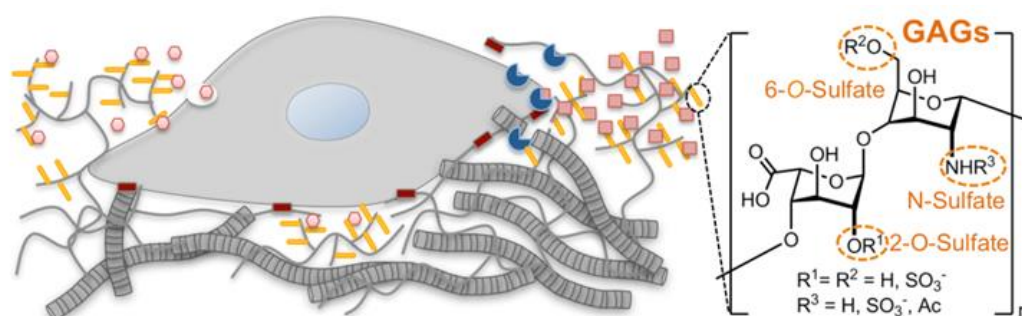
The extracellular matrix (ECM) provides cell instructive signals that control tissue formation and homeostasis. Particularly, glycosaminoglycans (GAGs), as one of the major components of the ECM, mediate various signaling functions of the ECM by presenting multiple soluble signaling molecules [104] and controlling the formation of morphogen gradients [147] (**Figure 2.6**). These fundamental roles of GAGs in the ECM ultimately regulate various important physiological processes in the body [88, 148-151]. In an attempt to recapitulate the instructive cell roles of the GAGs in living tissues, incorporation of GAG into the biomaterials are currently attracting considerable attention [152]. In addition to regulating the cell signaling function, the ECM also inherent various physical properties, structural heterogeneity, susceptibility to cell-mediated remodeling, and cell adhesion /attachment sites. Therefore, GAG-based biomaterials can further be tailored to recapitulate these fundamental features of the ECM through the rational design and processing of polymer networks to control the presentation of soluble factors, network structures, cell adhesiveness, shapes, and degradability of the matrices.

The *in-situ* encapsulation of soluble growth factors and cells within the MMP-degradable PEG-Hep hydrogels can be achieved using a cytocompatible, a Michael-type addition reaction scheme. This would allow for the investigation of more advanced cellular processes under a defined 3D cellular environment [3, 47]. The cell-mediated degradation and subsequent VEGF delivery were previously shown to enhance cell spreading and endothelial cell morphogenesis on the 2D surface of starPEG-heparin hydrogel [47]. The follow-up studies revealed that multiple pro-angiogenic growth factors (VEGF, FGF-2, and SDF-1 α) could synergistically enhance the formation of endothelial capillary networks in 3D [3]. Moreover, it has also been demonstrated that the co-culture of MSCs and HUVECs within RGD-modified, MMP-degradable, soft (~200 Pa) starPEG-Hep hydrogel matrix containing triple factors support the maintenance of a mature capillary network for at least a month *in vitro*. In an extension of that work, triple cultures of HUVECs, MSCs, and various breast and prostate cancer cell lines were established to generate a 3D tumor vascularization model [153]. Similarly,

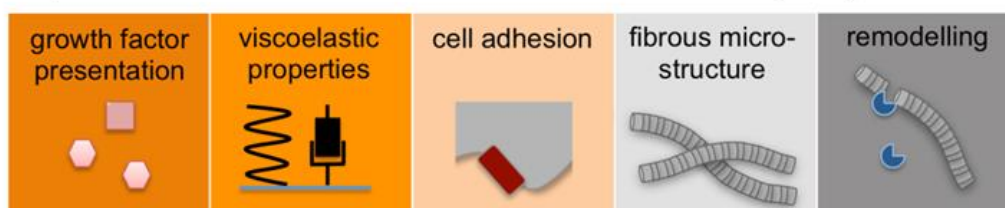
the platform has also been successfully applied to investigate the effect of different biochemical and biophysical properties of the matrix on the extent of renal tubulogenesis [154] and the hematopoietic stem cells cycling [155], highlighting the potential of the hydrogels for advanced organ culture models which could minimize the expensive and ethically challenging animal experiments [156].

The GAG-based hydrogel can entrap therapeutically relevant molecules and complexing the molecules through electrostatic interactions to control their local administration. Based on this property, starPEG-heparin hydrogel has been successfully adapted to control the release of various heparin-binding growth factors, such as FGF-2 [2], VEGF [4], BMP-2 [79], SDF-1 α [19], GDNF [157], NGF [158], TGF- β [35], IL4 [26], PDGF-BB [38], and EGF [159]. The relatively high gel heparin content also enabled multifactorial administration, such as for the combined delivery of FGF-2 and VEGF [5], and FGF-2 and GDNF [157].

The sulfation pattern of GAGs determines the GAG affinity for proteins, modulating the protein transport and bioactivity [160]. Therefore, the starPEG-Hep hydrogel platform was adjusted to exhibit different affinities for soluble signaling molecules via the incorporation of N-desulfated, 6O-desulfated, or 2O-desulfated heparin derivatives [39]. The rational design concept enables the formation of hydrogels with similar mechanical properties with different sulfation patterns [39, 79]. All the hydrogel containing desulfated heparin displayed anticoagulant activity. *In vitro* binding and release experiment of the VEGF from the hydrogel of different sulfation also revealed that VEGF release was unaffected by 2O-DSH, whereas 6O- and N-DSH enhance the VEGF release to a similar extent [6].



Key functional characteristics of extracellular matrices (ECM)



GAG-based, ECM-mimicking materials to adjust

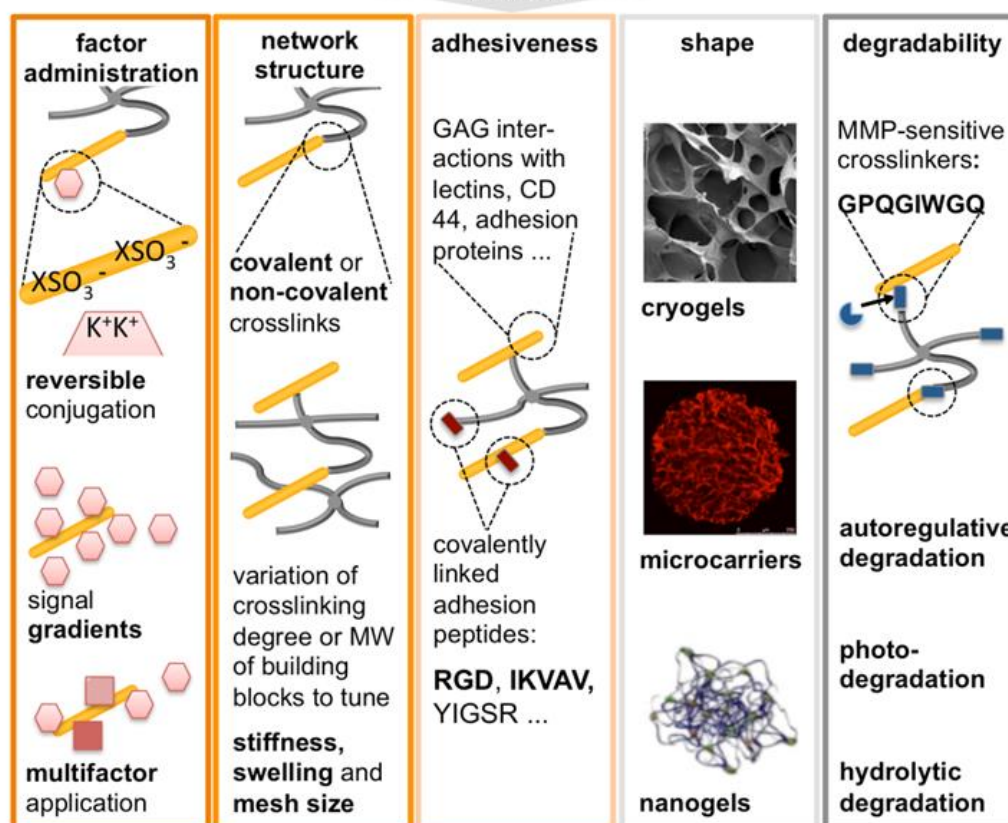


Figure 2.6. Modular starPEG-GAG biohybrid hydrogels. The starPEG-GAG hydrogel is tailored to recapitulate the fundamental characteristics of ECM, including the growth factor presentation, viscoelastic properties, provision of cell adhesion ligands, fibrous structures, and matrix remodeling. Adapted from [25]

3. Materials and Methods

3.1 Preparation of hydrogels

3.1.1 Binary GAG hydrogel systems

GAG component of the hydrogels, including maleimide-functionalized heparin (Hep) and heparin derivatives (6O- & 6ON desulfated heparin (6O-DSH & 6ON-DSH, MW ~ 15 000) were in house synthesized. The hydrogels were prepared as previously described with slight modifications [47]. Briefly, thiol functionalized 4-arm starPEG (starPEG-SH) (MW 10 000, Polymer Source, Inc., Dorval, Canada) and maleimide functionalized heparin/ heparin derivatives were dissolved in PBS at an appropriate molar ratio. To generate GAG-hydrogel with various mesh size/ crosslinking degree (molar ratio of starPEG to GAG), starPEG-SH solution at a concentration in the range of 1.8–4.4 mM was mix with an equal volume of GAG to reach a final GAG concentration of 1.5 mM (solid content ~ 3.2-4.4%). Similarly, the hydrogel with variable GAG sulfation patterns was produced with the final GAG content of 1.5 mM and prepared by reacting heparin or desulfated heparin with ~1.8 mM starPEG-SH (solid content ~ 3.2%). Furthermore, for the preparation of hydrogel with a lowered GAG concentration (0.5 and 1 mM), the Hep solution was mixed with 1.5 mM of starPEG-SH to produce hydrogels with a final solid content of ~2%. As a non-affine hydrogel control, pure PEG hydrogel was also prepared by reacting an equal volume of 3 mM of starPEG-SH with maleimide-functionalized starPEG (starPEG-Mal) (JenKem Technology, Plano, USA) at a final solid content of 2.2-3.2%. In general, upon the mixing of gel components, the hydrogels were formed instantaneously within several seconds. The pH of the starPEG-SH solution might be adjusted to 5.6 to have an efficient hydrogel component mixing allowing for the formation of homogenous hydrogel samples.

3.1.2 Ternary GAG hydrogel systems

A ternary system containing starPEG-SH, starPEG-Mal, and maleimide functionalized heparin was used to prepare GAG hydrogels with varied heparin

concentration in the range of 1.5-1500 μM . All the hydrogel components were dissolved in PBS. Subsequently, starPEG-Mal and maleimide functionalized heparin were mixed at an appropriate molar ratio to produce polymer containing maleimide mixture. The mixture was then combined with a starPEG-SH solution at an initial SH to maleimide molar ratio of 0.4-0.7 to produce hydrogels with different stiffness of a given heparin concentration (solid content of 2.6-4.5 %).

The hydrogels could be pre-functionalized with growth factors by gentle mixing of the growth factor with the polymer containing maleimide mixture before adding the starPEG-SH component. Additionally, cell encapsulation during the gelation process was carried out by incorporating the cell suspensions into the polymer containing maleimide mixture.

3.1.3 Synthesis of the starPEG-MMP cleavable peptide conjugate

The synthesis of matrix metalloproteinase-cleavable peptide (MMP) with a sequence of Ac-CGGPQG-IWGQGGCG and its conjugation with four arms polyethylene glycol (starPEG, Mw= 16,500 g/mol) was performed as previously described [8]. The starPEG-MMP conjugate was used for all the cellular experiments in place of non-cleavable starPEG-SH.

3.2 Physical characterization of hydrogels

3.2.1 Rheological and volume swelling measurements

67 μL of the hydrogel mixture was allowed to polymerize between two hydrophobic coverslips with a diameter of 9 mm to produce free-standing hydrogel discs. After the polymerization, the cover glass was removed, and the hydrogels were scanned using FLA 5100 fluorescent scanner (Fujifilm, Tokyo, Japan) before and after overnight swelling in PBS with excitation 473 nm and an emission filter of 510 nm. The diameter of hydrogels was then determined by analyzing the fluorescence images using the Fiji (ImageJ, NIH). The gel volumetric swelling, Q , was determined by the following equation:

$$Q = \left(\frac{d}{d_0} \right)^3 \quad (1)$$

where d_0 and d are the initial and final diameter of the gel disk, respectively. Subsequently, the storage modulus of the swollen hydrogels was also measured using rotational rheometry with 25 mm parallel plate geometry in an Ares LN2 (TA Instruments, Germany), as previously described [47]. The frequency sweeps were carried out at a shear frequency in the range of 10^{-1} rad s^{-1} to 100 rad s^{-1} with a strain amplitude of 2%. The mean values of the storage modulus were calculated from at least three independent hydrogel samples.

3.3 Protein diffusion studies in hydrogels

3.3.1 Fluorescent protein labeling and purifications

Recombinant human VEGF165, VEGF121, EGF (Peprotech, USA), and SDF1 α (Miltenyi Biotec, Germany) were labeled with Alexa 488 NHS esters (N-hydroxysuccinimide esters) (Thermo Fisher Scientific, Germany). Briefly, lyophilized proteins were dissolved in Milli-Q water, and an equal volume of 0.2 M sodium bicarbonate buffer (pH 8.3) was added to reach a final protein concentration of 0.5-1 mg/mL. The Alexa 488 NHS esters were then added at dye to protein molar ratio of 10:1 and 1.5:1 for a large (VEGF165 and VEGF121) and small proteins (EGF and SDF1 α), respectively. Afterward, the proteins were purified twice from the unreacted dyes using Zeba Desalting column with MWCO of 7 kDa (Thermo Fisher Scientific, Germany) following the manufacturer's instruction. The final concentration of the protein and conjugated dyes were measured using NanoDrop™ 1000 Spectrophotometer (Thermo Fisher Scientific, Germany) to determine the protein labeling degree.

3.3.2 Fluorescence recovery after photobleaching (FRAP)

FRAP measurement was used to evaluate the mobility of proteins within hydrogels or pure buffer. For the sample preparation, all hydrogel components were dissolved in PBS containing 0.1% BSA (**Figure 3.1A**). Fluorescently-labeled proteins were incorporated into the hydrogels during the gelation process. For this, the proteins were mixed with the Hep, 6O-DSH, 6ON-DSH, or starPEG-Mal at a final concentration of 5 μ M. Afterward, the mixture was reacted with starPEG-SH to prepare hydrogel with varied mesh size, heparin content, and

sulfation pattern as described above. To ensure that the diffusion coefficient measurement was carried out within the gel matrix and to specify the bleached spot's location within the scaffold, hydrogels were spiked with 1 mol% of ATTO 647 maleimide (Atto-Tec, Siegen, Germany). For the FRAP measurement, 3 μL of the hydrogel mixture was spread onto a glass slide to generate hydrogel with $\sim 120\ \mu\text{m}$ thickness, covered with 10 μL of buffer solution containing the same concentration of proteins as in the hydrogel, and sandwiched with another cover glass separated by an imaging spacer (Grace Bio-Labs SecureSeal, Sigma-Aldrich). Afterward, FRAP was carried out with a Leica TCS SP5 confocal using a 10x magnification objective (HC PL Fluotar 0.30 NA). For each measurement, a time-series of 20 pre-bleach images with a resolution of 256 x 256 pixels was recorded using an attenuated argon laser beam (80% output & 4% of transmission) every 141 ms (**Figure 3.1B**). A uniform disk with a radius of 20 μm in the middle of hydrogels was then bleached with high intensity of 488, 576, and 495 nm lines of an argon laser at 100% transmission for ~ 600 ms.

Immediately after the photobleaching, a stack of 100 and 120 images was acquired at low laser intensity (4% of transmission) for every 141 ms and 1 s, consecutively, to measure the extent of fluorescent recovery within the bleached spot. During all the experiments, the temperature was kept constant at 30 $^{\circ}\text{C}$. The diffusion coefficients (D) were extracted from the fluorescent recovery curve, as described elsewhere [38, 161]. Briefly, the mean fluorescent intensity in the bleached spot, $I_{\text{frap}}(t)$, was normalized to the intensity of a reference region for every time point t , $I_{\text{ref}}(t)$. $I_{\text{frap}}(t)$ was then normalized further by the intensity of a reference region, $I_{\text{ref}}(\text{pre})$, and the bleached area, $I_{\text{frap}}(\text{pre})$, before the photobleaching, using **Equation 2** to correct for possible bleaching during the image acquisition. Here, $f(t)$ is the normalized fluorescent intensity in the bleached spot.

$$f(t) = \frac{I_{\text{ref}}(\text{pre})}{I_{\text{ref}}(t)} \cdot \frac{I_{\text{frap}}(t)}{I_{\text{frap}}(\text{pre})} \quad (2)$$

Subsequently, $f(t)$ was normalized to a full scale, $F(t)$ using **Equation 3**. Here, $f(0)$ is the normalized fluorescent intensity of the bleached spot just after the bleaching, and $f(\text{pre})$ is the normalized fluorescent intensity before the bleaching.

$$F(t) = \frac{f(t) - f(0)}{f(\text{pre}) - f(0)} \quad (3)$$

Characteristics diffusion time, τ_D and the mobile fraction, a , were then extracted from the least square fit of $F(t)$ to the **Equation 4**, which is based on the 2D diffusion model for a circular spot as described previously by Soumpasis [162] (**Figure 3.1C**):

$$F(t) = a \cdot e^{-\frac{\tau_D}{2t}} \left[I_0\left(\frac{\tau_D}{2t}\right) + I_1\left(\frac{\tau_D}{2t}\right) \right] \quad (4)$$

I_0 and I_1 represent modified Bessel functions of the first kind of zero and first order, respectively. Finally, the diffusion coefficient, D , was obtained from **Equation 5**, where w is the radius of the bleached area.

$$D = \frac{w^2}{\tau_D} \quad (5)$$

To analyze the hydrogels network properties, hydrogels with heparin content of 1.5 mM were prepared in PBS with a molar ratio of starPEG/ heparin varied from 0.63-1.5. Fluorescein isothiocyanate–dextran (FITC-dextran) with different molecular weights (FD10, FD20, FD70, FD150, and FD2000) (Sigma-Aldrich, Germany) was then embedded during the gelation process at a final concentration in the hydrogel of 0.5 mg/mL. Subsequently, the procedures for the FRAP experiments, as described above, were followed.

To quantify the diffusion coefficient of proteins and dextran in the pure buffer, 10 μL of protein and dextran solutions were used at a final concentration of 2.5 μM and 0.5 mg/mL, respectively.

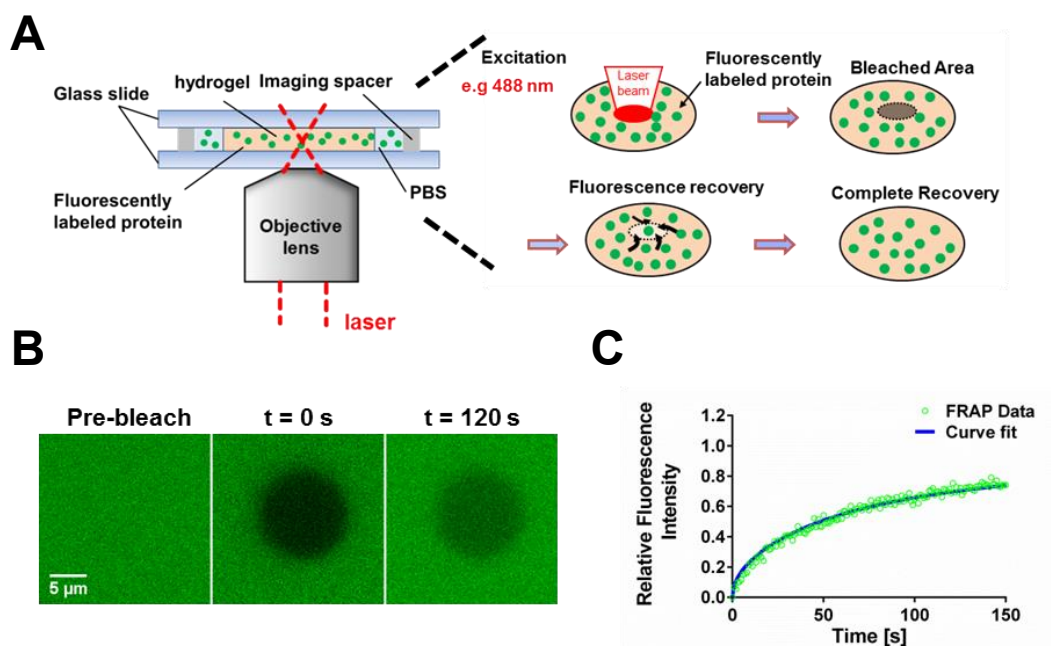


Figure 3.1. FRAP experiment set-up. (A) FRAP sample preparations. The hydrogels were preloaded with proteins, immersed in PBS, and sandwiched in between two glass slides separated by an imaging spacer. In general, the FRAP experiment consists of the photobleaching of protein samples using a high-intensity laser pulse and the monitoring of fluorescence recovery of the bleached spot until no further fluorescence recovery is observed. (B) The changes in the fluorescence inside the bleached spot before and after 120 s of the photobleaching. (C) The fluorescence intensity recovery curve of the bleached spot and the curve fit to a diffusion model for the quantification of a protein diffusion coefficient.

3.3.3 The formation of fluorescent protein gradient in microfluidic devices

As described in detail elsewhere [163], commercially available microfluidic chips were used to generate a biomolecular gradient within hydrogels. The microfluidic device contains three parallel channels, including the growth factor, hydrogel, and medium channels with a wide of 0.5, 1.3, and 0.5 mm, respectively (**Figure 3.2A**). The growth factor and medium channels are separated from the hydrogel channel by trapezoid posts that prevent the hydrogel precursor from leaking out to the medium or growth factor channels during the hydrogel loading. 0.1 mm spacing between the structures allows for the biomolecules' transport/ exchange between the hydrogel channel and the flanking growth factor and medium channels. The chips are designed to have a height of 0.2 mm, allowing the laminar

flow of liquid within the device. Any hydrogel, including the *in situ* forming, starPEG-heparin hydrogels, can be loaded into hydrogel channels by injection.

For the protein gradient characterization, the protein was labeled with Alexa-488 (Please see **section 3.3.1** for the protein labeling procedures), whereas the hydrogel was spiked with 0.1 mol % of ATTO-647. Moreover, for all the experiments involving this microfluidic device, 10 μL of hydrogel precursors were mixed thoroughly by pipetting it within a 500 μL Eppendorf tube. Subsequently, using a 20 μL micropipette, the mixture was injected into the hydrogel inlet until the solution reaches 2/3 of the gel channel length. The remaining solution was injected into the opposite hydrogels channel inlet until the front of the gel precursor was merged. The gels were allowed to polymerize for 5 min, and the gel inlets were then sealed with adhesive plastic sealant. Subsequently, the hydrogel was washed with PBS/ 0.1% BSA by injecting 15 μL of the solution into the growth factor and medium channels.

To initiate the gradient formation, 70 μL of 1 μM of fluorescently labeled protein, which is diluted with PBS/ 0.1% BSA solution, was injected into one of the growth factor channels, and an additional 50 μL of the growth factor solution was loaded from the opposite growth factor inlets. Similarly, a total of 120 μL PBS/ 0.1% BSA solution were loaded into the medium channel, of which 70 μL and 50 μL of the solution were injected from different ports. After adding the protein into the growth factor channel, the net diffusive transport of the protein from the growth factor to the medium channel initiated the formation of a protein gradient (**Figure 3.2B**).

For the time-lapse microscopy, 20 μL of mineral oil (Sigma-Aldrich, Germany) was added onto each medium and growth factor ports to prevent evaporation during the imaging. The fluorescence images were captured using a Leica TCS SP5 confocal (Leica Microsystems, Germany) every 30 min for a total duration of 72 H and subsequently used to analyze the spatial and temporal evolution of protein gradient.

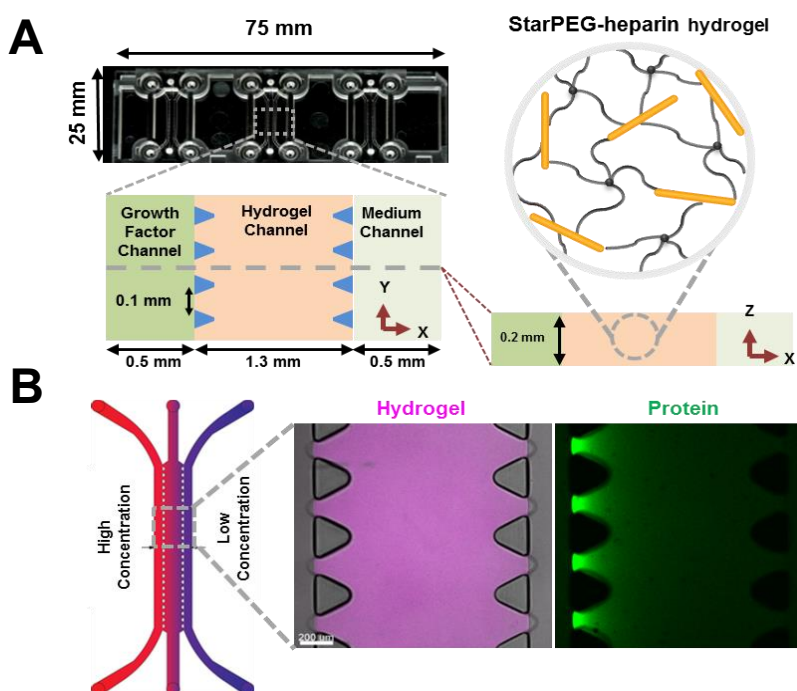


Figure 3.2. Generation of a biomolecular gradient within a microfluidic device. (A) The schematic of the microfluidic device used to generate a protein gradient. (B) The formation of a protein gradient across the loaded hydrogel. The fluorescence image represents the hydrogel and protein gradient formation after 48 H of the protein loading. Scale bar 200 μ m.

3.5 Protein release studies from hydrogels

10 μ l of hydrogels with variable GAG concentration or sulfation degree were loaded with a final protein concentration of 1.5 μ M and allowed to polymerize in 0.5 mL conical microcentrifuge low protein binding tubes LoBind (Eppendorf Tubes, Germany). 400 μ l of the release medium (Dulbecco's Modified Eagle Medium (DMEM; Gibco Life Technologies) supplemented with 0.1% BSA, 0.1% Procline, and 60 mM of HEPES buffer (Gibco Life Technologies) was then added to the samples and incubated at room temperature to initiate the release of protein from hydrogels. Release media was completely removed and exchanged with an equal volume of fresh media at $t = 0.125, 0.25, .5, 1, 3, 6, 24, 96, 168, 264,$ and 336 h. The collected media was split into two aliquots, stored and frozen at -80°C until the analysis. The amount of protein in the release media was quantified using enzyme-linked immunosorbent assay (ELISA) DuoSet kit (R&D Systems, Minneapolis, USA) according to the manufacturer's instructions ($n \geq 6$).

3.6 Cell cultures

Human umbilical vein endothelial cells (HUVECs) were isolated as previously described [164], cultured in Endothelial Cell Growth Medium (ECGM; Promocell, Heidelberg, Germany) containing supplemental mix and 2% FCS on fibronectin-coated 75 cm² culture flasks, and maintained at 5% CO₂ and 37 °C in a humidified incubator. After reaching 80% confluency, the cells were detached using 0.5% trypsin-EDTA (Sigma-Aldrich, München, Germany) solution, collected, centrifuged at 1000 rpm, and reseeded at appropriate density until further usage. Cells from passage 2-6 were used for all experiments.

3.7 *In vitro* assays

3.7.1 Endothelial cell vascular morphogenesis

To investigate the effect of GAG content on the endothelial cell morphogenesis within the binary hydrogel system, HUVECs were embedded within the hydrogels at a final heparin concentration of 0, 500, 1000, and 1500 µM. Besides, hydrogels with varied GAG sulfation patterns (Hep, 6O-DSH, 6ON-DSH) were prepared at a total GAG concentration of 1500 µM to study the influence of GAG sulfation patterns on the endothelial cell capillary morphogenesis. For these purposes, HUVECs were detached using Accutase (Sigma-Aldrich) for 5 min at 37 °C and resuspended in an ECGM medium containing a supplemental mix and 2% FCS at a final concentration of 40 x 10⁶ cells/ml. Next, the starPEG-GAG hydrogels were prepared as described previously [3] with slight modifications.

In brief, a degradable starPEG-MMP conjugate (MW 16,489) and heparin/heparin derivatives-maleimide conjugate (MW 15,000) was dissolved in the HUVEC culture medium. Subsequently, the adhesive peptide CWGGRGDSP (cRGD, MW 990) was supplemented into the heparin at a 2:1 molar ratio. After that, the heparin-RGD mixture was (non-reactively) functionalized with VEGF165 (PeproTech, USA) at a final concentration of 0-20 µg/ml, and an equal volume of HUVEC suspension was then added to generate a cell-heparin conjugate mixture. For the formation of hydrogels, the cell-heparin conjugate mixture was mixed with the starPEG conjugate solution in a 1:1 volume ratio to

form 20 μL of hydrogel droplets, which were cast onto hydrophobic μ -slides 8 well chambers (Ibidi, Germany). Following the *in situ* crosslinking, the gels were immediately immersed in the cell culture medium, and on day 3, the samples were fixed with 2% paraformaldehyde (PFA) for 10 min at RT and stained with fluorescence.

For the spatial patterning of endothelial cell morphogenesis in microfluidic chips, hydrogels and the growth factor were loaded into the device as described before in **section 3.3.3**. The final cell concentration within the hydrogel was adjusted to 10×10^6 cells/ml. The cells within the device were treated with 5 $\mu\text{g/mL}$ of VEGF dissolved in basal medium (ECGM containing 0.5% FBS) either as a gradient or uniformly distributed within the hydrogels. The cells treated with the basal medium was included as a control. The progress of morphogenesis was then observed daily, and on day 3, the cells were fixed with 2% PFA and stained with the fluorescence.

3.7.2 Endothelial cell chemotaxis

HUVECs chemotaxis assay was performed on μ -Slide Chemotaxis (Ibidi, Germany). This slide has been previously used for a long-term chemotaxis assay of various cells, including the immune cells, fibroblasts, and cancer cells under a two-dimensional (2D) or three-dimensional (3D) environment [165]. μ -Slide Chemotaxis contains three main chambers: observation and two large reservoirs area (**Figure 3.3**). The observation area is filled with the cell-laden hydrogels precursors, and the reservoir area can be filled with a cell culture medium only or in combination with a chemoattractant. Here, the effect of the VEGF gradient on the chemotaxis of HUVECs in 3D was investigated. Two other conditions where the hydrogels were not loaded with VEGF or uniformly loaded with VEGF were used as a control. For this purpose, cells were encapsulated within the hydrogels as described previously in **section 3.7.1** except that all hydrogel components were dissolved in basal medium (ECGM supplemented with 0.5% FBS), and the heparin concentration in the hydrogel was fixed at 500 μM . The observation channel was filled with 6 μL of hydrogel precursors, whereas the reservoir was

3. MATERIALS AND METHODS

filled with 65 μ L of medium with or without VEGF supplementation. No VEGF was added in the hydrogel or the reservoir chamber for the untreated control group, and all other compartments were filled up with the basal medium. For the gradient treated group, 5 μ g/mL of VEGF was supplied at one of the reservoir chambers, while the other reservoir chamber was filled with the basal medium only. On the other hand, for the treatment with a uniform VEGF distribution, VEGF was preloaded within the hydrogel during the gelation process, and no additional VEGF was supplied into the reservoir chambers.

Next, a live cell imaging was performed under 10x objective (HC PL Fluotar 0.30 NA) using a bright field imaging mode of a Leica TCS SP5 confocal (Leica Microsystems, Germany) equipped with a humidifier and CO₂ incubation. The image was captured every 15 min for up to 24 H. The XY coordinate of the cells for a particular field of view was extracted using manual tracking of Image J software. The cell migration parameters such as forward migration index (FMI), directness, accumulated distance, and the net migration distance between 6 and 16 hours were then analyzed using IBIDI chemotaxis and migration tool software. The directed cell migration was considered to be statistically significant if the FMI parallel to the direction of the gradient (FMI^{||}) is larger than the FMI perpendicular to the direction of the gradient (FMI[⊥]) and the p-value, $P < 0.05$ or if the FMI^{||} and FMI[⊥] of the control group are around zero and the p-value, $P > 0.05$.

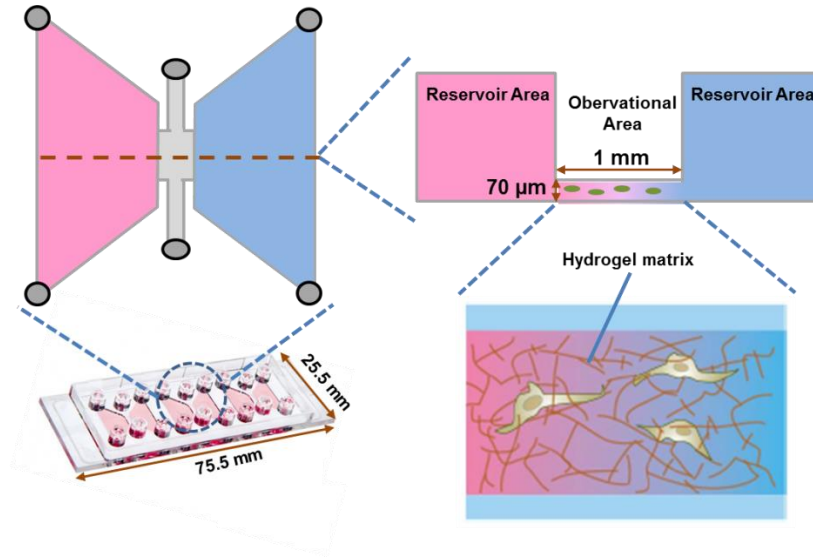


Figure 3.3. Schematic of μ -Slide Chemotaxis design for HUVECs chemotaxis assay. The cells are embedded within the hydrogel for the 3D cell migration experiment.

3.8 COMSOL mathematical modeling and simulation

A reaction diffusion-model was used to simulate the protein transport dynamics within GAG-based hydrogels. Notably, the model was applied to determine the concentration of free and bound protein within a hydrogel droplet, predict the protein release from hydrogels loaded within a conical microcentrifuge tube, and estimate the spatial and temporal changes of hydrogel-based protein gradients. Initially, this model was established by Crank [166] to describe the mass transport in an affinity-based controlled release system based on a simple binding kinetics and Fick's laws of diffusion. A similar model has also been adapted and successfully applied in a peptide-based [52] and metal chelating affinity hydrogels [129] to model the release of recombinant proteins from the polymer networks.

The binding ligand (GAG or GAG derivatives) in our system is covalently tethered within the hydrogel. Therefore, the freely diffusing protein is the only mobile fraction in the system. The protein reversibly binds to the GAG to form an immobilized protein-GAG complex, dissociate and diffuse through the hydrogel matrix. The equilibrium dissociation constant (K_D) (**Equation 6**) is expressed as the ratio between the dissociation rate constant (k_d) and the association rate constant (k_a); the value determines the strength of affinity interaction between

3. MATERIALS AND METHODS

protein and GAGs that eventually govern the protein mobility within- and the subsequent release from the scaffold.

$$K_D = \frac{k_d}{k_a} = \frac{C_P C_G}{C_{PG}} \quad (6)$$

Here, C_P is the concentration of free protein, C_G is the concentration of GAG and C_{PG} is the concentration of protein-GAG complexes. The diffusion coefficient of protein within the hydrogels (D_{gel}) and release media (D_{med}) were determined using FRAP, as described in **section 3.3.2**. In this case, the diffusion coefficient of affine-proteins within affine gel systems (GAG-containing hydrogels) was approximated by measuring the protein's diffusion within a non-affine PEG-PEG gel with a comparable stiffness. On the contrary, the diffusion constant of non-affine proteins was measured directly within the affine hydrogel systems.

The initial equilibrium concentration of free protein, GAG, and protein-GAG complexes within the hydrogel was determined according to the equations described as follows [167]:

First, the equilibrium dissociation constant (**Equation 7**) can be rearranged to:

$$C_P C_G = K_D C_{PG} \quad (7)$$

At equilibrium, the free protein and GAG concentration can be calculated by:

$$C_P = C_{P_Total} - C_{PG} \text{ and } C_G = C_{G_Total} - C_{PG} \quad (8)$$

Here, C_{P_Total} and C_{G_Total} are the initial protein and GAG loading concentrations in the gel precursors. Next, these equations were substituted into **Equation 7** and rearranged to solve for C_{PG} giving rise to:

$$C_{PG} = \frac{(C_{P_Total} + C_{G_Total} + K_D)}{2} - \sqrt{\frac{(C_{P_Total} + C_{G_Total} + K_D)^2}{4} - C_{P_Total}C_{G_Total}} \quad (9)$$

Conversely, free protein concentration can also be defined as:

$$C_P = C_{P_Total} - \frac{(C_{P_Total} + C_{G_Total} + K_D)}{2} + \sqrt{\frac{(C_{P_Total} + C_{G_Total} + K_D)^2}{4} - C_{P_Total}C_{G_Total}} \quad (10)$$

Afterward, a set of partial differential equations (**Equation 11-14**) was used to describes the diffusive transport and formation/ dissociation of protein-GAG complexes in the hydrogel (**Equations 11–13**) as well as the diffusive transport in the release media (**Equation 14**).

Here, the change in the free protein concentration overtime happened as a result of association and dissociation from GAG, and the diffusion within the hydrogel matrix is described as

$$\frac{\partial C_P}{\partial t} = D_{gel} \nabla^2 C_P - k_a C_P C_G + k_d C_{PG} \quad (11)$$

Similarly, the change in concentration of protein-GAG complexes overtime in the hydrogels was defined by

$$\frac{\partial C_{PG}}{\partial t} = k_a C_P C_G - k_d C_{PG} \quad (12)$$

Furthermore, the change in the free GAG concentration over time was expressed as

$$\frac{\partial C_G}{\partial t} = -k_a C_P C_G + k_d C_{PG} \quad (13)$$

Finally, the change in the protein concentration in the release medium due to the diffusion is given by

$$\frac{\partial C_P}{\partial t} = D_{med} \nabla^2 C_P \quad (14)$$

These equations were solved numerically using COMSOL Multiphysics 5.3a for different gel types and geometry as well as protein loading concentration. The dissociation rate constant of the model proteins from the heparin obtained from the literature was used as a starting point for the curve fitting to the experimental release of heparin-affine proteins. The best fit was obtained using the least-square method by systematic variation of K_D . In general, the reaction-diffusion model was used to describe molecular transport in all simulations. Variations in the assumptions and parameters of the numerical simulations and details about the hydrogel geometry will be addressed, specifically in **section 6.1.6**. Besides, all the parameters required to generate each figure containing the simulation results are summarized in **Table 6.1**.

3.9 Microscopy techniques and image analysis

3.9.1 Fluorescence staining and immunocytochemistry

To analyze the extent of tubular structure formation in a hydrogel. After fixation and washing with PBS, the samples were permeabilized using 0.1% TritonX-100 for 10 min. Samples were washed and incubated with Hoechst 33342 (Life Technologies; 1:200) and ATTO 610-phalloidin (Atto-Tec, 1:200) for two days at 4 °C. Next, the samples were washed three times and stored in PBS at 4 °C, covered with foil until the imaging using a Dragonfly Spinning Disc confocal microscope (Andor Technology Ltd., Belfast, UK). At least three images were taken at different positions within each hydrogel sample. Fields for imaging and quantification were chosen randomly for all conditions.

3.9.2 Image analysis

To quantify the extent of tubular structure formation in 3D, 100 μm thick z-stacks of 5 μm intervals at 50 μm above the glass slide were analyzed with Imaris (Version 9.2.1, Bitplane AG, Zurich, Switzerland) utilizing a filament tracer module. Briefly, a threshold loops algorithm was used to generate a 3D skeletonized image of the tubular structures obtained from the phalloidin staining. All the creation parameters used for the fluorescent image segmentation are listed in **Table 6.2**. Next, the resulting skeletonized images were used to calculate the total area and number of branch points of vasculatures. The skeletonized images were then visualized as a cone with a scale of 0.5.

3.10 Statistical analysis

All experiments were carried out with 2-3 independent experiments. Statistical analysis and graphing were performed using the GraphPad Prism 6 (San Diego, California). A one-way analysis of variance (ANOVA) followed by Tukey's multiple comparison post-hoc test was used to determine the significance level between the groups with different treatments. All values represent the mean \pm standard deviation for at least three independent samples. The difference between the means was considered to be statistically significant at the level of $P < 0.05$.

4. Results and discussion

4.1. Molecular transport of signaling molecules in the binary GAG-based hydrogel systems

4.1.1 Introduction

Soluble signaling molecules such as growth factors (GFs) and cytokines regulate many biological processes, including cell proliferation, survival, differentiation, and migration [168, 169]. Therefore, understanding the molecular transport of signaling molecules, in particular, within cell-instructive polymer networks, such as hydrogels, is critically important for the rational design of engineered living matters [170]. The mobility of bioactive proteins within- and the subsequent release from the hydrogel may not only affect the activity of the cells within the scaffold but also determine the host responses at the site of implantation [9-13]. For these reasons, several attempts to control the diffusivity of proteins within hydrogels have been made, including the incorporation of glycosaminoglycans (GAGs) [7, 10, 16, 25, 171, 172]. Owing to its negative charge, GAGs mainly sequester a wide range of positively charged proteins through electrostatic interaction, enabling the applications of GAG-based materials for controlled growth factor release [5], cytokines sequestration [7], and 3D cell culture [3, 153-155, 173, 174].

The mobility of signaling molecules within the polymeric biomaterials is controlled at the molecular level through its network properties. In general, the diffusivity of signaling molecules across the polymer networks is governed by the hydrogel mesh size. For the GAG-based hydrogels, the diffusion of such molecules is further affected by their binding to the gel matrix, which is primarily determined by the GAG volume density and affinity to the signaling molecules [28]. However, despite their critical roles, no studies have systematically reported the influence of different physical and biochemical parameters of the hydrogels on the mobility of embedded signaling molecules. The gained knowledge eventually can be essential for creating GAG hydrogels with a defined local growth factor

concentration that could precisely modulate cell fates through the soluble factor-mediated cell signaling.

Mathematical modeling can facilitate the development and design of biomaterials for controlled delivery of growth factors/ cytokines from affinity-based delivery systems [52, 113, 129, 175-177], including GAG-containing matrices [32, 61, 178]. However, most models developed so far have mainly investigated the role of affinity interaction between the proteins and affinity ligand while minimally taking into account the effect of steric interaction between the protein and hydrogels network [52]. Moreover, most of the models were developed based on ECM-derived matrices, which promiscuously bind to a diverse range of signaling molecules [34, 53, 61, 178-181] and suffer from a batch to batch variability, limiting the accuracy of the model prediction under various scenarios. Consequently, GAG-based biohybrid hydrogels with a fully defined composition and tunable biophysical and biochemical properties may be instrumental for studying the impact of the material properties on the transport of signaling molecules.

We have previously developed an *in situ* forming, cell-instructive, biohybrid starPEG-heparin hydrogel system based on a bio-orthogonal Michael-type addition reaction [22]. The system's mechanical and biochemical properties can be decoupled, allowing one to study the impact of different hydrogel network parameters on the cell fate control independently [22, 50, 66]. In the present work, we aimed to elucidate the effect of mesh size, heparin concentration, and heparin sulfation pattern of the system upon the mobility of signaling proteins with varying molecular size and affinity to heparin. Moreover, we also developed a mathematical model based on a reaction-diffusion model to analyze the transport and release of embedded signaling molecules from the polymer networks.

Herein, the binding of four relevant growth factors and cytokines, including EGF, SDF-1 α , VEGF121, and VEGF165 to the GAG building blocks of the hydrogels were first characterized using microscale thermophoresis (MST) [182] (**Section 6.2.1**). Subsequently, after the establishment of fluorescent recovery after photobleaching (FRAP) technique to measure the diffusivity of proteins within the

hydrogel samples or pure buffer [183] (**Section 6.2.2**), the mobility of proteins within a set of hydrogels with various properties was systematically investigated. The effective diffusion coefficient of the model proteins in hydrogels with varied sulfation degree derived from the FRAP analysis was then validated with the experimental release. Afterward, a reaction-diffusion model was developed and applied to predict the release of heparin affine proteins (VEGF165 and SDF1 α) from the gel constructs (**Section 3.3.8 & 6.1.4**). Finally, the sensitivity analysis of different model parameters, including the GAG content and affinity to signaling molecules, on the VEGF165 release from the hydrogels was performed to understand the global transport phenomena of signaling molecules within GAG-based materials.

4.1.2 Protein mobility in GAG-based hydrogels

4.1.2.1 Effect of protein physical sizes and affinity to GAG

Four model proteins were chosen to represent small and large signaling molecules with a strong affinity to heparin (SDF1 α and VEGF165) and no affinity to heparin (EGF and VEGF121). The affinity of SDF1 α and VEGF165 to heparin derivative was first confirmed by MST analysis (**Section 6.2.1**). Despite the difference in their molecular size, both proteins displayed a comparable affinity (K_D) to heparin (0.9 and 1.2 μ M for SDF1 α and VEGF165, respectively) (**Figure 4.1A**).

To fully characterize the effect of protein size on their mobility within the hydrogels, we analyzed the protein diffusivity in solutions as well as in non-affine PEG/PEG gels and affine PEG/Hep gels. The storage modulus of these hydrogels was adjusted to be comparable to exclude the influence of steric interaction with the hydrogel network (**Figure 4.1B**). FRAP analysis revealed that the mobility of proteins in solutions was inversely proportional to their molecular weight (**Figure 4.1C**), similar to the mobility of VEGF pair (VEGF165 vs. VEGF121) in a pure PEG hydrogel. Surprisingly, the SDF1 α diffused faster than the EGF in the non-affine PEG gels despite the slightly larger physical size (8 kDa vs. 6.2 kDa, for SDF1 α and EGF, respectively). The discrepancy could probably be attributed to the differences in the overall shape and compaction of their 3D structures.

4. RESULTS AND DISCUSSION

The diffusion of model proteins in an affine PEG/Hep hydrogel displayed an opposite trend as those in pure PEG/PEG systems. The mobility of small and large affine proteins (SDF1 α vs. VEGF165) within the affine PEG/Hep hydrogel was quite similar ($D = 4 \mu\text{m}^2/\text{s}$). In contrast, the in-gel diffusivity of the non-affine proteins within the affine hydrogel was affected by their molecular size. Similar to their diffusion in the non-affine gel, small non-affine EGF diffused through the hydrogel network faster than the larger non-affine VEGF121 with the diffusion coefficient of ~ 60 and $20 \mu\text{m}^2/\text{s}$, respectively.

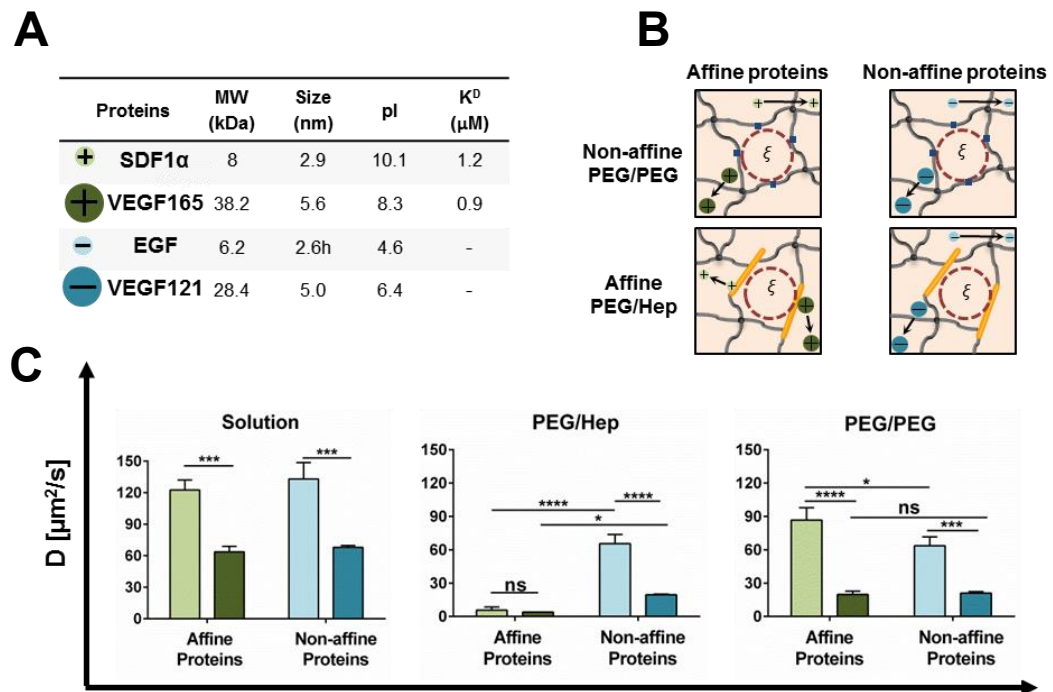


Figure 4.1. Effect of protein physical size and affinity to GAG on the mobility of proteins. (A) Physicochemical properties of the model proteins used in this study. The mobility of model proteins in an affine PEG/Hep and non-affine PEG/PEG hydrogel with a comparable stiffness/ mesh size was evaluated using FRAP. (B) A pictogram illustrating the effect of protein size and affinity to GAG on their mobility within PEG/Hep and PEG/PEG hydrogels, which are mostly affected by the electrostatic interaction between the protein and the GAG building block. (C) The diffusion coefficient (D) of the model proteins in solution or hydrogels as determined by FRAP. Data represents mean \pm SD ($n = 3$), 'ns' stands for not significant, * $P < 0.5$, *** $P < 0.001$, **** $P < 0.0001$.

4.1.2.2 Effect of hydrogel mesh size

The hydrogels' mesh size can be tailored to regulate the transport of embedded signaling molecules [8, 16]. Since the stiffness of hydrogel is correlated to the mesh size, we varied the stiffness of the gels by adjusting the molar ratio of starPEG to heparin while keeping the heparin content constant to investigate the effect of hydrogel mesh size on the mobility of signaling molecules independently from their heparin content (**Figure 4.2A-B**). This rational design strategy was previously shown to allow for decoupling the effect of starPEG-Hep hydrogel mechanical properties from the biomolecular characteristics [47].

It is hypothesized that decreasing the mesh size of hydrogels could increase the steric interaction between the free proteins and the hydrogel network, therefore slowing their mobility within the gel matrix (**Figure 4.2A**). Three different hydrogels with stiffness varied from ~0.2-6 kPa were generated while keeping the gel heparin concentration around 1500 μM . Based on the rubber elasticity theory [2], this range of stiffness corresponds to the gel mesh size of 9-28 nm (**Figure 4.2B and section 6.2.3**), which is significantly larger than the hydrodynamic diameter of the model proteins used in this study (**Figure 4.1A**).

FRAP analysis showed that small or large heparin-affine proteins' mobility was not affected by the hydrogel mesh size. The diffusion coefficient of SDF1 α and VEGF165 in the starPEG-heparin system was quite similar; each fell within the range of 4 $\mu\text{m}^2/\text{s}$ (**Figure 4.2C**). In contrast, the diffusivity of non-affine proteins (EGF and VEGF121) was influenced by hydrogel mesh size. It was shown that the effect of mesh size was more pronounced on the protein mobility of VEGF121 than for the smaller EGF. Accordingly, the increase in the mesh size of hydrogel from 9 to 11 nm significantly raised the diffusivity of the VEGF121 by ~ 30%. In contrast, the diffusivity of EGF only increased by ~ 20% if the mesh size of hydrogel was enlarged to ~ 28 nm. Probably, the VEGF121 experienced a stronger steric hindrance in the hydrogel network due to the larger size, even with a slight decrease in the mesh size of hydrogels.

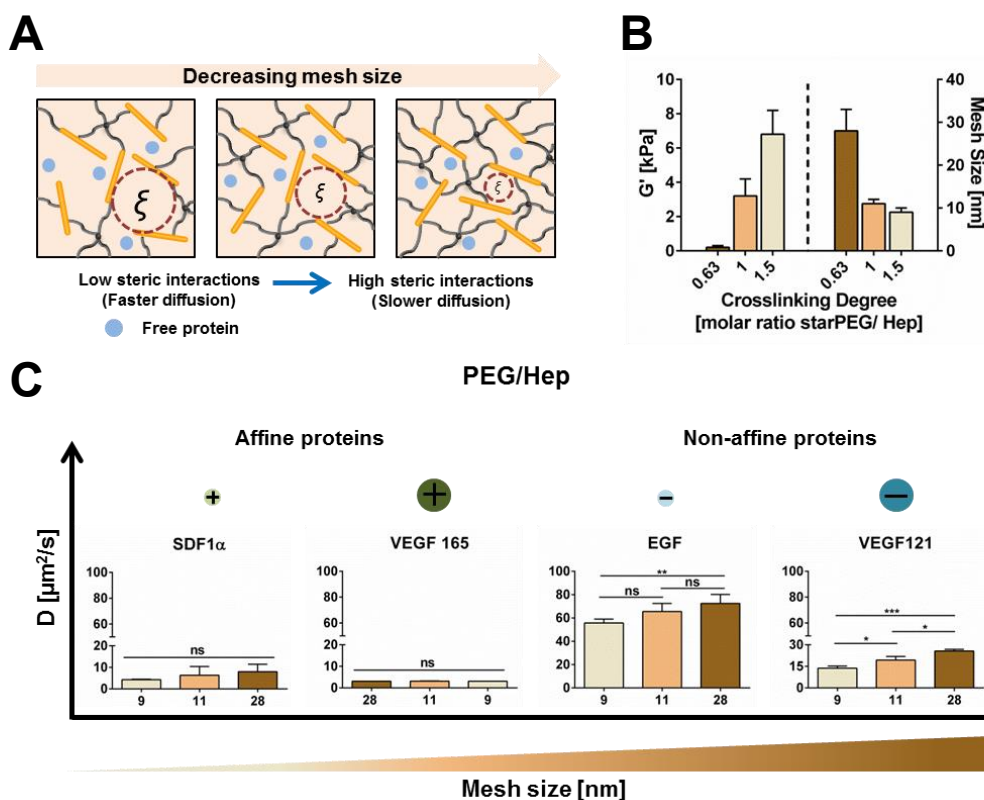


Figure 4.2. Effects of hydrogel mesh size on the mobility of proteins. The mobility of model proteins in PEG/Hep hydrogels at a pre-defined crosslinking degree with an overall GAG concentration of 1500 μM . (A) A pictogram illustrating the effect of adjusting the mesh size of hydrogel on the steric interaction between the free protein and the hydrogel network, which negatively correlates to the in-gel mobility. (B) Tunable mechanical properties/ mesh size of hydrogels can be obtained by varying the molar ratio of starPEG to heparin. (C) The diffusion coefficient (D) of the model proteins in hydrogels as determined by FRAP. Data represents mean \pm SD ($n = 3$), 'ns' stands for not significant, *P<0.5, **P<0.01, ***P<0.001.

4.1.2.3 Effect of GAG concentration

starPEG-GAG hydrogels containing fully sulfated heparin were used as a model system to investigate the effect of overall GAG concentration on signaling molecules' mobility. As previously described, the gel system could maintain a constant heparin content of approximately 1500 μM independent of their stiffness [47]. However, based on our rational design strategies, the overall solid content, crosslinking degree, and GAG building block can be adjusted further to prepare hydrogel variants with tunable biochemical characteristics (GAG content/ sulfation degrees) of comparable mechanical properties [47] (**Figure 4.3A**). As

shown in **Figure 4.3B**, the hydrogel with variable heparin content and pure PEG gel control can be produced with overall stiffness of ~ 200 Pa. With this storage modulus, the hydrogels were estimated to have a mesh size of about 30 nm, which is significantly larger than the hydrodynamic radius of proteins used in this study (**Figure 4.1A**). It is hypothesized that decreasing the hydrogel's GAG content could increase the free protein fraction within the system. Therefore, it could enhance the overall mobility of signaling proteins within the hydrogel.

Based on our FRAP analysis, we showed that the inclusion of heparin into the hydrogel could significantly lower the mobility of heparin affine proteins (**Figure 4.3C**). The diffusivity of the SDF1 α significantly decreased from $\sim 80 \mu\text{m}^2/\text{s}$ in pure PEG/PEG system to $\sim 15 \mu\text{m}^2/\text{s}$ or lower (≤ 5 factors) in the heparin-containing hydrogels. A similar trend was also observed for the VEGF165; the mobility of the protein in PEG/Hep hydrogel with the lowest heparin content decreased by approximately 40% compared to the PEG/PEG hydrogel. Although VEGF165 and SDF1 α displayed a comparable affinity toward heparin, the mobility of VEGF165 declined to a less extent than SDF1 α in the PEG/Hep hydrogel. This observation could have resulted from its higher molecular weight that already exerts a more substantial steric interaction with the hydrogel network.

While gradually adjusting the heparin content of the PEG/Hep hydrogels further from 500 to 1500 μM could still significantly decreased the mobility of heparin affine proteins, the mobility of small or large non-affine proteins (EGF and VEGF121, respectively) was not affected. The diffusivity of non-affine proteins within the hydrogels was comparable despite the variation in the heparin content, and the magnitude was inversely correlated to their molecular size (~ 20 and $60 \mu\text{m}^2/\text{s}$, for large and small non-affine proteins, respectively). This result suggested that the mesh size of the hydrogels was comparable. Thus, a similar extent of size filtering effects controlled the mobility of these proteins.

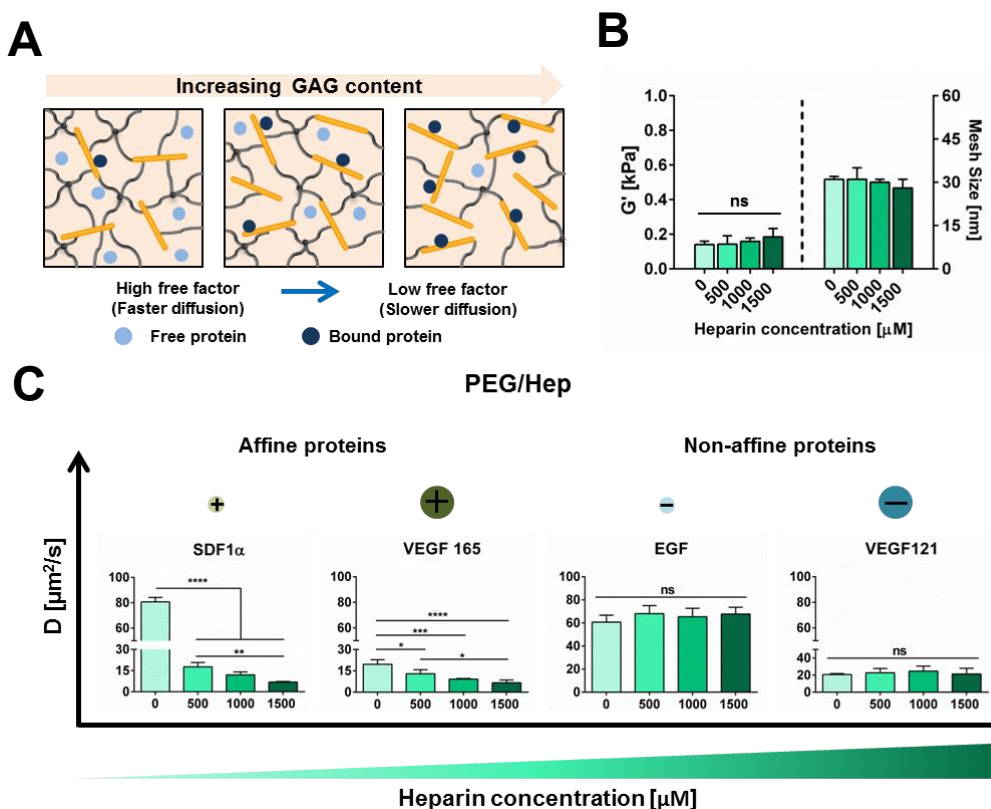


Figure 4.3. Effect of GAG concentration on the mobility of proteins. The mobility of model proteins in PEG/Hep hydrogels with a total GAG concentration of 0, 500, 1000, and 1500 μ M. (A) A pictogram illustrating the effect of tuning the GAG concentration of hydrogels on the free protein concentration, which positively correlates with the in-gel mobility. (B) Comparable mechanical properties/ mesh size of the hydrogels with variable GAG content. (C) The diffusion coefficient (D) of model proteins in the hydrogels as determined by FRAP. Data are presented as mean \pm SD (n = 3), 'ns' stands for not significant, *P<0.5, **P<0.01, ***P<0.001, ****P<0.0001

4.1.2.4 Effect of GAG-sulfation pattern

Next, we investigated the mobility of signaling molecules within the hydrogels with varied GAG sulfation patterns. Heparin was selectively desulfated at the 6-O- (6O-DSH), or both at the N-, and 6-O- (6ON-DSH) positions and functionalized with maleimide moieties to produce heparin derivatives which are reactive toward thiol-functionalized starPEG [38] (**Figure 4.4A**). The hydrogels with variable sulfate content of \sim 100% (PEG/Hep), 67% (PEG/6O-DSH), and 33% (PEG/6ON-DSH) relative to the fully sulfated heparin can be produced with a comparable stiffness of \sim 250 Pa, allowing us to decouple the impact of GAG sulfation from the gel matrix stiffness on the transport of signaling molecules

(**Figure 4.4B**). As described in **section 6.2.1**, heparin-binding proteins' affinity to heparin was regulated in a sulfation-dependent fashion with a declining affinity toward decreasing the sulfation degree of heparin. Therefore, we expected that lowering the heparin sulfation degree could enhance the amount of free protein within the hydrogel, increasing their effective diffusion coefficient.

In general, the diffusivity of non-affine proteins (EGF and VEGF121) within the hydrogels was not affected by the GAG sulfate content, and the diffusion rate was controlled primarily by the molecular weight (**Figure 4.4C**). Accordingly, the larger VEGF121 diffused with a diffusion coefficient of $\sim 18 \mu\text{m}^2/\text{s}$ while the smaller EGF diffused at a faster rate of $60 \mu\text{m}^2/\text{s}$ in all hydrogel types tested, confirming the similarity of the mesh size of hydrogels with a variable of GAG sulfation patterns.

While non-affine proteins' mobility was not dependent on the heparin sulfation patterns, the mobility of heparin affine proteins was inversely correlated to the GAG sulfate content (**Figure 4.4C**). However, a specific sulfate group of heparin seems to have a more noticeable impact on a given heparin-affine protein's mobility. For instance, the diffusivity of SDF1 α significantly declined from $\sim 30 \mu\text{m}^2/\text{s}$ in PEG/6ON-DSH hydrogel to $\sim 9 \mu\text{m}^2/\text{s}$ in PEG/6O-DSH, suggesting the critical role of N- sulfate group for the SDF1 α binding to heparin. Although we saw a lower diffusion coefficient of the SDF1 α in PEG/Hep compared to that in the PEG/6O-DSH gel, no significant difference was observed. Interestingly, the influence of 6O and N sulfate on the mobility of VEGF165 showed the opposite trends as those on the SDF1 α . VEGF165 diffused nearly 3-fold faster in PEG/6O-DSH gel than in the PEG/Hep gel. Moreover, the VEGF165 diffusivity in PEG/6ON-DSH gel behaved similarly to that in the PEG/6O-DSH hydrogel.

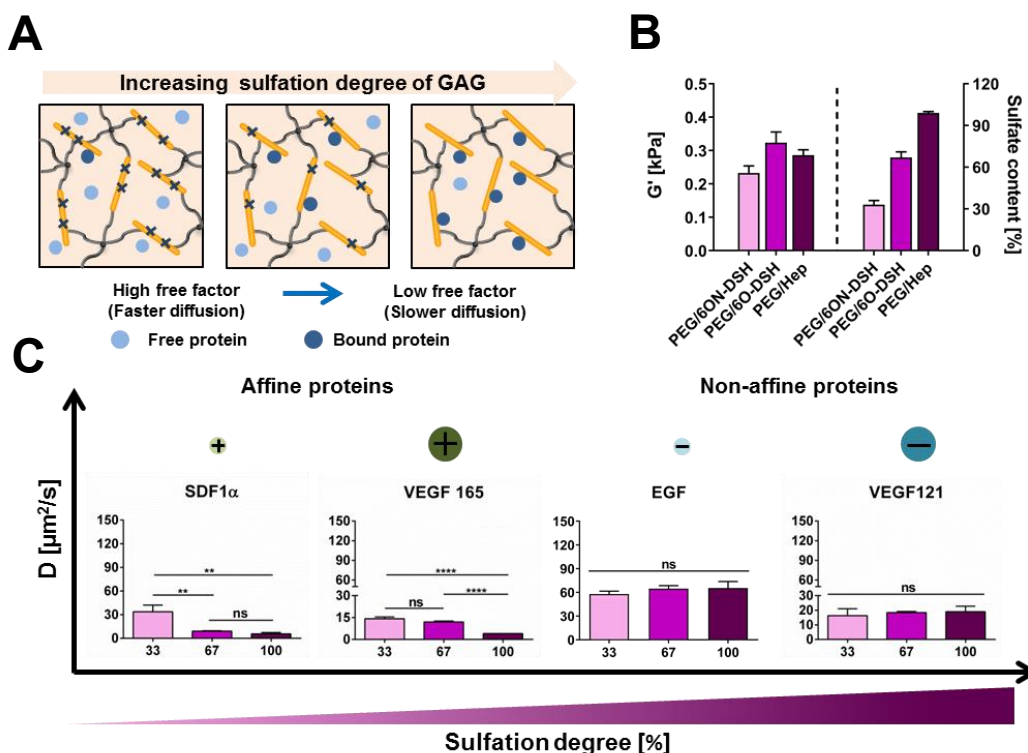


Figure 4.4. Effect of GAG sulfation pattern on the mobility of proteins. The mobility of model proteins in PEG/6ON-DSH, PEG/6O-DSH, and PEG/Hep hydrogels with an overall GAG concentration of 1500 μM . (A) A pictogram illustrating the effect of tuning the sulfation pattern of the GAG building block on the free protein concentration, which positively correlates with the in-gel mobility of the proteins. (B) Comparable mechanical properties of hydrogels with variable sulfation pattern and the respective theoretical sulfate content relative to the PEG/Hep hydrogel. (C) The diffusion coefficient (D) of the model proteins in the hydrogels as determined by the FRAP. Data are presented as mean \pm SD ($n = 3$), ‘ns’ stands for not significant, * $P < 0.5$, ** $P < 0.01$, **** $P < 0.0001$.

4.1.3 Protein release from GAG-based hydrogels

The release of model proteins from a set of GAG hydrogels with varied overall sulfate content (PEG/Hep, PEG/6ON-DSH, PEG/PEG) was investigated. Subsequently, the experimental release profiles of the proteins were fitted to a mathematical model, which is based on the reaction-diffusion model to obtain their translational diffusion coefficient within the hydrogel network. Here, the resulting diffusion coefficient is called an effective diffusion coefficient because it considers the binding and unbinding of the proteins to (from) the hydrogel network during its translational motion [166, 184]. Consequently, the value is

comparable to the diffusion coefficient obtained from the FRAP experiments. As described previously in **section 4.1.2.4**, PEG/Hep and PEG/6ON-DSH hydrogels were expected to have an approximately 100% and 33% sulfation degree, respectively. In addition to this, the PEG/PEG gel containing no sulfate was used as a control. Together, all the gel variants could represent GAG-based matrices with variable affinity to soluble signaling molecules.

The release of SDF1 α , VEGF165, EGF, and VEGF121 from the hydrogels was analyzed throughout 360 H (**Figure 4.5, left panel**). Depending on their sulfate content, all hydrogels showed an initial burst release of heparin affine proteins within the first 24 H, followed by nearly constant slow linear release throughout 360 H (**Figure 4.5A-B**). The release of VEGF165 and SDF1 α from the hydrogels with the highest sulfate content only reached almost 1% of the initially loaded amounts even after two weeks, indicating the proteins' strong affinity to the hydrogel scaffold. Decreasing hydrogels' sulfate content to 33% (PEG/6ON-DSH) enhanced the affine proteins' release by almost two factors, independent from their physical sizes, suggesting the important role of negatively charged sulfate groups for the binding of proteins to the GAG backbones. Remarkably, even if the remaining sulfate content of the PEG/6ON-DSH hydrogel was already as low as 33%, the overall protein release from this gel was still relatively low ($\leq 5\%$). The considerably higher GAG concentration than the protein loading amount in this gel matrix (1500 μM vs. 2.5 μM) might counteract the impact of its reduced affinity on the protein release, allowing them to still behave as a molecular sink of cationic proteins.

Moreover, the release rate of small or large affine proteins from the pure PEG/PEG system was significantly much higher than from the GAG-containing hydrogels, with nearly 70% of the protein released was observed after 48 H. Notably, the release of both affine and non-affine proteins from the PEG/PEG hydrogels never reaches 100%, even up to two weeks of the release studies, despite the protein repellant properties (**Figure 4.5A-D**).

While the affine-proteins displayed a low release from the PEG/HEP or the PEG/6ON-DSH hydrogels after 360 H, the release of non-affine proteins (EGF

and VEGF121) was quite similar for all examined hydrogel formulations (**Figure 4.5C-D**). Like the release of affine proteins from the PEG/PEG hydrogels, the non-affine protein attained a maximum release close to 60% of the initial loading amount within 48 H in any hydrogel types tested. This result could be explained by the absence of electrostatic interaction between the proteins and hydrogel building blocks. Therefore, the proteins only experienced a hindered diffusion caused by the hydrogel network, which only delays their release for a short period [16].

The release experiments are generally accepted as the gold standard and most available methods to compare biomolecules' transport in different gel systems. For this reason, we compared the effective diffusion coefficient of proteins in the hydrogels obtained from the FRAP with those from the experimental release (**Section 4.1.2.3-4** and **Figure 4.5**). For all cases, the obtained values from release experiments were almost twice as high as ones from the FRAP measurements. However, similar trends in the diffusion coefficient of the proteins in different gel formulations were obtained from both methods. While the diffusivity of heparin-affine proteins declined as the hydrogel's sulfate content decreases, the non-affine protein diffusion remained constant irrespective of the hydrogel sulfate composition. Also, similar to the trends obtained from the FRAP measurements (**Figure 4.1.2.1**), the impact of protein size and affinity on their mobility within the hydrogel can also be determined using the diffusion coefficients derived from the release studies. Small and affine protein (SDF1 α) diffused faster than large and affine protein (VEGF165) in the non-affine gel system (PEG/PEG), while their diffusivity was quite similar in the GAG-containing hydrogels (PEG/Hep or PEG/6ON-DSH). Besides, small non-affine proteins (EGF & VEGF121) were also observed to diffuse much faster than the bigger counterpart in all hydrogels tested (**Figure 4.5C-D, right panel**).

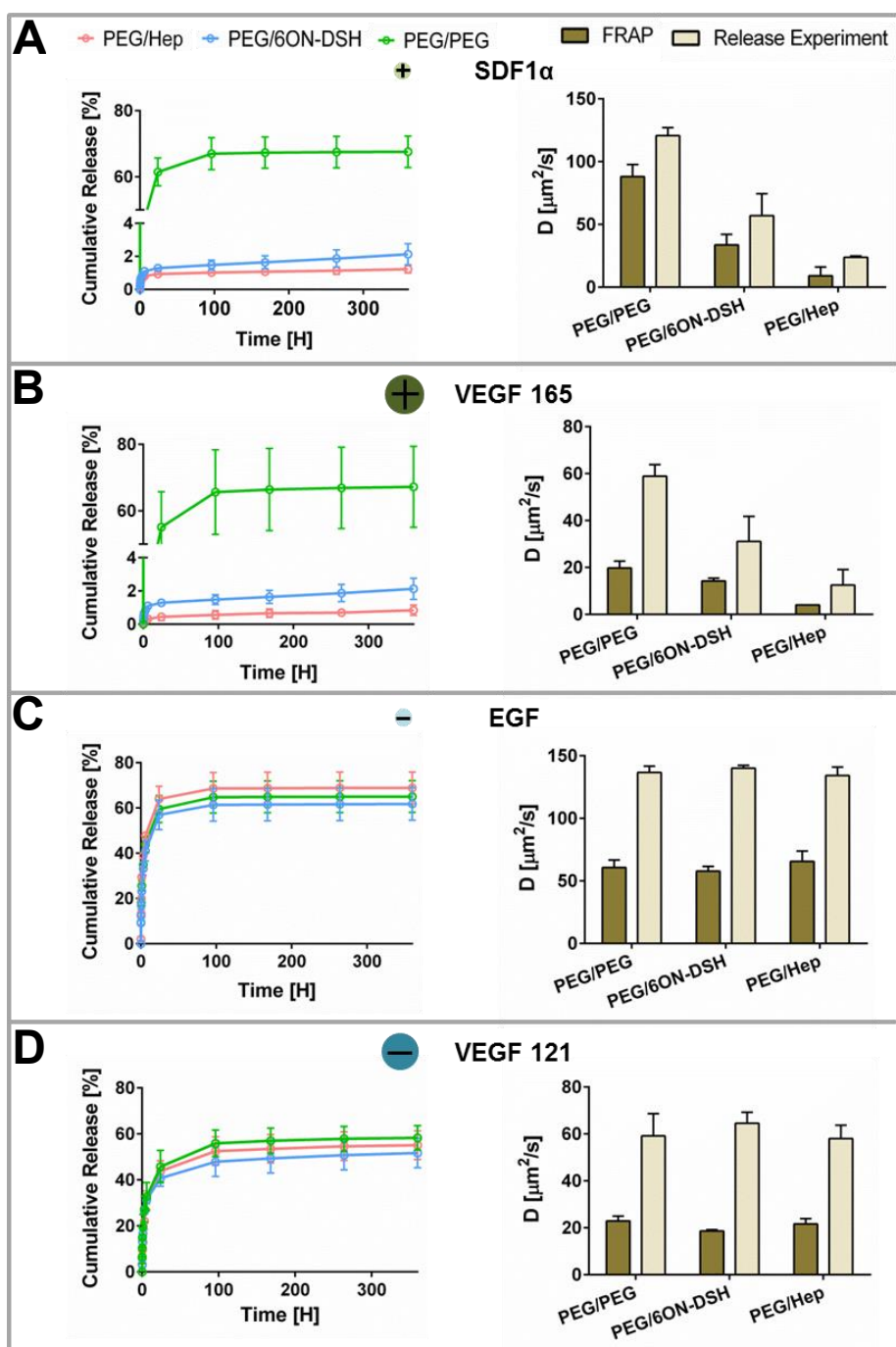


Figure 4.5. The release characteristics of model proteins from binary GAG hydrogels containing different GAG sulfation patterns. (A) The release of SDF1 α , (B) VEGF165, (C) EGF, (D) VEGF121 from PEG/Hep, PEG/6ON-DSH, PEG/PEG hydrogels for a period of 360 H at room temperature. For all conditions, the hydrogels were pre-loaded with 2.5 μ M of proteins. The release curve for each protein was then fitted with a Fickian diffusion model to extract the proteins' effective diffusion coefficient in hydrogels. The resulting diffusion coefficient (D) was then compared to those obtained from the FRAP experiments. Data represent mean \pm SD (n = 3)

4.1.4 Modelling the transport of protein within GAG-based hydrogel systems

To evaluate the applicability of the reaction-diffusion model to predict the release of proteins from the GAG hydrogel with varied sulfation, the experimentally determined release curve of two heparin-binding proteins, including VEGF165 and the SDF1 α throughout 360 H was fitted to the model using the least-squares method (**Figure 4.6**). The simulation could approximate the K_D value of the protein-GAG complex within the hydrogel (**Figure 4.6** and **Table 4.1**). Subsequently, the K_D values obtained from the MST were compared to those obtained from the release experiments.

In general, the reaction-diffusion model could not describe the release profile of both VEGF165 and SDF1 α at early time points (**Figure 4.6**). Especially, the model underestimated the protein release within the first 24 H. However, at 100 H or longer, the experimental release of both proteins was in good agreement with the simulation. Notably, the model could better predict proteins' release from the PEG/Hep gel than from PEG/6ON-DSH gel.

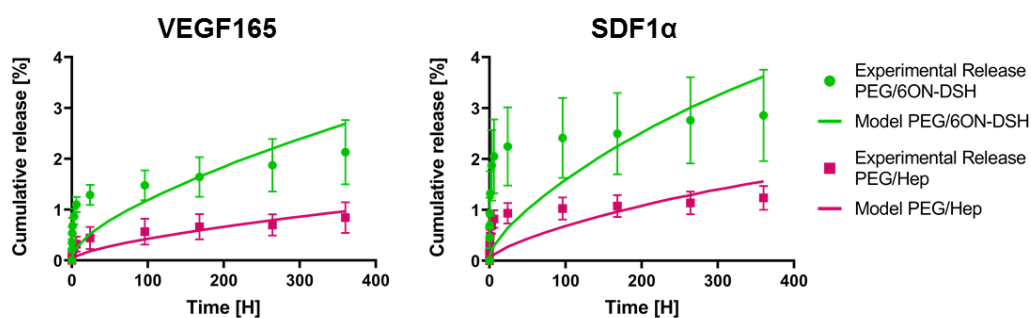


Figure 4.6. Experimental release (data points) and the resulting least-squares best fit of the data using the reaction-diffusion model (solid line) of VEGF165 and SDF1 α from GAG hydrogels with variable sulfation.

Table 4.1. Affinity constants of the VEGF165 and SDF1 α to the heparin or heparin derivatives as determined by microscale thermophoresis (MST) and the release simulation based on the reaction-diffusion model (model) from the GAG hydrogels with variable sulfation.

Protein	GAG	K _D _MST [M]	K _D _Model [M]
VEGF165	Hep	9.00 x 10 ⁻⁷	2.13 x 10 ⁻⁶
	6ON-DSH	3.33 x 10 ⁻⁵	6.67 x 10 ⁻⁶
SDF1 α	Hep	1.20 x 10 ⁻⁶	2.21 x 10 ⁻⁶
	6ON-DSH	ND	5.48 x 10 ⁻⁶

4.1.5 Sensitivity analysis of different COMSOL model parameters on the release characteristics of protein from hydrogel

To understand the effect of each model parameters on the release of heparin affine protein from the hydrogels, the release of VEGF165 from starPEG-heparin hydrogels loaded at the bottom of the microcentrifuge tube was simulated (Please see section 6.1.6.1 for the detailed geometry of the system). The influence of different hydrogel network biochemical properties, including the total concentration of heparin, the affinity of heparin to protein, the dissociation rate constant of protein from the heparin, and the impact of protein loading concentration was investigated (Figure 4.7). The detailed parameters used for the simulations for each graph were listed in Table 6.1.

According to the simulations, the initial growth factor concentration did not affect the overall release of VEGF from the hydrogel, especially at a high concentration of heparin (1500 μ M) (Figure 4.7A). In such conditions, VEGF's release increases only from ~1% to ~6% over two weeks, when the protein loading concentration was raised to 1500 μ M. However, this concentration is physiology irrelevant. Therefore, increasing the growth factor concentration was not the best choice to enhance the release from hydrogels as the burst leakage of the growth factor, especially those with a narrow margin of safety, may cause severe side effects. Interestingly, we could fine-tune the release rate of protein from hydrogel by varying the initial protein loading concentration only when hydrogels' heparin

content was lowered by 100 times to 15 μM . Notably, the overall release efficiency was higher for the gel prepared with a low heparin content. Moreover, over two weeks, the total protein release could also be adjusted from 30% to 80% by merely changing initial protein loading from 1.5 to 150 μM .

Altering heparin's affinity to protein was also shown to effectively control the protein release from hydrogels (**Figure 4.7B**). The protein release could be varied from 30% to 80% at low heparin content only by modulating heparin's affinity. The strategy to modulate protein affinity to GAG has been previously described, such as removing certain sulfate groups of the heparin that determine the specific binding to a particular protein [6]. Although decreasing the GAG building block's affinity to the protein of interest could also modulate their release from the hydrogel containing high heparin content, the overall release amount was still low. The protein's cumulative release only increased to 8% at high heparin content when the heparin's affinity declined by ten factors. This indicated that hydrogels containing high content/ density of binding ligands, even those with a low affinity for the signaling molecules, are suitable more as a sequestration biomaterial than a controlled delivery system of bioactive proteins.

The affinity of GAG to signaling molecules is determined by the ratio of dissociation and association rate of the protein to GAG. As several combinations of the association (k_a) and dissociation rate constant (k_d) of the protein-GAG interaction pair results in the same value of K_D ($K_D = k_d/k_a$), we then examined whether these rate constants could influence the protein release from the hydrogel. The impact of k_d on the protein release was investigated at a high and low heparin content (**Figure 4.7C**). In both cases, varying the dissociation rate constant from 1×10^{-2} – 1×10^{-5} /s did not change the overall release of VEGF. Remarkably, decreasing the dissociation rate constant (increasing the resident time) at given strength of affinity interaction (K_D) could lower the overall protein release only when physically irrelevant rate constant (1×10^{-9}) for a typical GAG-protein interaction was used for the simulation. Besides, this effect was proportional to the heparin concentration of the hydrogel. At high heparin content, decreasing the rate constant to 1×10^{-9} decreased the total release by almost ten factors whereas,

at a low heparin content, the same rate constant only declined the entire release by two factors.

Finally, since adjusting the affinity or initial growth factor concentration did not significantly affect VEGF's overall release when the heparin concentration is high, we extended our simulation to understand the effect of gel heparin concentration on the protein release (**Figure 4.7D**). For the simulation, the heparin was varied in the range of 1.5 to 1500 μM while the affinity of heparin to growth factor was either set to low ($K_D = 21300 \text{ nM}$) or high ($K_D = 2130 \text{ nM}$). Remarkably, the VEGF release could be finely tailored from as low as 1% to as high as 80% over two weeks by varying the hydrogel's heparin content at both K_D values. In general, the gel heparin content was inversely proportional to the amount of protein release. Overall, incorporating a graded amount of heparin into the GAG hydrogels seems to be a more robust strategy to gradually adjust the release of protein from the gel matrix than modifying the heparin affinity to the signaling molecules.

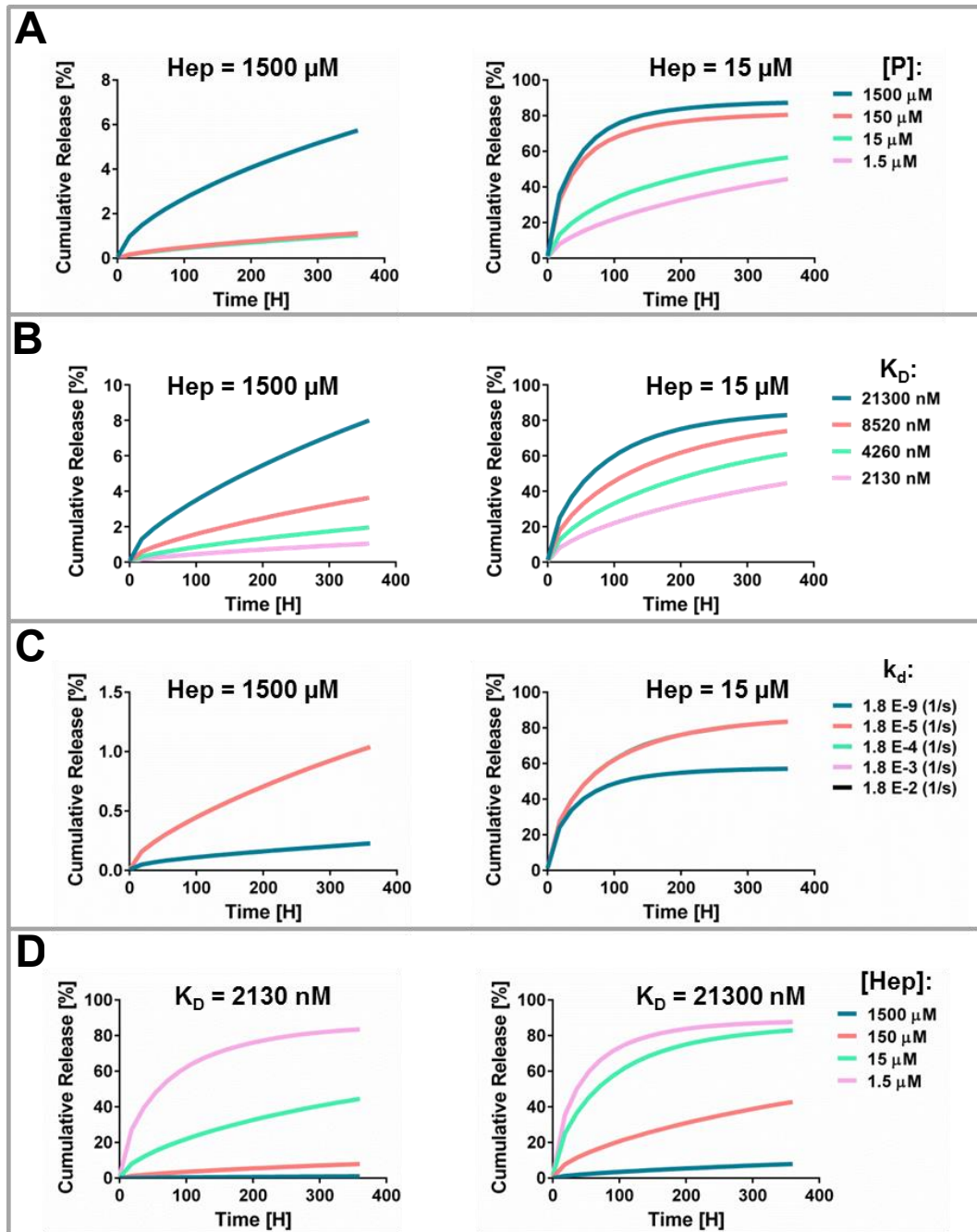


Figure 4.7. COMSOL simulations of the VEGF165 release from GAG hydrogel systems. The effect of different input parameters of the COMSOL model, including (A) the initial protein loading concentration, (B) the protein affinity to GAG, and (C) the dissociation rate constant (k_d) of the protein, on the release of the protein from hydrogels containing a high (1500 μM) and a low (15 μM) heparin concentration. (D) The effect of heparin concentration of the hydrogel on the protein release at a strong ($K_D = 2130$ nM) and weak ($K_D = 21300$ nM) protein-GAG affinity interactions. The initial VEGF concentration was 2.5 μM for all simulations, except for (A) when the effect of protein loading concentration was investigated.

4.1.6 Discussion and summary

The capacity of GAGs to control the mobility and retention of cytokines/ GFs within polymer networks has been widely applied in biomaterial research to control physiological processes, including wound healing, stem cell renewal, and differentiation, and tissue vascularization [7, 19, 43, 155]. However, the impact of GAGs incorporation into the biomaterial on the cellular responses is often difficult to predict because of the GAG-protein interactions that could suppress and enhance biological signaling depending on the context of presentation [28, 36, 185-188]. Accordingly, signaling molecules' interactions with GAG resulted in their partition within the polymer network into a matrix-bound and free factor. Such separation eventually controls their retention within the gel matrices and influence the bioactivity [54]. Therefore, one potential approach to effectively predict the effect of GAG on the cell fate control within such materials is to apply a mathematical model that estimates the total amount of growth factors retained within the polymer matrices and the fractions that can be delivered to the cells.

In this part of the thesis, we investigated the role of different biophysical and biochemical parameters of GAG-based hydrogels on the transport of selected signaling molecules that differ in their molecular sizes and binding affinity to the GAG. Using our previously established tunable starPEG heparin hydrogels systems [38, 47], we could dissect the impact of steric (hydrogel mesh and protein size) as well as the affinity interactions (which depends on the heparin concentration & GAG-sulfation degree) between the polymer network and model proteins, including VEGF165, VEGF121, SDF1 α , and EGF, upon their in-gel mobility. Finally, a mathematical model based on the diffusion of signaling molecules or in combination with their binding to GAG building block was developed to interpret the overall processes governing the diffusivity within the hydrogels matrix and their subsequent release from the system. Thus, our systematic study could potentially serve as guidelines for designing materials that could precisely induce desirable cellular responses through growth factors-based biological signaling.

Modulation of steric interactions between the hydrogel network and embedded signaling proteins through adjustment hydrogel mesh size is a common strategy to control the in-gel mobility or the release kinetics of proteins from polymer matrices [16, 189]. The relative difference between the protein and hydrogel mesh size dictates the magnitude of the steric hindrance. Hydrogel mesh size can be modulated either by the concentration and the chemistry of polymer and crosslinker or by introducing external stimuli [16]. In this study, the GAG-hydrogels' mesh size was gradually adjusted by changing the molar ratio of the starPEG to heparin while keeping the heparin concentration constant [47]. This strategy effectively generated hydrogels with mesh size ranging from 8-30 nm of similar biochemical characteristics, making them suitable to control the mobility of many therapeutically relevant cytokines and GFs [7, 38]. Molecular diffusivity studies using FRAP revealed that the mobility of non-affine proteins within the GAG-hydrogels was primarily influenced by the protein's molecular weight and the hydrogel's mesh size (**Figure 4.2**). Similar to the mobility of these proteins in a pure buffer/ in a non-affine gel system (PEG/PEG), we found that smaller non-affine protein (EGF) diffuse faster than the bigger ones. These effects could be clearly explained by the higher steric hindrance that the larger proteins experienced as it diffuse through the hydrogel network in comparison to the smaller proteins. Similarly, increasing the steric constraint within the starPEG-heparin hydrogels by decreasing the hydrogel mesh size could restrict the diffusivity of both small (EGF) and large (VEGF121) non-affine proteins.

In contrast, the diffusion of heparin-affine proteins (VEGF165 & SDF1 α) was not significantly affected by their molecular size. We believe that the impact of overall electrostatic interactions between positively charged affine proteins and the high density of negatively charged heparin (750:1, heparin/ protein molar ratio) at pH 7.4 surpassed the effect of steric interaction between the proteins and the hydrogel network. In line with this, our previous finding reported that starPEG-heparin hydrogel could efficiently sequester a significant amount of many different cationic proteins *in vitro* and *in vivo* [7]. Similar effects of the protein size and charge on their in-gel mobility have also been documented in self-assembling peptide hydrogels [9, 189]. Here, the release of the bovine serum

albumin (BSA) and trypsin inhibitor as representative of small and large, negatively charged protein models, respectively, was studied. Accordingly, the larger protein exhibited a more prolonged-release than, the smaller ones at a pH where the electrostatic interaction between the protein and nanofiber was negligible [189]. On the contrary, the release of positively charged cytokines (β FGF/ basic fibroblast growth factor & BDNF/ brain-derived neurotrophic factor) from a variant of the peptide hydrogel that has a net negative charge was comparable despite the difference in their molecular weight [9].

The mobility of proteins in affinity-based delivery systems, including the GAG-based hydrogel, is affected by the steric interactions with the hydrogel network and their affinity interactions with the binding ligand, which depends on the concentration of ligand and the strength of interaction [16, 52]. Based on this concept, recently, we have introduced GAG-hydrogels with varied GAG-sulfation patterns to modulate the affinity of the encapsulated Platelet-Derived Growth Factor (PDGF) and control the release kinetics from hydrogels [38]. In the present study, we varied the heparin content along with hydrogels' crosslinking degree to maintain a similar gel stiffness.

The results of our study showed that the mobility of affine proteins decreased as the hydrogel heparin content increased (**Figure 4.3**). This finding is similar to what Jha and coworkers reported for the diffusion of TGF β 1, another heparin-binding protein, in heparin-containing hyaluronic acid hydrogels [43], where the amount of added heparin did correlate to a substantial decrease in the mobility of proteins. Similarly, the increase of gel heparin content in a PEG-hyaluronic acid hydrogel was demonstrated to decrease VEGF's mobility and the subsequent release from the polymer matrices [77].

Unlike the impact of heparin concentration, the effect of specific GAG-sulfation pattern on the diffusion of heparin-affine protein within the hydrated polymer network seems to be more exclusive for a particular affine protein. We showed that the removal of 6O-sulfate from the heparin building block did not significantly affect the mobility of SDF1 α , but it significantly enhanced the mobility of VEGF165 (**Figure 4.4**). In line with this finding, previous studies

investigating the interactions between the growth factors or cytokines and heparin have also demonstrated a preferential protein interaction with a distinct sulfate group of heparin for the efficient binding [36, 167, 190-193]. For example, the N- and 6O- sulfate of heparin was known to a greater extent mediate the heparin-binding of VEGF165, whereas the interaction with the SDF1 α mainly involved the 2O- and N- sulfate group [190, 193]. Overall, the results of the study suggested the potential application of our hydrogel as a defined 3D *in vitro* model to recapitulate growth factor presentation/ transport in the ECM.

The release of GAG-affine proteins from the hydrogel was inversely correlated to the sulfation degree of GAG building blocks, similar to their in-gel diffusivity trend measured by the FRAP method (**Figure 4.5**). Contrary to this, the release of non-affine proteins was not affected by the hydrogels' GAG sulfation. Interestingly, both the GAG-affine and non-affine proteins did not reach a complete release from the pure PEG/ PEG hydrogel despite the absence of affinity interactions. In line with this finding, Koutsopoulos and coworkers have also documented the release of proteins from a peptide-based-hydrogel scaffold that rarely reached 100% irrespective of the protein sizes and affinity peptide fibers [189]. Accordingly, the hydrogel network domain's entanglement might limit the free movement of encapsulated macromolecules within the hydrogel matrix, which eventually precluded their complete release from the system. Also, the growth factors usually possess a short half-life both *in vitro* and *in vivo* [15, 194, 195]. Thus, it was possible that during the release studies, proteins were denatured or forming aggregates preventing their detection by the ELISA or the release from the gel constructs [52, 196, 197].

Fluorescence recovery after photobleaching (FRAP) was a robust technique to quantify protein diffusion within various systems [183]. However, its applicability to analyze the diffusion process underlying the release of therapeutically relevant proteins from an affine GAG-based hydrogel system has yet to be proven. In this study, we observed similar trends of the diffusion coefficient of model proteins in the hydrogels with varied sulfation obtained either from the FRAP measurement or release experiment (**Figure 4.5**). In general, the values of diffusion constants derived from the release curve were consistently higher than those acquired from

the FRAP, which is in good agreement with the previous studies on the diffusion of macromolecules within crosslinked-polymeric networks [161]. One possible explanation for such discrepancies might be attributed to the differences in the experimental setups [198-200]. Alternatively, the relatively higher protein concentration used for the FRAP measurement than the release experiment [201], might cause protein aggregation that would slow down the protein diffusion. Moreover, the slow scanning speed of the confocal microscope might also allow the diffusion to happen during the photobleaching stage of the FRAP measurements. These conditions could further contribute to the underestimation of diffusion coefficients obtained from the FRAP [202], especially when both slowly and rapidly diffusing protein fractions exist within the hydrogel [161].

Overall, the FRAP can be adapted as an alternative to the release experiments to evaluate the relative contribution of different GAG-hydrogel network parameters on the transport of embedded signaling molecules because the determined diffusion coefficient values were correlated well with those obtained from release studies. Considering the speed and precision of the FRAP measurement, both methods can complement each other to rapidly evaluate the potential of new GAG-based/ GAG-inspired materials for controlling the administration of growth factors or other bioactive molecules.

A mathematical model can be instrumental for guiding the design of a cell-instructive hydrogel with desired growth factor transport characteristics. Here, we applied a reaction-diffusion model to understand the binding and diffusion process within the GAG-based hydrogel system and predict the release kinetics of signaling molecules (**Figure 4.6**). In general, the model underestimated the protein release within the first 24 H, especially those from hydrogels containing 6ON-DSH. However, at later time points, the experimentally determined release of both proteins well agreed with the simulation. Two different protein populations that were not considered in the model may exist within the hydrogel: weakly and strongly binding proteins. The weakly binding protein was released much faster at early time points, whereas the strongly binding protein population sustainability was released from the hydrogel matrix over a more extended period.

Consequently, as the model only accounts for single protein species with a strong affinity to the GAG, it could better capture the protein release dynamic at later time points. Additionally, for the PEG/ 6ON-DSH hydrogel with a low sulfation degree, much more weakly bound proteins may also present in the gel matrix. Together, these reasons might explain the model's poor curve fitting result to the experimental release of proteins from the PEG/ 6ON-DSH hydrogel. Moreover, the convective flow that speeded up the gels' protein release during the buffer replacement step of the experiments might also exist, especially at initial time points when the procedure was done more frequently. In this study, the buffer exchange was done more often at the beginning of release studies to capture the protein release dynamic, especially from the pure PEG/PEG gel, where the diffusion was relatively fast. For future studies, the time scale to analyze affine proteins' transport in the GAG-based hydrogel system needs to be adjusted independently. As such, the release media should be exchanged less frequently to minimize the convective flow that complicates the subsequent analysis using the reaction-diffusion model.

Despite these shortcomings, the developed computational model could still provide valuable information to predict the total protein release from the GAG hydrogel with varied sulfation patterns. The developed model could also estimate the K_D value characterizing the interaction between the protein and GAG crosslinked within the hydrogel based on the experimental release. In general, the resulting K_D values obtained from the release experiment were positively correlated to those obtained from the MST measurement (**Table 4.1**). Besides, the variation in the K_D obtained from both methods felt within the same order of magnitude of variability range of the K_D values determined using different methods [115, 116, 127, 182]. Overall, we could see a positive correlation between the K_D values derived from the model and the overall amount of protein release from the hydrogel, except for the interaction between the SDF1 α and 6ON-DSH, where the K_D value could not be determined using MST. Besides, the K_D values also decreased with increasing sulfation degree of GAG building block of hydrogels. Therefore, the reaction-diffusion model that we developed here is

instrumental to directly quantify the strength of interactions between the protein and GAG immobilized within a biomaterial.

The model that we developed based on the binding and diffusion of molecules within the hydrogel might also serve as a guideline to design and characterize the biomaterial. By utilizing the K_D of the interaction between the protein and linear/soluble GAG measured using methods such as SPR [116], ITC [115], or BLI [117], it is possible to predict the release of proteins from the GAG-based hydrogels quantitatively. The adjustment of input parameters of the model, including the growth factor loading, GAG content, GAG affinity to the proteins (e.g., GAG sulfation patterns), and the gel geometry, can further be applied to predict the transport of protein within and out of the gel matrices in a more complex *in vivo* or *in vitro* scenario.

Sensitivity analysis of GAG-hydrogel network parameters revealed that adjusting the GAG content of hydrogel was the most effective way to modulate the release of GAG-affine proteins (**Figure 4.7**). The effect of protein loading concentration, GAG affinity to the signaling molecules, and the dissociation rate constant of the GAG-protein complex did not significantly influence the release of GAG-affine proteins, especially at a high concentration of GAG. Regioselective desulfation or the introduction of additional sulfate moieties to the GAGs regulates their affinity for signaling molecules and thereby could be applied to modulate the retention and release kinetics of proteins from engineered matrices [38, 203]. However, the complicated procedures and the difficulty in achieving a tunable release of the growth factors from the materials may limit their usage. As demonstrated by the simulations results, heparin's affinity to the protein could also dynamically control the release of growth factor from the matrices at the low heparin concentration. Therefore, combining selective heparin desulfation and tuning the hydrogels' heparin concentration may provide valuable options to precisely tailor the release rate of signaling molecules for various applications.

Previous studies investigating the influence of binding rate constant on the release kinetics of protein from affinity-based growth factor delivery systems have reported conflicting results. Some studies suggested that the dissociation rate

constant is essential for determining the release of proteins from the gel matrix [129], while other studies have shown the opposite [178]. Here, we found that altering the dissociation rate constant did not change the overall release of protein as long as a physically relevant rate constant value for a typical GAG-protein interaction was used. Therefore, for the subsequent simulation employing this model, it is unnecessary to utilize the exact value of rate constant between the protein and heparin or heparin derivatives to predict the release from scaffolds. This knowledge is particularly useful, especially when the rate constants' values are not available/ failed to be determined using available methods.

Taken together, in this section of this thesis, fluorescent recovery after photobleaching has been successfully optimized and implemented to analyze the transport of signaling molecules within the binary GAG-based hydrogels. Our systematic study on the mobility of proteins revealed the key parameters of the gel network that govern the transport of signaling molecules. A mathematical model that describes the binding and diffusion of signaling molecules within the GAG-based hydrogel has also been developed utilizing the data derived from the protein diffusion and binding studies under various scenarios. Overall, the obtained results allow for the customization of signaling protein transport in GAG-based biohybrid hydrogels for tissue engineering and regenerative medicines.

4.2 Tuning the activity of pro-angiogenic growth factor within binary GAG-based hydrogels

4.2.1 Introduction

The vascular network is essential to provide the cells with a continuous supply of nutrients and oxygen. Previous *in vitro* studies revealed that the formation of vascular structures involves the interplay between endothelial cells, supporting cells [3], and biophysical and biomolecular cues of the scaffold such as matrix degradability [66, 204], stiffness [3, 205], cell adhesiveness [206], and functionalization with pro-angiogenic growth factors [3, 140]. Among the previously identified pro-angiogenic growth factors, vascular endothelial growth factor (VEGF) is the key player of *in vivo* angiogenesis. The factor controls multiple aspects of vascular function and development by stimulating proliferation, migration, survival, and differentiation of endothelial cells [69-72]. However, the VEGF has a relatively short half-life [14, 15, 207], and a narrow therapeutic window [17, 208]. Therefore, maintaining the delivery of bioactive VEGF within- and out of the scaffold can be instrumental for the application in vascular tissue engineering.

Incorporation of sulfated glycosaminoglycans (GAGs) has been widely applied for the sustained delivery of signaling molecules from engineered biomaterials [4-6]. This methodology offers a powerful means to modulate the retention and release kinetics of heparin-binding proteins because the negatively charged GAGs can reversibly interact with the molecules through their positively charged surfaces. The affinity of GAG to a given signaling molecule, and the overall GAG content, determine the relative concentration of free and matrix-bound factor within the hydrogel [32, 51-53]. Therefore, adjusting the overall GAG content of the polymer network as well as the GAG sulfation pattern to modulate the GAG affinity to signaling molecules have been widely applied to control the administration of signaling molecules, including the VEGF from the GAG-based scaffolds [6, 38, 43]. The effect of GAG content and GAG sulfation patterns of GAG-based matrices on the bioactivity of the released VEGF has been previously investigated [4-6, 77]. However, the influence of both parameters on the activity

of gel embedded VEGF to control cell fates within cell-instructive polymer networks has not been systematically studied.

To unravel the impact of GAG content and GAG sulfation patterns of the hydrogel on the transport and bioactivity of VEGF, herein we applied a previously introduced platform of binary GAG based-hydrogel made from heparin and four-arm poly(ethylene glycol)-(starPEG) peptide conjugates (**Figure 4.8A-B**) [47]. As described before, the overall GAG content and GAG sulfation pattern of the system can be varied to tailor the overall space charge density and local charge density of the GAG component, respectively, to modulate the binding of various cytokines and growth factors (**Figure 4.8C-D**) [78]. Besides, the system is compatible with a direct encapsulation of human umbilical veins endothelial cells (HUVECs) and has been adapted as a robust 3D *in vitro* model of angiogenesis [3]. As the VEGF plays a vital role in the early regulation of angiogenesis [12, 209, 210], controlling extracellular availability is critically important to direct the tubular morphogenesis of endothelial cells.

In this study, hydrogels containing different heparin (Hep) content (0,500,1000, and 1500 μ M) or heparin derivatives with varied sulfation patterns were first prepared and thoroughly characterized for their swelling and mechanical properties. A mathematical model to predict free and bound VEGF availability within the gel matrices was then developed and experimentally validated. Furthermore, we investigated the relevance of free VEGF availability and specific heparin (derivatives) sulfation patterns on the formation of HUVEC tubular structures within the hydrogels. Finally, by utilizing the microfluidic technique, we also demonstrated the effect of a graded distribution of VEGF on the HUVEC chemotaxis and the spatial pattern of the emerging endothelial cell capillary structures.

4.2.2 Physical properties of hydrogels

Heparin (Hep) was regioselectively desulfated at 6O- position to generate 6O-desulfated heparin (6O-DSH), or both at 6O- and N- position to synthesize 6ON-desulfated heparin (**Figure 4.8A**). This strategy enabled the generation of heparin derivatives with a sulfation degree of ~67% and ~33%, respectively, relative to the fully sulfated heparin (Hep). Subsequent functionalization of Hep or its derivatives with maleimide moieties further allowed for an efficient reaction with thiol-containing starPEG through Michael type addition scheme to form a hydrogel with a stable thioether bond in the presence of biological fluid (**Figure 4.8B**). Due to the reaction's specificity, the crosslinking reaction is also compatible with a direct encapsulation of cells or various growth factors during the gel formation.

To modulate hydrogels' affinity for given signaling molecules, the GAG-building block with a variable sulfation degree can be selectively chosen for the in-situ cross-linkable hydrogel formation to generate hydrogel with variable local sulfate density (**Figure 4.8C**). Besides, the heparin content of hydrogels was also varied by adjusting the overall solid content (**Figure 4.8D**). This strategy is rationally applied to adjust the number of protein binding sites within the system, modulating the binding and transport of signaling molecules.

Endothelial cell morphogenesis within engineered materials is controlled both by the presence of pro-angiogenic growth factors and the scaffold's mechanical properties, such as stiffness [3, 143, 211]. As described before, the formation of endothelial capillary structures within starPEG-heparin hydrogel can be achieved in a soft hydrogel with a storage modulus of ~200 Pa [3]. Therefore, to investigate the effect of heparin content and heparin sulfation patterns on the VEGF-mediated vascular morphogenesis, a set of hydrogels with the various heparin content or heparin-sulfation degree was prepared with this stiffness range (**Figure 4.8E-F**).

For investigating the effect of heparin content on the transport and bioactivity of VEGF within the scaffold, hydrogels containing fully sulfated heparin were produced with a total GAG concentration in the range of 500-1500 μM (**Figure 4.8E**). Besides, pure PEG hydrogel was used as a control. We could prepare

hydrogels with a stiffness of approximately 200 Pa by adjusting the overall solid content in the range from 2-3.6% and the molar ratio of starPEG to heparin. Volume swelling measurement of all hydrogels indicated an increase in the volume of only less than 30% from its original, with the highest swelling was observed for the hydrogel containing the highest heparin content (1500 μ M).

Next, to understand the effect of GAG affinity on VEGF's bioactivity, hydrogels containing fully sulfated heparin, 6O-desulfated heparin, and 6ON desulfated heparin were prepared at a total GAG concentration of 1500 μ M. All the hydrogel with varied GAG sulfation patterns could be produced with a 200 Pa stiffness by merely altering the GAG building block choice while fixing the total GAG content constant (**Figure 4.8F**). Interestingly, similar to the hydrogel prepared with a low GAG content (**Figure 4.8E**), slightly lower volume swelling was observed for the hydrogels containing GAG building block with the lowest sulfation degree compared to the fully sulfated heparin. These results might be attributed to the decrease in hydrogel hydrophilicity due to the reduced volume density of sulfate groups.

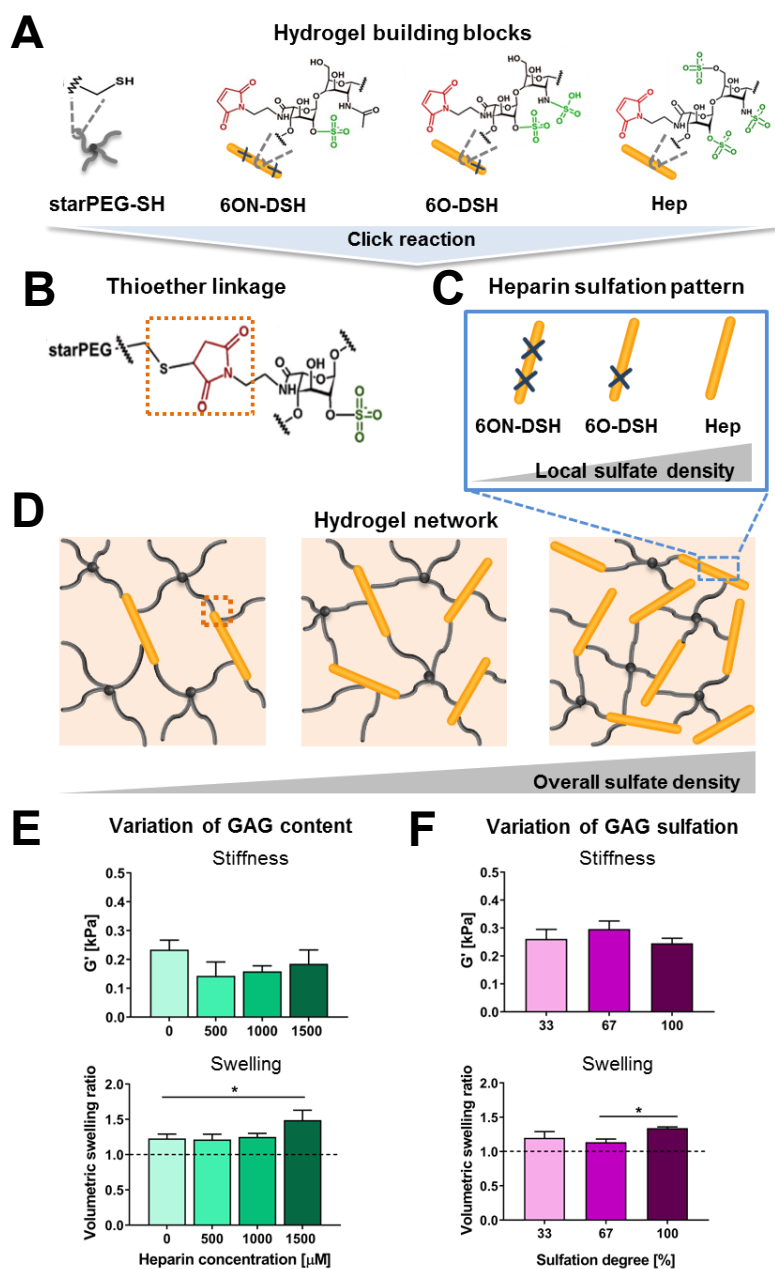


Figure 4.8. The formation and physical properties of the GAG-based hydrogel with adjustable local and overall sulfate density. (A). The building block of hydrogels consists of thiol-functionalized starPEG (starPEG-SH), maleimide functionalized heparin (Hep)/ heparin derivatives, which were selectively desulfated at 6O- (6O-DSH), or 6O- and N- position (6ON-DSH). (B) The starPEG-SH can be instantaneously reacted with maleimide-functionalized heparin to form a hydrogel network containing a stable thioether linkage. (C) Variation in hydrogels' local sulfate density can be achieved by incorporating heparin/ heparin derivatives with different sulfation degrees. (D) The overall heparin content of hydrogels can also be adjusted to control the overall sulfate density. (E) Stiffness and volumetric swelling of the hydrogels with varied heparin content. (F) Stiffness and volumetric swelling of the hydrogels with different GAG sulfation patterns.

4.2.3 VEGF release from hydrogels with varied GAG content and GAG sulfation patterns

The effect of heparin content of hydrogels and the sulfation pattern of GAG on the release of VEGF165 was evaluated throughout 360 H. Due to the biorthogonal crosslinking scheme, the protein can be encapsulated during the gel formation [212]. All hydrogels were adjusted to have a similar stiffness to specifically dissect the impact of both parameters on the protein release.

The release of VEGF from PEG-PEG hydrogel displayed a significant initial burst (**Figure 4.9A**). More than 60% of the initially loaded protein was released within the first 24 H. At 72 H, the VEGF release reached a maximum amount (~ 70%), and no more protein release occurred at later time points.

Nevertheless, in all hydrogels with varied heparin content, more than 97% of the loaded VEGF can be retained throughout 360 H (**Figure 4.9B**). The hydrogels could also maintain a sustainable release of VEGF with a minimal burst release. The release of VEGF165 can be gradually adjusted by varying the heparin concentration. Decreasing the hydrogel's heparin content from 1500 μ M to 500 μ M could enhance the overall VEGF release by a factor of three, which is proportional to the total decrease in the heparin content.

Similarly, hydrogel containing different GAG sulfation also displayed variation in the release profile (**Figure 4.9C**). Sulfation degree of the GAG-building block inversely correlated to the amount of VEGF release from the hydrogel. The VEGF release rise from ~1% to ~2.5% when the GAG building block was switched from fully sulfated heparin (Hep) to 6O-desulfated heparin. Incorporation of 6ON-desulfated heparin further enhanced VEGF release to more than 4% throughout 360 H. Although 6ON-DSH contains only ~30% of the sulfate group of the heparin, 96% of the proteins were retained within this hydrogel even after two weeks, which is significantly higher than the amount remaining in the PEG-PEG hydrogel. This result indicated that the desulfated heparins maintain a higher affinity for the VEGF than the PEG, which was reported to be inert [213].

To understand if the release of VEGF from the hydrogel is governed both by the diffusion of protein through the hydrogel network and the binding to the GAG

building block, the experimental release data was fit to the reaction-diffusion model [52], in COMSO Multiphysics. The curve fitting resulted in an estimated strength of an interaction between the VEGF and GAG or GAG derivatives within the crosslinked polymeric network. A similar model has been previously applied in several affinity-based systems [52], including the GAG-based materials [32, 33, 53]. Several parameters, including the free diffusion coefficient of protein in the hydrogel (D_{gel}), dissociation rate constant of the protein-GAG interactions (k_d) as well as the GAGs and initial protein loading concentration after the hydrogel swelling, were required for the curve fitting (**Table 6.1**). It is important to note that the curve fitting of the VEGF release from PEG/PEG hydrogel mainly required the diffusion coefficient of protein in the gel since no protein affinity to the PEG building block was assumed.

Interestingly, the reaction-diffusion model could describe the release profile of proteins from all gel formulations. The resulting K_D values obtained from the curve fitting for each GAG-derivatives were listed in **Figure 4.9D**. VEGF's binding strength to the GAG crosslinked within the hydrogel was inversely correlated to the GAG building blocks' sulfation degree. In general, the obtained K_D values are lower than those obtained using microscale thermophoresis for a linear GAG in solutions. However, the values are still within the variability range of the K_D values of protein-GAG interaction measured using various techniques [167, 193].

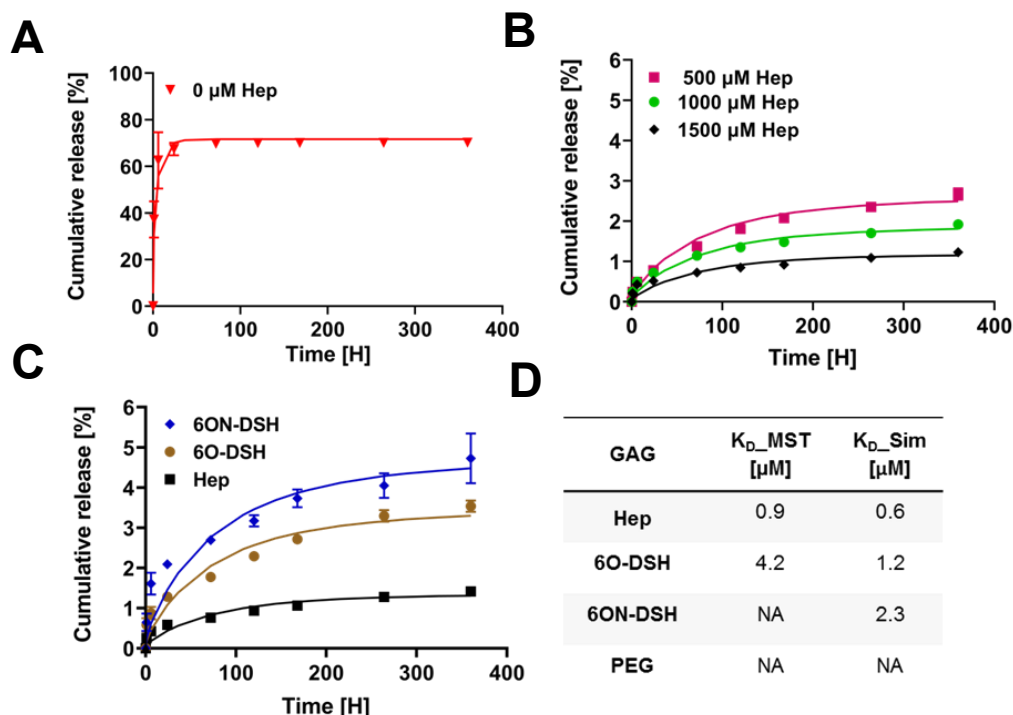


Figure 4.9. GAG content and GAG sulfation patterns modulate the release of VEGF from hydrogels. (A) The release of VEGF from hydrogel with varied heparin content. (B). The release of VEGF from hydrogel containing variable GAG sulfation patterns. (C) The release of VEGF from non-affine pure PEG/PEG hydrogel. The release experiment was conducted at 37° C in endothelial growth medium (EGM) supplemented with 0.1% BSA over 360 H. The data points and solid lines indicate the experimental release and resulting curve fit to the reaction-diffusion model, respectively. Data represent mean \pm SD ($n \geq 3$). (D) Comparison between the binding constant of VEGF to the GAGs obtained from the microscale thermophoresis and the curve fitting of experimental release.

4.2.4 Effect of GAG concentration and sulfation pattern on the formation of vascular structures of endothelial cells within hydrogels

The VEGF is the major growth factor that controls proliferation, migration, survival, and differentiation of endothelial cells [70-72, 214]. Previously, it has been incorporated into the starPEG-GAG hydrogel to initiate the capillary-like structure formation [3]. Here, we investigated the role of GAG content and GAG sulfation on the extent of VEGF-induced endothelial cell vascular morphogenesis. As described before, the HUVECs and VEGF can be directly encapsulated into a droplet of hydrogel during the gel formation and eventually form vascular structures within three days [3] (**Figure 4.10 A-B**). After three days, the cells were fixed and stained with fluorescence (**Figure 4.10C**). A stack of images was

acquired in the middle of the hydrogel, skeletonized, and subsequently analyzed for the vessel area and branching (**Figure 4.10D**).

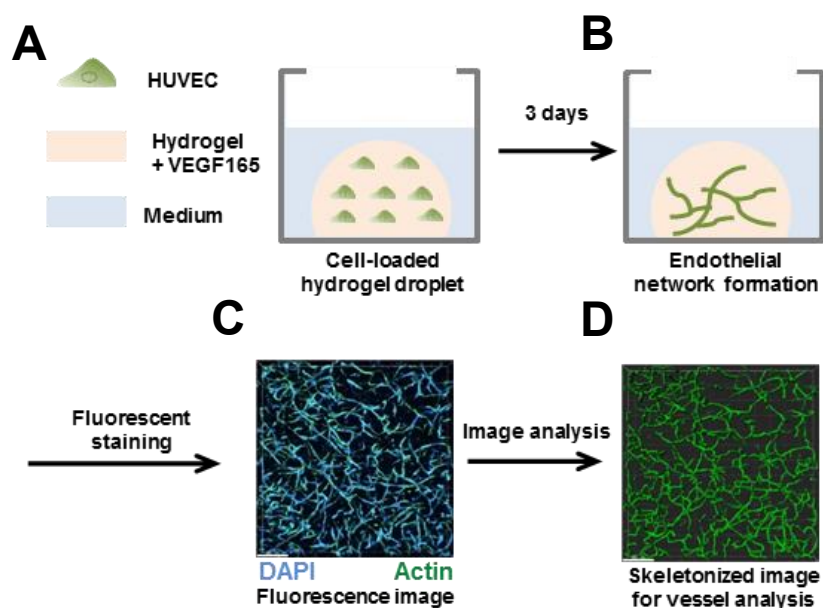


Figure 4.10. Schematic view of *in vitro* assay of endothelial morphogenesis within the hydrogel. (A) Uniform encapsulation of HUVEC and VEGF within a hydrogel droplet. (B) After three days of culture, HUVEC capillary-like structures were formed. (C) Fluorescence image of HUVEC vascular structures within the hydrogel, DAPI was used as a nuclear counterstain, and the actin filament was visualized using ATTO-633-phalloidin. (D) The skeletonized image obtained from the fluorescence image using the Imaris software was used to quantify the number of branching and the total vessel area of HUVEC capillary networks.

We have shown that the VEGF induced metabolic activity of HUVECs on 2D at a concentration of 1-100 ng/mL, in a dose-dependent manner (**Figure 6.7A**). Similarly, others have also reported that 10 ng/mL (260 pM) of VEGF was sufficient to induce the proliferation of HUVECs [193]. However, our previous work reported that a much higher concentration of VEGF (at least 5 $\mu\text{g/mL}$) was needed to prime endothelial cell vascular morphogenesis in the starPEG-GAG hydrogels [3]. Therefore, we hypothesized that free VEGF availability is crucial for the induction of proliferation and metabolic activity of endothelial cells within the hydrogels. A numerical simulation based on the reaction-diffusion model was performed utilizing the K_D obtained from the release experiment (**Figure 4.9D**) to determine the amount of free factor exposed to the cells after the gelation (0 H)

and at 72 H when the endothelial capillary-like structures were formed (**Figure 4.11**).

According to the simulation, free VEGF concentration is inversely proportional to the hydrogel's GAG content. At $t = 0$ H, the pure PEG gel has the highest free VEGF content (> 250 pM), whereas the corresponding concentration within the hydrogel containing 500, 1000, and 1500 μM of heparin was found to be 170 pM, 110 pM, and 60 pM, respectively. After 72 H, a significant portion of the VEGF was already released from the PEG/PEG gel. In contrast, all hydrogels functionalized with the GAG retained almost all the loaded VEGF.

Similar trends were also observed in the hydrogels with varied sulfation patterns, the hydrogel with the highest GAG sulfation maintain around 60 pM of free VEGF, and the values increase to around 160 pM and more than 200 pM for the hydrogel with 67% and 33% of GAG sulfation degree, respectively. Even after 72 H, all hydrogels with varied GAG sulfation also maintain a similar amount of free factor compared to 0 H, with the amount of free VEGF in the media inversely correlated to the sulfation degree of GAGs.

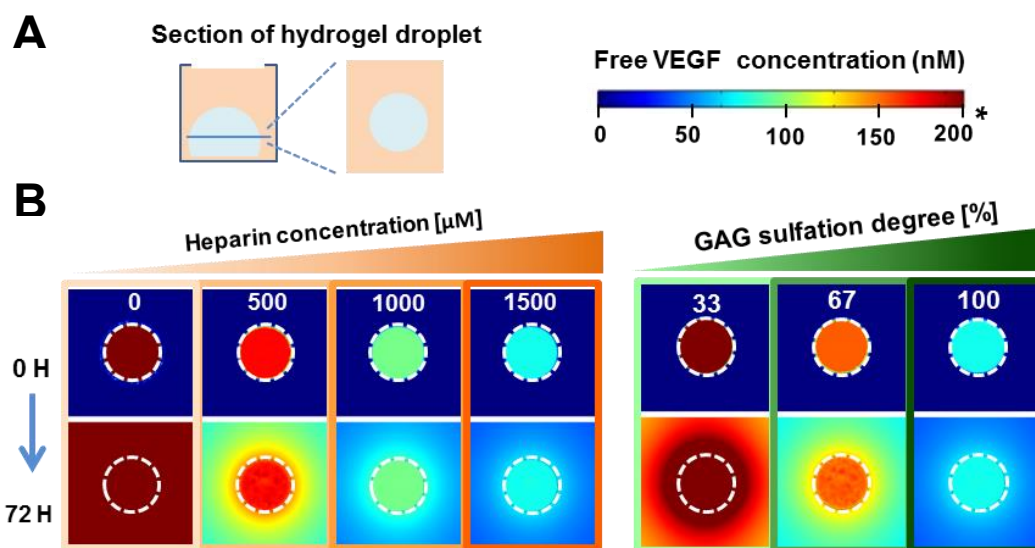


Figure 4.11. COMSOL simulation of the free VEGF concentration in hydrogel droplets with varied GAG content and GAG sulfation. (A) Schematic view of the hydrogel droplet for endothelial cell culture and the cross-section view at the middle part of the hydrogel. (B) The color map shows the distribution of free VEGF in media and hydrogels with varied GAG content (left panel) or varied GAG sulfation of fixed GAG content (right panel) just after the formation of the hydrogels (0 H) or 72 H after the incubation with media. The gels were pre-loaded with 5 $\mu\text{g/ml}$ of the VEGF. The color legend represents the free VEGF concentration in nM. The free factor with a concentration of 200 nM or higher is shown with the same color (dark red) as indicated by the * sign.

Next, the effect of GAG content and GAG sulfation on the bioactivity of VEGF to regulate vascular morphogenesis within the hydrogel was examined. VEGF's initial loading was varied from 0-20 $\mu\text{g/mL}$ to further modulate the free VEGF concentration within the hydrogels. The hydrogel containing the lowest GAG content displayed a superior formation of endothelial cell tubular structures at any VEGF loading concentration than any other hydrogels tested (**Figure 4.12A**). The total vessel area and the number of branch points of the vascular network in the hydrogel with 500 μM of GAG were significantly higher than for the hydrogels with 1000 μM or 1500 μM of GAG (**Figure 4.12B-C**). In general, the extent of vascular morphogenesis decreased as the GAG content of the hydrogel increased. This effect was directly correlated to the amount of free VEGF within the hydrogel.

Furthermore, the amount of VEGF loading enhanced the formation of vasculatures in a concentration-dependent manner. In particular, we observed a

greater extent of vascular structure formation in the hydrogel with the low and medium GAG content as more VEGF was loaded into the gels. Interestingly, the hydrogel with the lowest GAG content also required a less VEGF concentration to induce an extensive vascular network formation. Although 1 $\mu\text{g/ml}$ of VEGF was enough to induce vascular morphogenesis in the hydrogel with the lowest GAG content, increasing the VEGF loading up to 20 $\mu\text{g/mL}$ in hydrogels with the medium or high GAG content could not promote a similar extent of vascularization. Interestingly, while the pure PEG hydrogel contained the highest amount of free VEGF compared to any other hydrogels, a minimum of vascular morphogenesis was observed within this hydrogel. Similar to the VEGF bioactivity in culture medium (**Figure 6.7B**), probably the activity of VEGF in the PEG hydrogel also decreased over time since a slight increase in the vascular structure formation was seen when the VEGF loading was raised to 5 and 20 $\mu\text{g/mL}$ (**Figure 12A**).

Similar to the effect of VEGF in the hydrogel with varied GAG content, the VEGF enhanced the vascular morphogenesis in a concentration-dependent manner in any hydrogels with varied GAG sulfation patterns (**Figure 4.13A**). Increasing the free factor concentration by removing the 6O sulfate or 6O and N sulfate from GAG enhanced HUVEC tubular structures' formation. Compared to the hydrogel with the fully sulfated GAG, the hydrogel containing 6O-DSH or 6ON-DSH produced vasculatures with a larger area and higher number of branch points (**Figure 4.13B-C**). Interestingly, at a lower VEGF loading concentration of 1 and 5 $\mu\text{g/mL}$, hydrogel containing 6O-DSH induced a superior vascular structure formation compared to the one with 6ON-DSH, despite the higher estimated free VEGF in the 6ON-DSH hydrogels. However, increasing the VEGF loading to 20 $\mu\text{g/ml}$ resulted in no significant difference between the vasculature area in both types of hydrogels. Notably, in the absence of VEGF, the hydrogel containing the GAG with the lowest sulfation promoted larger vessel area formation than those with higher GAG sulfation.

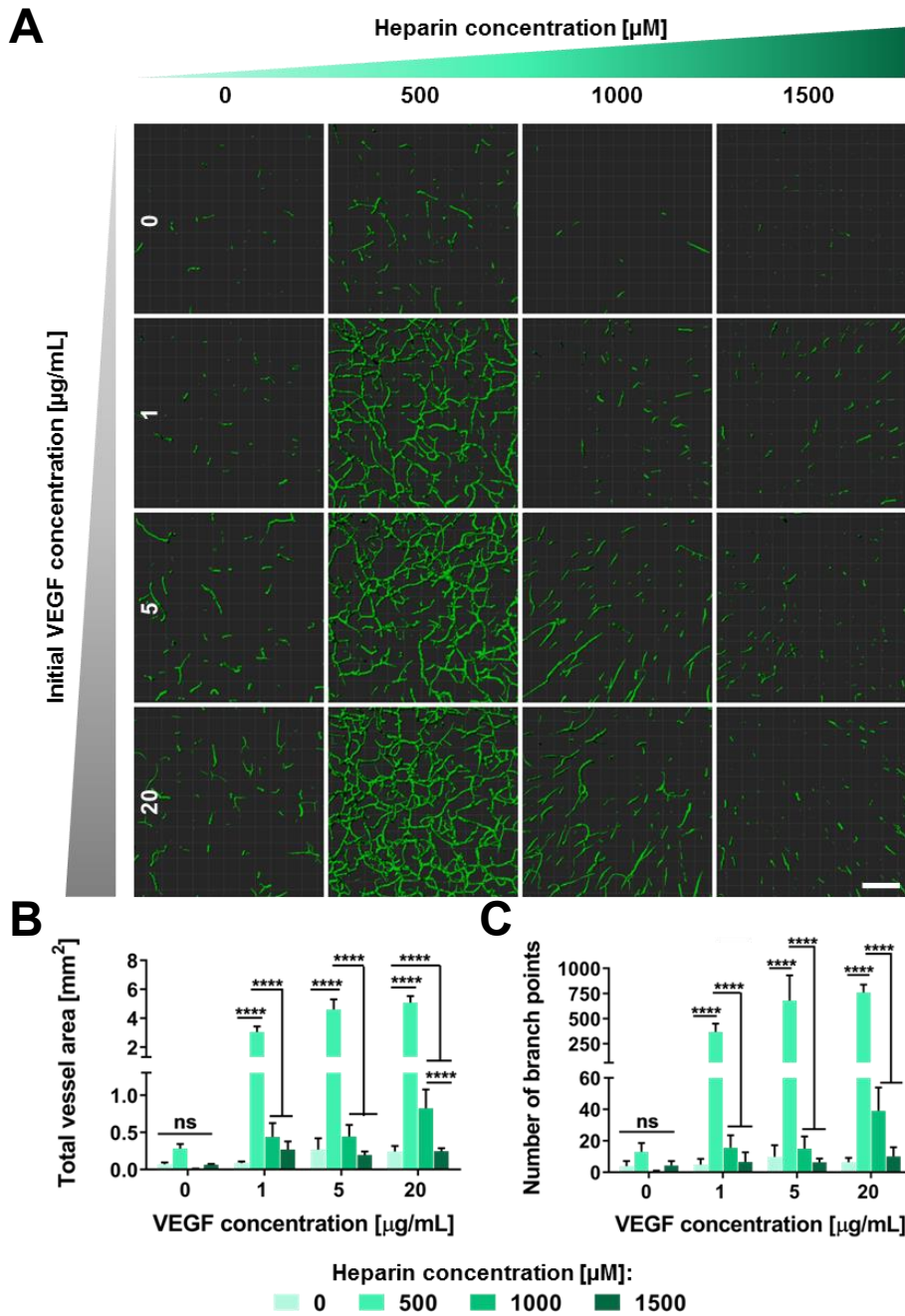


Figure 4.12. Effect of heparin content of the hydrogel on the endothelial cell capillary morphogenesis at various VEGF loading. (A) Representative skeletonized images of endothelial vascular structures formed within the hydrogels with varied heparin concentration (0, 500, 1000, and 1500 μM) over three days. One image per condition was chosen arbitrarily to represent different hydrogel conditions. Fixed samples were stained with phalloidin and DAPI, and Imaris software was used to process and skeletonize the fluorescence images. (B) Total vessel area of the vascular structures. (C) The number of branch points of the endothelial network. Scale bar = 200 μm . Data represents mean \pm SD (n = 5-8 cultures), 'ns' stands for not significant, ****P<0.0001.

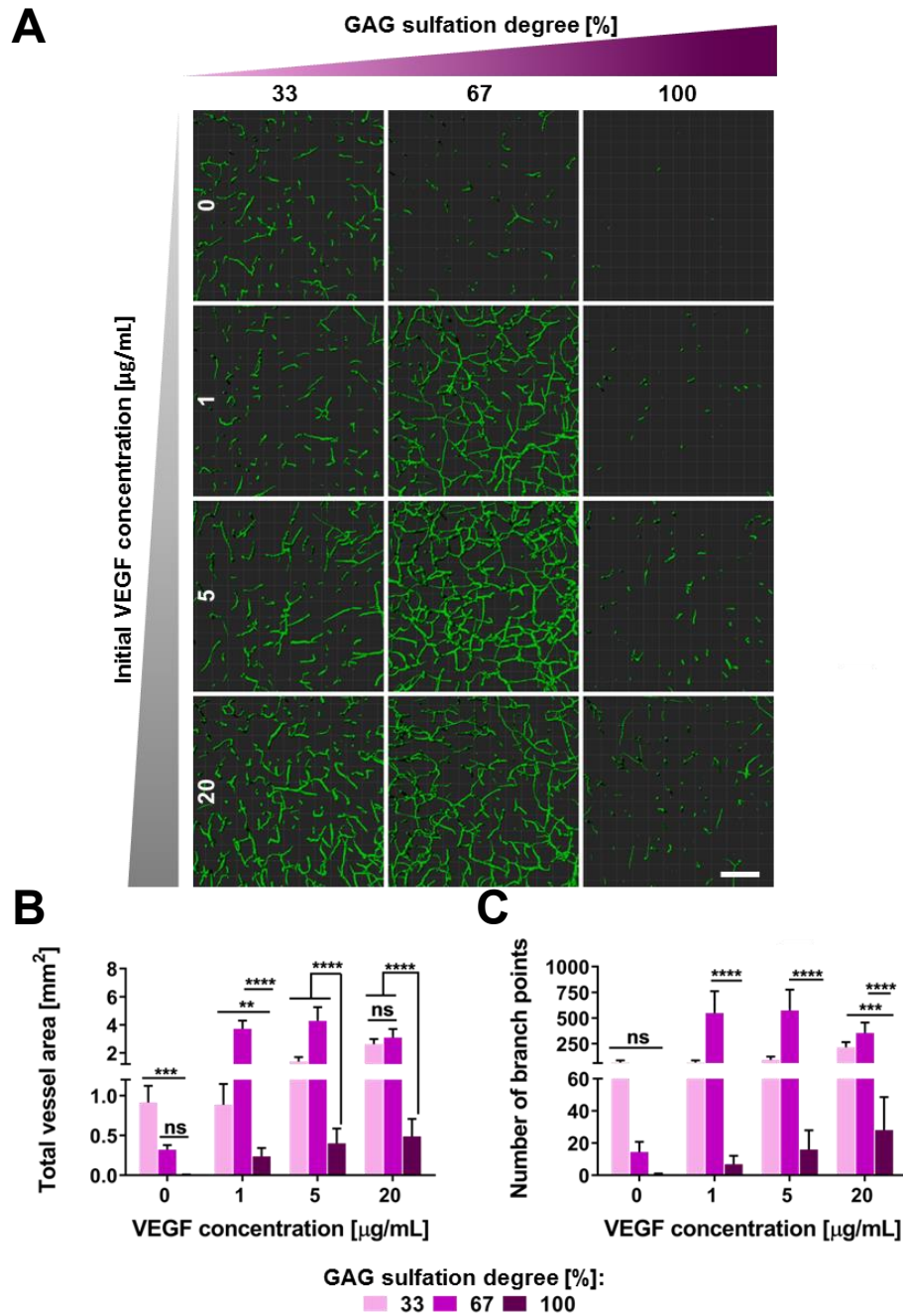


Figure 4.13. Effect of GAG sulfation pattern of the hydrogel on the endothelial cell capillary morphogenesis at various VEGF loading. (A) Representative skeletonized images of endothelial vascular structures formed within the hydrogels containing GAG building blocks with varied sulfation degrees (33, 67, & 100 %) over three days. One image per condition was chosen arbitrarily to represent different hydrogel conditions. Fixed samples were stained with phalloidin and DAPI, and Imaris software was used to process and skeletonize the fluorescence images. (B) Total vessel area of the vascular structures. (C) The number of branch points of the endothelial network. Scale bar = 200 μm . Data represents mean \pm SD (n = 5-8 cultures), 'ns' stands for not significant, ** P<0.01, *** P<0.001, ****P<0.0001.

4.2.5 Spatial patterning of cellular activity within hydrogel matrices

4.2.5.1 Patterning of endothelial cell morphogenesis in response to angiogenic growth factor gradients

GAG binds to various positively charged growth factors, restricts their diffusive transport, and initiates a growth factor gradient in the ECM [215, 216]. Hydrogel prepared with the lowest GAG content and functionalized with a uniform distribution of VEGF could support a remarkable vascular network formation. To test the applicability of material to direct the spatial organization of endothelial cell tubular structures within the hydrogel, the VEGF was presented as a gradient using microfluidic devices as previously described [163]. The microfluidic platform contains three parallel channels for loading medium containing growth factors, the hydrogel precursors, and the medium alone.

To characterize the VEGF gradient's spatiotemporal profile, fluorescently labeled VEGF was loaded into one of the side channels and allowed to diffuse into the hydrogel for 72 H. The fluorescent images revealed the spatial differences in the fluorescent intensity across the hydrogel channel (**Figure 4.14A**). Immediately after adding growth factors into the source channel, significant protein accumulation was observed near the medium-gel interface. Even after the 72 H of the protein uptake, the gradient of VEGF remained visible. The simulation of the spatial and temporal profile of the VEGF gradient using the reaction-diffusion model revealed that the gradient only spans within the first 300 μm from the source of growth factors and remained stable throughout 72 H (**Figure 4.14B**). In good agreement with the simulation results, the fluorescent protein gradient spanned within the first half of the hydrogel channel from the source of growth factors. The gradient was not depleted after 72 H, although no medium flow was applied to the medium nor the growth factor channel (**Figure 4.14C**).

To examine the effect of the VEGF gradient on the spatial formation HUVEC tubular structure, HUVECs were embedded within the hydrogel and subsequently exposed to medium only, the gradient of VEGF, or homogenously distributed VEGF (**Figure 4.14D**). After three days of culture under these conditions, the

extent of vessel area near the sink channel, the source channel, as well as within the hydrogel channel were quantified (**Figure 4.14E**). As such, the hydrogel treated with the medium only did not support any vascular structures' formation. On the other hand, the hydrogels containing the gradient of VEGF supported a higher density of tubular structures toward the higher concentration of VEGF (**Figure 4.14F**). Moreover, when the VEGF was homogeneously distributed within the hydrogel, the extent of the tube-like structure formation in the source and sink area was comparable.

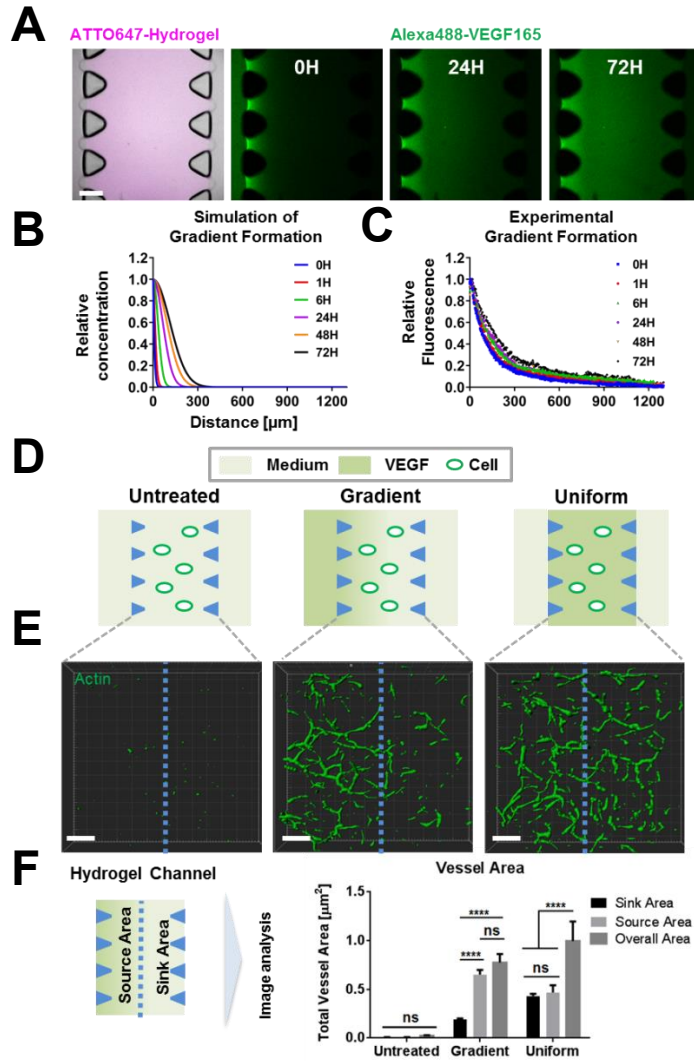


Figure 4.14. The gradient of VEGF modulates the spatial organization of endothelial cell vascular structures within the hydrogel. (A) fluorescence images representing the gradient of fluorescently labeled VEGF formed within the microfluidic device throughout 72 H. (B) The theoretical gradient profile of VEGF (C) The experimental gradient profile of fluorescently labeled VEGF. (D) The experimental set-up to investigate the effect of the VEGF gradient on the spatial organization of HUVEC vascular structures. The endothelial cells loaded within the hydrogel are either treated with no VEGF, the gradient of VEGF or homogenously distributed VEGF. (E) Skeletonized images of endothelial vascular structures resulting from VEGF treatment of different spatial presentations over three days. One image per condition was chosen arbitrarily to represent different hydrogel conditions. Fixed samples were stained with phalloidin and DAPI, and Imaris software was used to process and skeletonize the fluorescence images. (F) Quantification of the total area of HUVEC vascular structures at a different location within the hydrogel channel. The source area is defined as the half portion of the hydrogel channel closed to the VEGF source, whereas the sink area is defined as the half portion of the hydrogel channel closed to the medium channel containing no VEGF. Scale bar = 200 μm. Data represents mean ± SD (n = 3), ‘ns’ stands for not significant, ****P<0.0001.

4.2.5.2 3D chemotaxis of endothelial cells in response to angiogenic growth factor gradients

The formation of new vasculatures involves a series of steps initiated by the degradation of the ECM and followed by a directed endothelial cell migration toward non-vascularized tissues, cell proliferation, and the formation and stabilization of vascular lumens [217]. The VEGF is a potent chemoattractant that functions to modulate cell motility [218]. Herein, the effect of the VEGF gradient on the endothelial cell chemotaxis within the hydrogel was investigated. Two main conditions where the VEGF was either distributed homogeneously or presented as a gradient within the hydrogel were tested. As a control, the migration pattern of the HUVECs in the absence of VEGF was also examined. Accordingly, the HUVECs treated with the VEGF gradient displayed as strong chemotaxis toward the source of VEGF (**Figure 4.15A**). The HUVECs exposed to the VEGF gradient displayed a greater forward migration index (chemotaxis index) than the untreated cells or the ones treated with uniform distribution of VEGF (**Figure 4.15B**). In the presence of VEGF, the cells also migrated farther and more efficiently compared to the non-treated cells, as indicated by the higher directness and net migration distance and the lower accumulated distance.

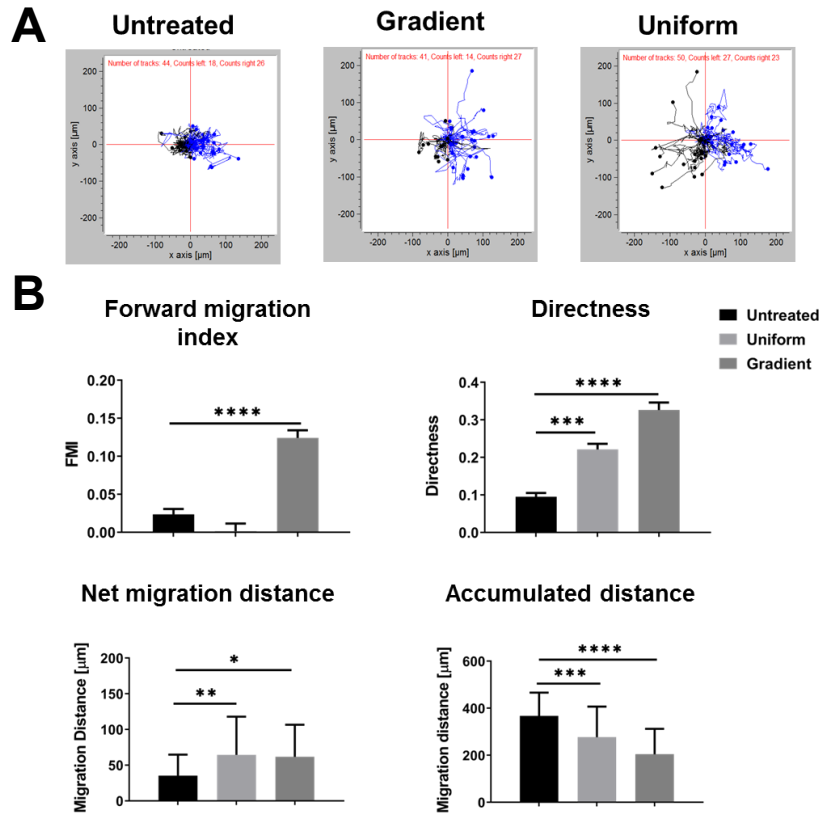


Figure 4.15. Endothelial cell chemotaxis in response to the VEGF gradient. (A) Representative trajectory plots of the HUVECs treated with various VEGF presentations. (B) Analyzed cell migration parameters, including a forward migration index, directness, net migration distance, and accumulated distance.

4.2.6 Discussion and summary

Strategies to maintain the stability of VEGF and the retention within polymeric biomaterials include covalent immobilization [23, 219], engineering growth factor variants with higher affinity for particular matrices [21], and incorporation of GAGs into the polymer networks [4, 6]. While the first two approaches might compromise the functionality of the growth factors, the later offers unprecedented options to control the bioactivity of VEGF due to the ability of the GAG to enhance protein stability and to facilitate the growth factor binding to the receptors [7, 22, 29, 54, 220-222]. However, maintaining a subtle balance of retention and cellular delivery of the growth factors can be crucial in determining the cell fate decisions. The fraction of free and bound factor within GAG-based material is determined by the affinity of growth factor to the GAG building block

and the total content of GAG within the system. Controlling the sulfation degree of GAG has been previously explored to modulate the growth factors' affinity and thereby determine the release from polymer networks [6, 38, 39]. However, the influence of the hydrogels' GAG content and GAG sulfation patterns on the bioactivity of gel-embedded VEGF was not yet determined.

In this part of the thesis, we investigated the role of GAG content and GAG sulfation patterns of the starPEG-GAG hydrogel system on the VEGF-mediated endothelial cell vascular morphogenesis [47]. Hydrogels with varied GAG content and GAG sulfation were prepared and characterized for their physical properties. Analysis of VEGF release from the hydrogel using a mathematical model revealed the VEGF transport dependency on the binding and diffusion of the molecules within the polymer network. Finally, mathematical modeling and HUVEC tubular morphogenesis studies in hydrogels with varied GAG content and GAG sulfation patterns revealed the relevance of free VEGF availability and specific GAG sulfation patterns on the formation of tubular structures of endothelial cells. Moreover, the VEGF gradient was shown to modulate the chemotaxis of endothelial cells and the spatial organization of the emerging tubular structures within the hydrogel.

The ability to tune the mechanical and biochemical properties of the scaffolds is essential to dissect the influence of GAG content as well as GAG sulfation patterns on the cell-fate control. The rational design concept has enabled the independent modulation of the starPEG-heparin hydrogels' mechanical properties from their heparin concentration and the GAG building block sulfation patterns [38, 39, 47, 79]. Supporting this finding, we could produce a set of soft hydrogels with varied GAG sulfation (**Figure 4.8**). Besides, for the first time, we demonstrated that the heparin content of the starPEG-GAG could also be tuned while maintaining their similar stiffness by merely adjusting the molar-ratio of starPEG to heparin of the hydrogel precursors. The capacity to decouple the GAG content and the GAG sulfation of hydrogels from the mechanical properties will broaden the applicability of the materials for dissecting their relevance on the organ or disease development such as cancer, in which the stiffness, GAG sulfation, GAG content of the ECM played essential roles [223].

The GAG volume density of hydrogels modulates the transport of signaling molecules. In the present study, we expanded the starPEG-GAG hydrogel system's tunability to allow for the formation of hydrogels with varied heparin concentrations. This strategy could further improve our hydrogel platform's versatility to control the diffusivity of signaling proteins at various levels. The effect of heparin content on the in-gel mobility of heparin-affine proteins, here as we demonstrated using the VEGF165, was also correlated with the release from the hydrogel matrices (**Figure 4.3 & Figure 4.9B**). Similarly, we have observed less VEGF released from the hydrogel as more heparin was incorporated into the hydrogel. In line with this finding, the modulation of the VEGF's retention and release rate from various hydrogels, including PEG-hyaluronic acid hydrogel matrices, and polycaprolactone-alginate scaffolds, could also be achieved by tuning the heparin content of the system [45, 77].

GAG sulfation patterns determine the affinity for signaling molecules, thereby, governs the transport of growth factors within GAG-based materials [38]. The N- and 6O- sulfate of heparin was known to a greater extent, mediate the binding of VEGF165 to heparin [190, 191, 193]. In line with this, the diffusivity of VEGF165 in the hydrogels containing 6O-DSH and 6ON-DSH was significantly higher compared to that in the hydrogels containing Hep (**Figure 4.4**). Furthermore, the degree of GAG sulfation inversely correlated to the amount of VEGF release from the hydrogel (**Figure 4.9C**). The hydrogel containing 6O-DSH significantly released more VEGF than that containing fully sulfated Hep. Furthermore, the VEGF release slightly increased when the hydrogel's GAG building block was changed from 6O-DSH to 6ON-DSH heparin, which further confirmed the importance of both 6O- and N- sulfate for the VEGF binding to heparin or heparin derivatives. Similarly, the influence of 6O desulfation of heparin on the VEGF release from the starPEG-GAG hydrogels of different crosslinking schemes has also been reported before [6]. However, no significant differences were observed between the release of VEGF from the GAG hydrogel containing 6O-DSH and 6ON-DSH. The discrepancy might be explained by the differences in the hydrogel thickness as well as the loading amount and entrapment procedures of VEGF, which could affect the initial distribution within

the hydrogel, the absolute amount of release, and the subsequent detection by the ELISA. Interestingly, only less than 10% of the proteins were released throughout 360 H from the hydrogel containing 6ON-DS despite the low sulfate content. The remaining negative charges on the GAG derivative due to the carboxylic acid and residual sulfate groups and the molar excess of GAG compared to the protein loading in the hydrogels (100: 1, GAG/ protein molar ratio) collectively might explain this observation.

A mathematical model could be instrumental in designing materials that achieve the desired rate of morphogen transport [32, 55], to precisely modulate cell fate decisions [30, 38]. Notably, the mathematical models have been previously applied to predict the transport characteristics of growth factors within GAG-based materials in the presence or the absence of matrix degradation [33, 53, 55, 57]. In most of these studies, the experimental release confirmed the impact of the heparin to growth factor ratio on the overall release of the growth factor. However, a direct comparison between the theoretical and the resulting experimental release was not presented. In this study, VEGF's release from the hydrogel with varied GAG content and GAG sulfation can be well described using a reaction-diffusion model. The decrease in the heparin sulfation resulted in a weaker interaction between the protein and GAG within the hydrogels. Besides, the estimated binding strength of the VEGF to the GAG crosslinked within the hydrogel was comparable to the value determined by the MST for the growth factor interaction with the linear GAG in solution (**Figure 4.9D**). This indicates the applicability of the model for the quantitative prediction of different GAG-binding proteins' transport by merely providing necessary input parameters. For example, the diffusion coefficient of the protein in the hydrogel as can be determined by molecular diffusion techniques, and the binding constant value (K_D) of the protein to the linear GAGs as can be measured using methods such as SPR [127], ITC [115], or BLI [117].

Apart from that, here, the mathematical model was also developed to investigate the transport of signaling molecules within biohybrid GAG-based hydrogels with predefined constituents. Therefore, it would allow us to precisely determine all possible molecular interactions between the growth factors and the gel

components (e.g., GAG units). In contrast, previous studies developed the model to predict the transport of signaling molecules in GAG-based biopolymer-derived matrices [33, 53, 55, 57]. In such matrices, the inherent affinity of the biopolymer components for a broad spectrum of growth factors [181], and their batch to batch variability would make it difficult to accurately estimate the strength of interactions between the factors and the GAG building blocks. Furthermore, to improve the accuracy of the model predictions in more complicated in vivo settings, we also envisioned considering parameters such as the competitive binding of serum-borne proteins to affinity ligands [58] and the altered GAG affinity after the chemical modifications [224] in our mathematical model.

In the context of VEGF administration, the GAG content of polymer networks determines the overall VEGF retention and the available amount that can stimulate the embedded cells. We hypothesized that only the unbound VEGF could bind to the endothelial cell surface receptor and subsequently trigger the VEGF-dependent vascular morphogenesis. Therefore, we applied the mathematical model to predict the amount of VEGF that forms a complex with the GAG and the one that freely diffuses within the hydrogel network.

Despite the high retention of VEGF ($\geq 90\%$) in all hydrogels containing heparin (**Figure 4.9**), only the hydrogel with the lowest heparin concentration displayed an extensive endothelial network formation (**Figure 4.12**). Based on our simulation results, the hydrogel containing 500 μM of heparin maintains the free VEGF concentration of about 170 pM for at least up to 3 days of culture without the supplementation of growth factor in the media (**Figure 4.11**). This concentration is comparable with the VEGF dose required to prime endothelial network formation in the standard tube formation assays (520 pM) [225]. The enhancement in the cellular delivery of free VEGF with decreasing GAG content of hydrogels probably played a significant role here since the concentration of bound VEGF in all hydrogels containing heparin was comparable and significantly higher than 260 pM (>117 nM, data not shown). However, out of our set of gels, only the material containing the lowest heparin content supported the vascular morphogenesis. (**Figure 4.12**). It is important to note that increasing VEGF loading in the hydrogel with the high or medium heparin content to 20

$\mu\text{g/mL}$ did not enhance vascular morphogenesis as much as in the hydrogel with the lowest heparin content despite the elevated free VEGF concentration. Heparin is known to promiscuously bind to various growth factors [7], probably the bioavailability of endogenously secreted factors that also regulate the vascularization was affected by the excess amount of heparin in the hydrogel with a medium or high concentration of heparin.

The effect of VEGF availability on the formation of tubular structures of HUVECs strongly depends on the specific GAG sulfation pattern. According to the simulation, complete removal of the heparin (as in the pure PEG/PEG gel) or the substitution of fully sulfated Hep with the 6ON-DSH could significantly increase the availability of free VEGF to a greater extent than in the hydrogel with 6O-DSH (**Figure 4.13**). However, we could not see a similar extent of endothelial tubulogenesis in these hydrogels. Heparin has been recognized to prolong the half-life of the heparin-binding proteins in culture by increasing their stability [26, 226]. Moreover, as previously demonstrated for heparin-binding BMP-2, N-DSH, and 6ON-DSH were not as effective as the native heparin in preserving the bioactivity of BMP-2 against thermal denaturation [227]. Therefore, we hypothesized that the N-sulfate group of heparin is essential to modulate vascular morphogenesis by maintaining VEGF activity. The capacity of the starPEG-GAG hydrogels to enhance the activity of VEGF could also explain the relatively low concentration of free VEGF required to stimulate endothelial vasculatures formation within these hydrogels. In particular, the hydrogel with the lowest heparin content could stimulate the endothelial cell vascular morphogenesis at a lower free VEGF concentration (~ 40 pM, data not shown) whereas in other hydrogel systems containing no growth factor sequestering moieties, a significantly higher VEGF concentration (≥ 50 ng/mL (1300 pM)) was required [66, 228, 229].

Finally, the ability to localize the VEGF activity to spatially control the formation of endothelial capillary-like structures was evaluated within the hydrogel with the lowest GAG content due to its superiority in supporting the vascular morphogenesis. Previously, spatial patterning of the vascular tube formation within the hydrogels could be achieved through light guided photocrosslinking

[230], and controlling the RGD ligand presentation [231]. In our study, we harnessed the natural capacity of the GAG to restrict the mobility of pro-angiogenic growth factors within the ECM [106, 107], to modulate the distribution across the polymer network. Simulation-based on the reaction diffusion-model enabled the prediction of the spatial and temporal distribution of VEGF within the hydrogels (**Figure 4.14B-C**). We have shown that presenting the VEGF as a gradient within the GAG-based hydrogel matrices allowed for the spatial control over the directed endothelial cell migration in 3D as well as the local formation of endothelial vascular structures within the hydrogels (**Figure 4.14D-F & Figure 4.15**). Further modulation on the hydrogel's transport properties, for example, through the use of GAG with different binding affinity to the VEGF, could modulate the gradient profiles within the hydrogels that further control the spatial organization of cellular fates. Moreover, the application of computational modeling to predict the transport of growth factors within hydrogels *in silico* can rationally guide the design of materials with precise regulation over the presentation of growth factors.

Overall, we have shown the impact of GAG content and GAG sulfation patterns of biohybrid hydrogels on cellular morphogenesis by modulating the local availability of signaling molecules. In the elaborated example, computational modeling allowed for the prediction of transport and bioavailability of VEGF within the biomaterials. The gained knowledge could further be applied for the precision engineering of GAG-based material for vascular tissue engineering and regenerative medicines.

4.3. Cell-instructive ternary hydrogel system with variable GAG content

4.3.1 Introduction

Soluble signaling molecules control a diverse range of cellular responses and orchestrate the formation of tissues and the developmental processes [20]. In particular, pro-angiogenic growth factors stimulation is essential for the physiological formation of *in vivo* vasculatures [232]. Therefore, engineering delivery strategies that could sustainably maintain their local concentration within a therapeutic window could be instrumental for therapeutic vascularization or vascular tissue engineering [65]. Glycosaminoglycan-based hydrogel offers unprecedented options to modulate the retentions as well as the activity of pro-angiogenic factors due to the ability of GAGs to reversibly bind positively charged surface patches of the growth factors through electrostatic interactions [25, 26] (**Figure 4.16A**).

Recent progress in tuning the administration of pro-angiogenic growth factors within the GAG-based polymeric network has been made to precisely modulate cellular responses [4-6, 19]. For example, Zieris et al. varying the initial growth factor loading of the starPEG-heparin hydrogel to control the release of VEGF and FGF-2 from the hydrogel matrices [5]. In related work, a matrix-metalloproteinases cleavable peptide has been incorporated into the hydrogels to mediate polymer network degradation in response to cell-secreted proteases, which could further enhance the growth factor release [19, 50]. More recently, selectively desulfated heparins have also been applied to modulate various growth factors' binding affinity to the GAGs and control their release from the scaffold [6, 38, 39, 78]. The tunable release can be achieved either by adjusting the local sulfate density of the GAG or the overall hydrogel sulfate content [6]. However, removing a specific sulfate group from the GAG might affect the activity of the molecules to stabilize various GAG-binding proteins [227]. Besides, the chemical procedures to selectively remove specific sulfate group of the GAG was also complicated [227].

Incorporating a graded amount of fully sulfated GAG into the cell-instructive polymer networks can be applied as an alternative strategy to modulate the binding, as well as the transport of pro-angiogenic growth factors. Besides, simulation using the reaction-diffusion model described in **section 4.1.5** also revealed that adjusting the hydrogel's GAG content is the most effective strategy to control the release of GAG-affine proteins from the hydrogel matrix. Notably, modulation of the retention and release rate of heparin-affine proteins from various hydrogels, including PEG-hyaluronic acid hydrogel matrices [43], and polycaprolactone-alginate scaffolds [45], has been demonstrated by tuning the amount of incorporated heparin. Despite the effectiveness of this approach to achieve a tunable release of the growth factor, the ability to decouple the GAG content from the mechanical properties of GAG-based biomaterials is often difficult to achieve, especially when the GAG is used as the major building block of the scaffold [47, 233, 234]. In such a system, producing a hydrogel with a low GAG content is limited by the minimum solid content for the hydrogel crosslinking reaction to occur.

To address this challenge, here we developed a set of ternary GAG-based materials with a precise adjustment over GAG content to control the administration of pro-angiogenic growth factors. The materials were formed by extending a previously established binary GAG-based hydrogel synthesis protocol [47]. Specifically, the hydrogel was prepared by combining thiol-terminated starPEG units, maleimide-functionalized GAG, and maleimide-terminated starPEG units in different ratios through a Michael type addition crosslinking scheme to freely modulate the heparin content over a broad range of gel stiffness (**Figure 4.16B-E**). In this study, the hydrogel materials with varied heparin content were thoroughly characterized for their network and transport properties, as well as the applicability of the matrices to support endothelial cell vascular morphogenesis. Besides, the GAG content of the hydrogel was also tuned to modulate the gradient of GAG-affine proteins. Overall, the new GAG-based materials that we developed here could pave a new way to precisely control the administration of pro-angiogenic growths rationalizing their future applications as advanced 3D cell culture platform and tissue engineering matrices.

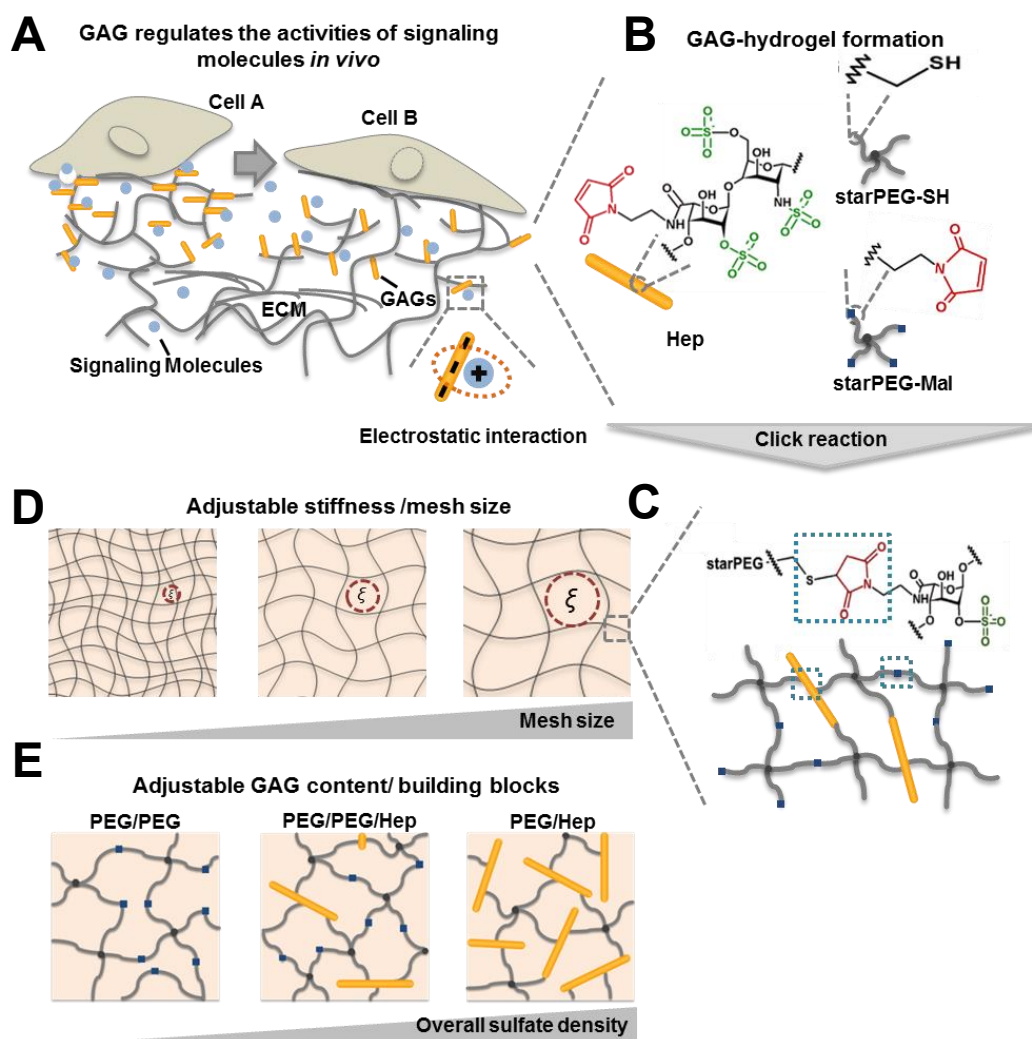


Figure 4.16. Ternary GAG hydrogel systems with tunable GAG content and mechanical properties. (A) In the extracellular matrix (ECM), cellular fate is controlled by the GAG's ability to modulate the presentation of signaling molecules through electrostatic complexation. (B) The building blocks of ternary hydrogel systems consist of thiol-functionalized starPEG, maleimide-functionalized starPEG, and maleimide-functionalized GAG. (C) The network of ternary hydrogel systems formed by Michael-type addition (click) reaction between the thiol and maleimide terminated polymers. (D) The stiffness/ mesh size of the hydrogel can be customized by adjusting the overall solid content or the molar ratio of thiol to maleimide-containing polymers. (E) The GAG content/ overall sulfate density of the gel can be varied while maintaining a comparable gel stiffness by adding an appropriate amount of starPEG-Mal.

4.3.2 Physical properties of ternary hydrogels

Rational design strategies of the binary starPEG-heparin hydrogel have enabled the development of hydrogel materials with a stiffness in the range of 0.2-8 kPa at a relatively invariant heparin content of 1500 μM [47]. To further modulate the transport of signaling molecules, binary hydrogels with a heparin concentration in the range of 500-1500 μM were formed by altering the solid content and crosslinking degree of the hydrogel. However, as we decreased the heparin content of the hydrogel, a more crosslinking degree (ratio of starPEG-SH to heparin) was required to initiate the gel formation (**Figure 6.8**). For example, 200 Pa hydrogel with a heparin concentration of 1500 μM could be formed at a crosslinking degree of 0.63. In contrast, a comparably stiff hydrogel with a heparin concentration of 500 μM was formed only at a higher crosslinking degree of 1.5. Furthermore, we did not observe gelation at heparin concentration below 500 μM because of the low solid content of the reacting solution ($< 2\%$).

We included starPEG-Mal as the third component of the ternary hydrogel to maintain a similar solid content between different gel preparations allowing us to decouple mechanical properties and heparin content of the hydrogels (**Figure 4.17A**). Accordingly, hydrogels with heparin content of 0-1500 μM can be prepared with variable stiffness in the range of 0.2-4 kPa by merely adjusting the total solid content. Interestingly, hydrogels with similar stiffness but varied in their heparin content displayed a similarity in the volumetric swelling with a softer hydrogel swells relatively more than the stiffer ones. (**Figure 4.17B**).

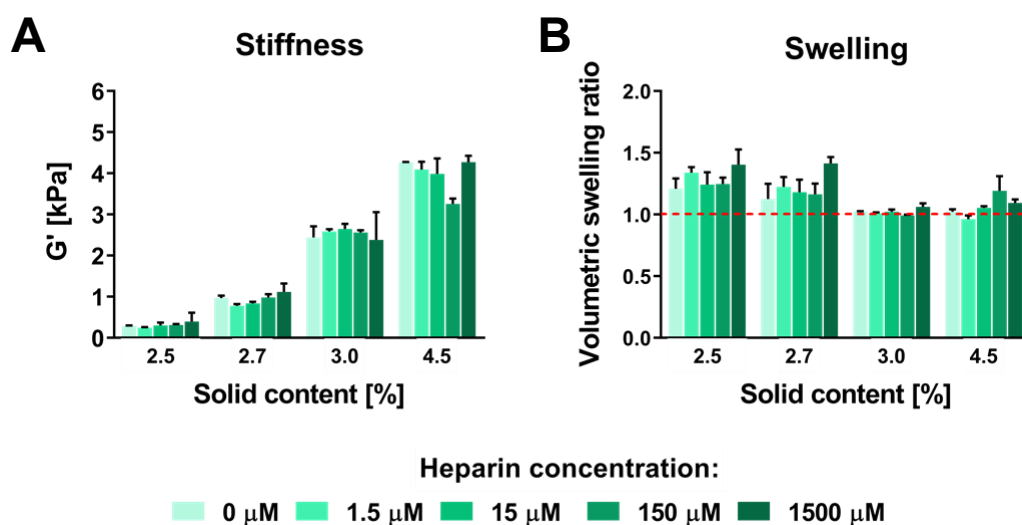


Figure 4.17. The physical properties of ternary hydrogels with variable GAG content. (A) The Stiffness and (B) the volumetric swelling of the hydrogel at various solid content.

4.3.3 Mobility of heparin affine proteins within- and the release out of ternary hydrogels

The in-gel mobility of heparin affine proteins (VEGF165 and SDF1 α) within the ternary hydrogels with varied heparin content was investigated using FRAP. It is hypothesized that as the heparin content of the hydrogel decreases, more unbound proteins exist, resulted in the enhancement of the mobility of affine proteins. FRAP measurements were carried out in the hydrogels with the stiffness of ~ 2.5 kPa. Based on the rubber elasticity theory [2], hydrogels prepared with this stiffness were estimated to have a mesh size of 10 nm, which is significantly larger than the molecular size of the VEGF165 and SDF1 α . The similarity in the stiffness of the hydrogels containing variable heparin content also allowed for the dissection of the effect of heparin content on the mobility of these proteins independently from the impact of steric interaction within the polymer network (**Figure 4.18A-B**).

In general, the mobility of large and small heparin affine proteins was affected by the hydrogels' heparin volume density (**Figure 4.18C**). For example, VEGF diffusivity increased from $\sim 4 \mu\text{m}^2/\text{s}$ in the hydrogel with the highest heparin content to nearly $20 \mu\text{m}^2/\text{s}$ in the hydrogel with the lowest heparin concentration.

4. RESULTS AND DISCUSSION

Interestingly, the effect of decreasing the heparin content of hydrogels was more pronounced on the mobility of SDF1 α as compared to the VEGF165. The mobility of SDF1 α was raised by ~15 factors in the hydrogel with the lowest heparin content, whereas the mobility of VEGF165 increased by only five factors. The lower steric interaction might explain that the small affine protein diffused faster than the larger ones in the hydrogel with the lowest heparin content. Similarly, as shown in pure PEG-PEG gels, which show a minimum protein binding, the diffusivity of SDF1 α was significantly higher than the VEGF165.

The effect of varying GAG content of hydrogels on protein release was also investigated (**Figure 4.18D**). The release of VEGF165 and SDF1 α from the PEG/PEG gel displayed a burst release and reached a maximum after 24 hours. Interestingly, no additional protein release was observed even after 360 H. The release of both proteins from the pure PEG/PEG gel also did not reach 100%. Nearly only 50% and 85% of the VEGF165 and SDF1 α , respectively, was released from the gel constructs after 360 H.

Incorporating a graded amount of heparin into the hydrogel modulated the release of VEGF165 and SDF1 α . In the hydrogel with the highest heparin content (1500 μ M), only less than 1% of the VEGF165 or SDF1 α was released after two weeks. In contrast, the hydrogel with the lowest heparin (1.5 μ M) content significantly released a higher amount of proteins, with nearly 20% of the proteins was released within the same period.

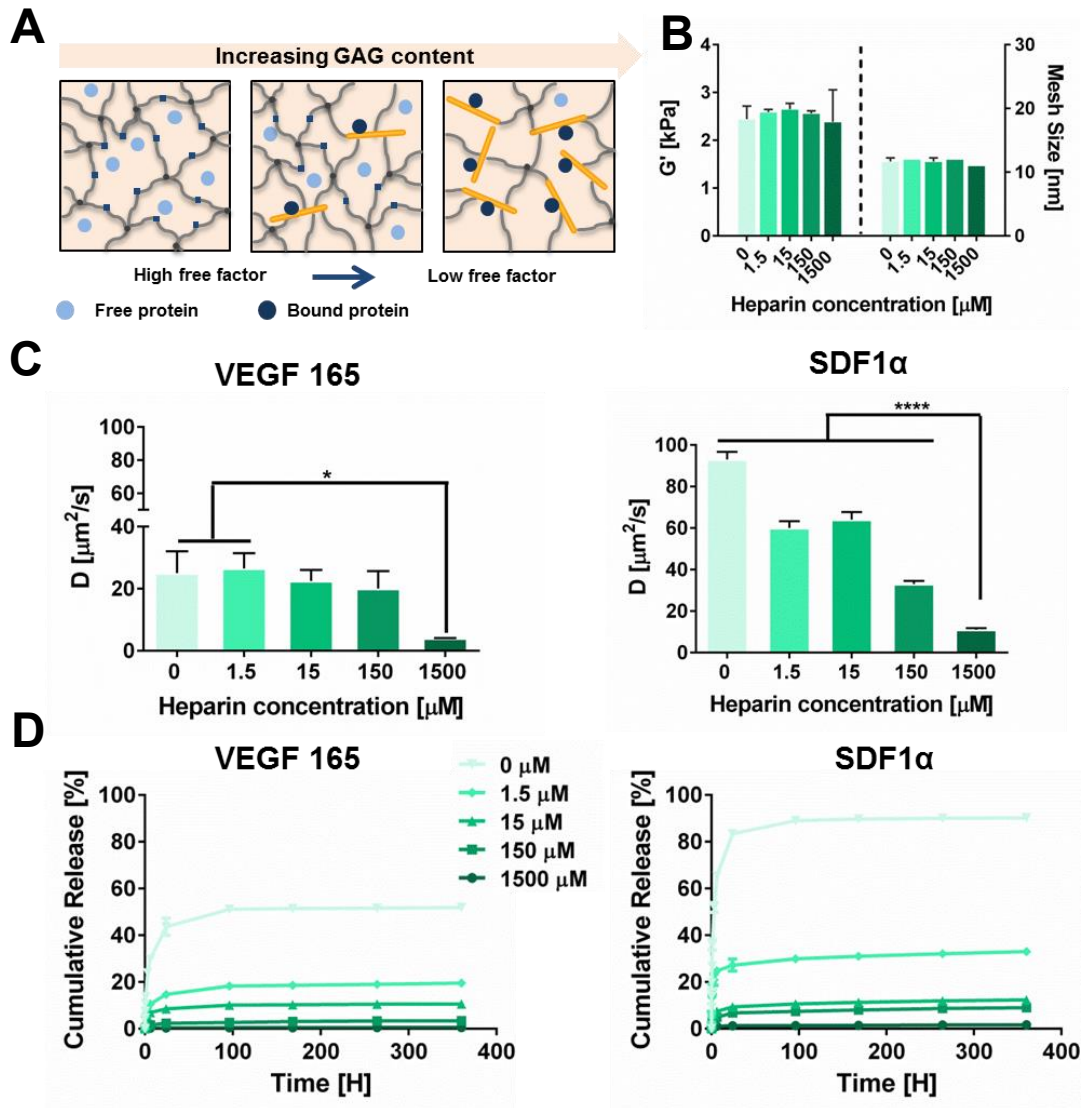


Figure 4.18. The GAG content of ternary hydrogels modulates the in-gel mobility and release of GAG-affine proteins. (A) A schematic illustrating the effect of GAG content of ternary hydrogel on the free protein concentration within the hydrogel network, which positively correlates to the diffusivity of proteins. (B) Comparable stiffness/ mesh size of ternary hydrogel with varied heparin content (C) The diffusion coefficient (D) of VEGF165 and SDF1 α within the hydrogels with different heparin content as determined by FRAP. (D) The release of VEGF165 and SDF1 α from ternary hydrogel with varied heparin content. Data represents mean \pm SD (n = 3), ‘ns’ stands for not significant, *P<0.5, ****P<0.0001

4.3.4 The gradient of signaling molecules within ternary hydrogels

The ability of GAG hydrogels to modulate the gradient of signaling molecules with different properties was evaluated using a microfluidic platform. Accordingly, the gradient of large or small heparin-affine proteins could be maintained stably over 48 H without a continuous replenishment of growth factors (**Figure 4.19A**). Fluorescent microscopy revealed that the heparin-affine proteins were mostly accumulated near the hydrogel and growth factor channel interface. The resulting gradient was steep and only spanned across half of the gel channel even after 48 H (**Figure 4.19B**). In opposite to these observations, the gradient of non-affine EGF was depleted quickly. In less than 6 H, the protein already reached an equilibration within the hydrogel. Interestingly, although the VEGF121 did not have an affinity toward heparin, the gradient could still be observed after 48 H. However, the gradient profile spans at a much broader range than those of the affine proteins.

The experimental gradient profile of proteins within the GAG hydrogel was also compared with the simulation-based on a reaction-diffusion model (**Figure 4.19B**). In good agreement with the theoretical modeling, the gradient of affine proteins was developed quite slowly and only spanned near the growth factor's source. Based on the simulation, the gradient of SDF1 α and VEGF165 only developed within the first 600 μm and 300 μm , respectively, from the hydrogel channel over 48 H.

Similarly, the gradient of non-affine proteins can also be approximated using the same model by only considering the free diffusion coefficient within the hydrogel. In particular, the EGF was shown to diffuse rapidly into the hydrogel, and the gradient was nearly depleted after 6 H of the protein uptake. In line with the experimental data, a similar EGF gradient profile can be predicted accurately using theoretical modeling. In contrast, the experimental gradient of VEGF121 could not be described with the simulation results. Experiment results showed that the gradient of VEGF121 evolved slowly and remain visible after two days. Based on the model prediction, the gradient of VEGF121 should have only lasted for less than 24 H due to the minimal interaction with the heparin. However, dynamic

light scattering analysis showed the formation of VEGF121 aggregates with a size up to a few μm shortly after the dilution in the medium (**Figure 6.9**). The protein aggregations might retard the diffusion of VEGF121 from the source to the sink channel. Hence, as the hydrogel's mesh size was within the range of nm, μm -sized aggregate remained to persist in the hydrogels and visible as a stable gradient.

In an attempt to modulate the spatiotemporal profile of heparin affine protein gradients in the hydrogel, the heparin content of ternary hydrogels was varied from 0-1500 μM (**Figure 4.20**). In the absence of heparin, both VEGF165 and SDF1 α diffused rapidly into the hydrogel and formed a gradient that lasted only for a few hours (**Figure 4.20A**). Nearly after 6 H of the protein uptake, the gradient of proteins was utterly depleted. Remarkably, the gradient of affine proteins could be gradually adjusted by increasing the hydrogel's heparin content with a shorter-range, and a steeper gradient profile was observed as more heparin was loaded into the hydrogels. The stability of gradients was also varied with increasing heparin content. Time-lapse microscopy demonstrated that the hydrogel with the heparin content of 15 μM maintains a long-range gradient of heparin affine proteins that lasted for up to 24 H (**Figure 4.20B**). In contrast, hydrogels with heparin content of 150 μM or higher could stably maintain a short-range gradient of the growth factors even up to 48 H.

Mathematical modeling was also applied to predict the gradient of heparin-affine proteins in a set of hydrogels with a graded amount of heparin after 48 H of the protein uptake (**Figure 4.20B**). While the gradient of VEGF165 in all hydrogels preparations was in good agreement with the simulation, the experimental gradient of SDF1 α exhibited a slightly different profile from the simulated ones, especially for the hydrogel with a heparin content of 150 and 15 μM . In contrast to the model prediction, the experimental gradient of SDF1 α in these hydrogels displayed a steeper profiler and evolved more slowly. This discrepancy might indicate protein aggregations, which could be affected by the intrinsic properties of proteins, as this case was not observed for the VEGF165.

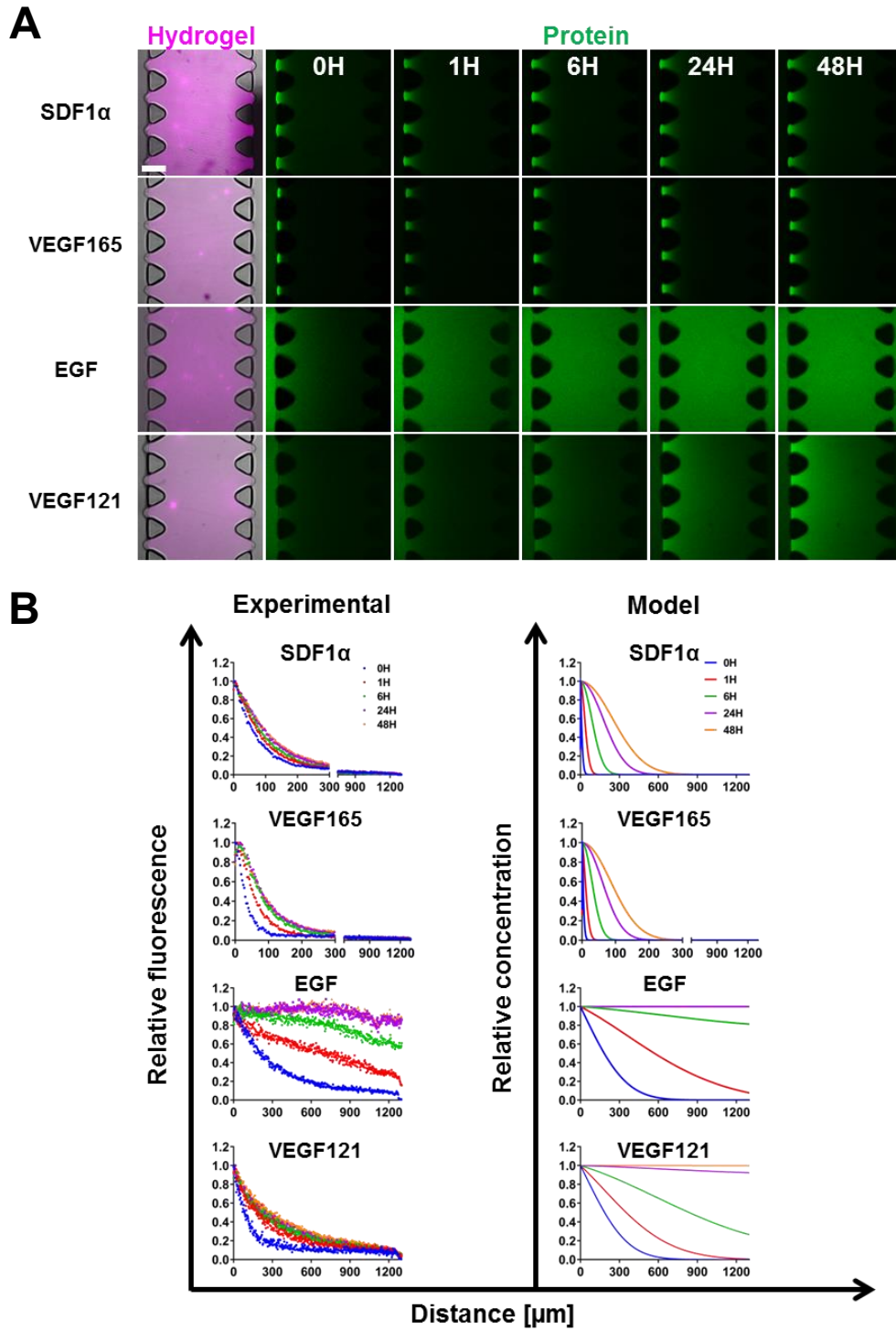


Figure 4.19. The gradient of signaling molecules with different molecular sizes and affinity to the GAG. (A) Fluorescence images representing the gradient of various fluorescently- labeled proteins (SDF1 α , VEGF165, EGF, and VEGF121) established using the microfluidic device within the hydrogel containing 1500 μ M of heparin throughout 48 H. (B) The theoretical and experimental gradient of proteins within the hydrogels after 48 H.

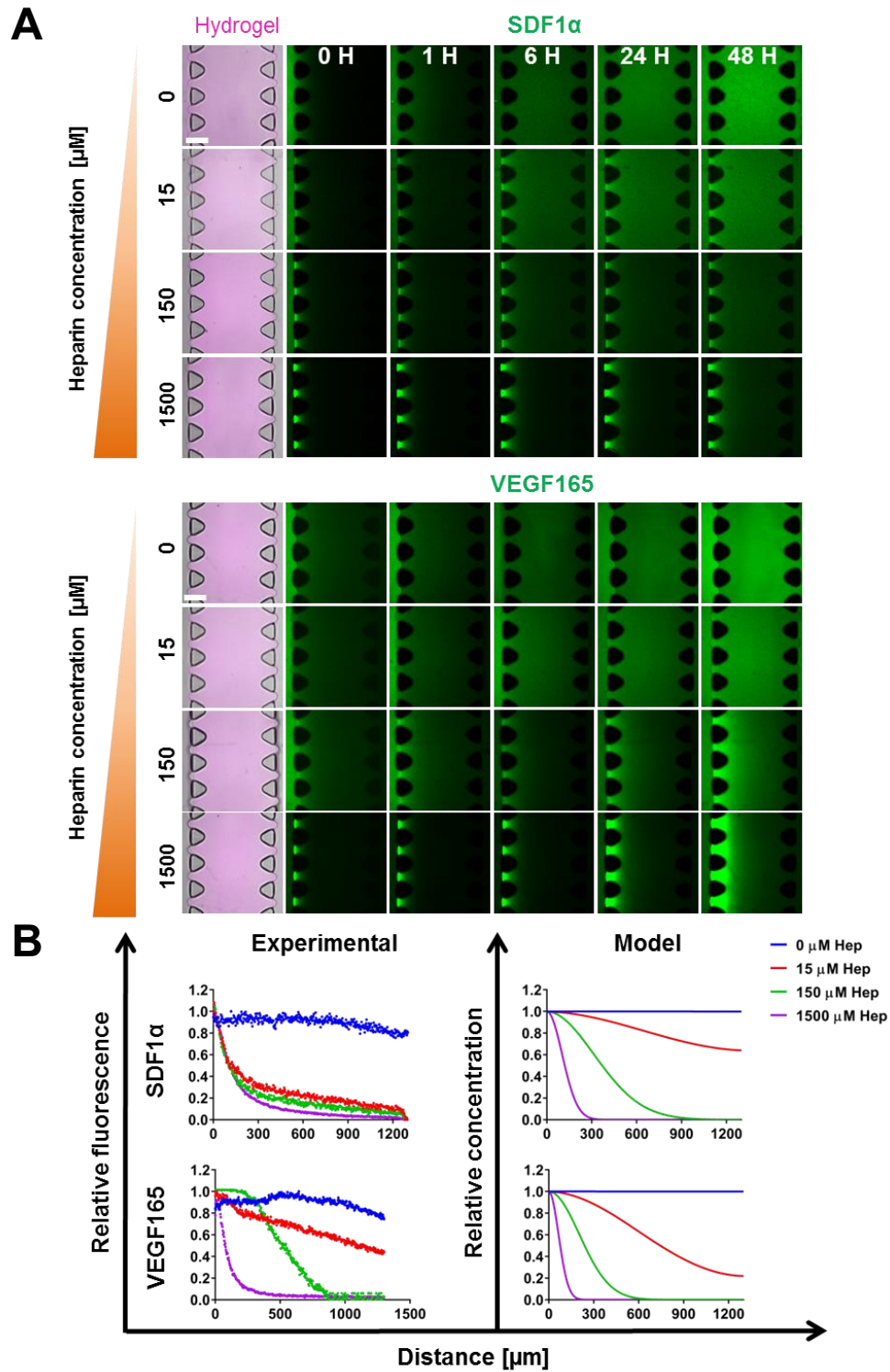


Figure 4.20. The GAG content of ternary hydrogels modulates the gradient of GAG-affine proteins. (A) Fluorescence images representing the gradient of various fluorescently- labeled proteins (SDF1 α , VEGF165, EGF, and VEGF121) established using the microfluidic device within ternary hydrogels containing 0-1500 μ M heparin throughout 48 H. (B) The theoretical and experimental gradient of proteins within the hydrogels after 48 H.

4.3.5 Endothelial cell capillary morphogenesis within ternary hydrogels

Previously, the binary GAG-based hydrogel has been shown to support endothelial cell vascular morphogenesis *in vitro* [3]. Here, we also evaluated the applicability of ternary hydrogels for the 3D culture of endothelial cells. HUVECs cultured in ternary hydrogels with heparin content of 0-500 μM initiated the formation of capillary-like structures approximately three days after the cultures (**Figure 4.21A**). The variation in the heparin content of hydrogels was shown to modulate the vascular morphogenesis within these hydrogels. Accordingly, ternary hydrogels containing 5 μM of heparin promoted a more extensive vascular structure formation than ones functionalized with 50 μM of heparin or higher (**Figure 4.21B**). Moreover, this gel also induced a higher vascularization in comparison to the pure PEG hydrogel control.

The extent of vascular morphogenesis in the ternary hydrogels was also compared to the binary gel containing 500 μM heparin. HUVEC tubular structures were observed in ternary gels with variable heparin volume density. However, HUVECs formed a larger total vessel area in the binary hydrogel with 500 μM heparin than the ternary hydrogels with any heparin content tested. As a result, future works may aim to optimize other parameters of the ternary gel network, such as the molecular weight of the PEG component, to enhance the vascularization of the hydrogels.

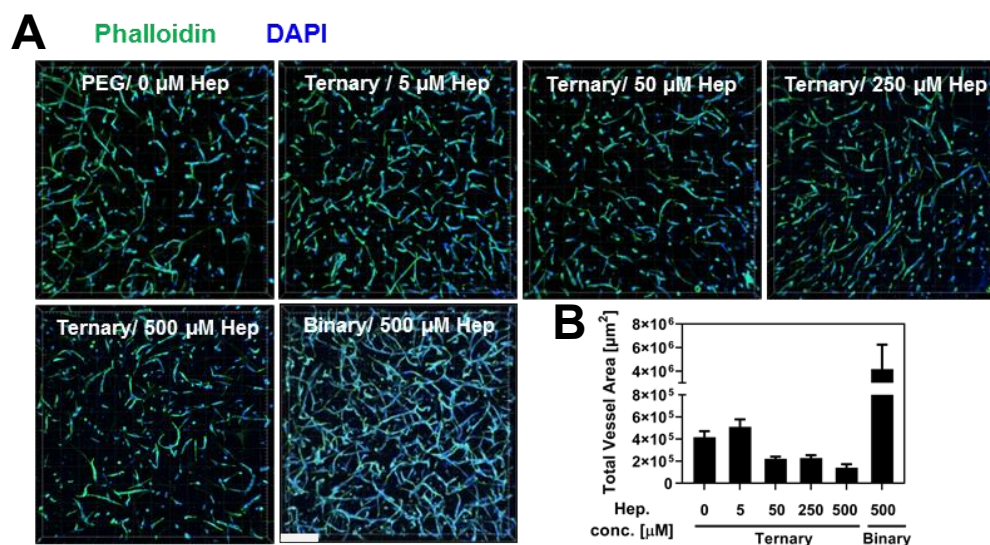


Figure 4.21. The ternary hydrogel system supports endothelial cell vascular morphogenesis. (A) Capillary-like structures of endothelial cells formed within the hydrogels containing varied heparin concentrations after three days of culture. One image per condition was chosen arbitrarily to represent different hydrogel conditions. Fixed samples were stained with phalloidin and DAPI. After the confocal imaging, Imaris software was used to process and analyze the fluorescence images. Scale bar = 200 μm . (B) Total vessel area of the endothelial cell vascular structures.

4.3.6 Discussion and summary

Tissue formation is a complex process involving the interplay between physical and biomolecular cues of the extracellular matrix [235]. In particular, the *in vivo* formation of blood vessels requires the cell-instructive signals provided by pro-angiogenic growth factors [209, 236, 237]. Various strategies have been developed to control the administration of pro-angiogenic growth factors to stimulate the vascularization of diseased tissues or engineered living matters [45, 219, 238-240]. However, in the field of tissue engineering, maintaining a sustained delivery of bioactive growth factors remained challenging.

To overcome this, polymeric biomaterials have been exploited to incorporate glycosaminoglycans (GAGs) to maintain the sustained delivery and long-term bioactivity of growth factors [25]. Various GAG-based hydrogels have been developed for the controlled administration of pro-angiogenic growth factors [4, 6, 46, 77, 137, 239, 241-243]. In general, network properties of the system,

including the GAG content, sulfation pattern of the GAG building blocks, degradability of the network, as well as the growth factor loading concentration, could be adjusted to modulate the retention and release. Nevertheless, no studies have reported the development of GAG-based materials with tunable mechanical properties over a broad range of GAG concentration.

In this study, the ternary hydrogel system based on the heparin-maleimide, starPEG-maleimide, and starPEG-thiol, was developed by extending our previously established binary hydrogel platform [47], to precisely customize the administration of pro-angiogenic growth factors. The hydrogel with tunable mechanical properties was developed to incorporate heparin in the concentration range of 0-1500 μM (**Figure 4.17**). Tuning the heparin content of hydrogel was shown to modulate the in-gel mobility and release of pro-angiogenic growth factors as well as the formation of gel-based growth factor gradients. Moreover, the system was also shown to support endothelial cell morphogenesis.

Previously, hydrogels with variable GAG content have been developed to control the administration of soluble signaling molecules [48, 137, 244-246]. Nevertheless, in most studies, the influence of heparin content on the overall network properties of hydrogels was not investigated. In this study, rational design strategies have been successfully applied to developed ternary hydrogel system with variables GAG content and tunable mechanical properties. Compared to the previously established binary hydrogel system [47], the ternary system allowed for the formation of hydrogels at much lower heparin concentration while retaining tunable mechanical properties.

The ability to tune the mechanical properties of the materials independently from the heparin content is particularly beneficial for investigating the effect of heparin content on the cellular process in which the matrix stiffness plays a significant role. For example, osteogenic differentiation of mesenchymal stem cells was primarily induced by a stiff substrate, whereas neurogenic differentiation occurs on a more compliance matrix [247]. Similarly, GAG-based hydrogels might be applied to stimulate vascularization in tissues with different stiffness. The design of a controlled release system with mechanical properties matching to the

implantation sites could minimize foreign body responses and rejection of implants [248]. Therefore, ternary hydrogels with a programmable heparin content and mechanical properties could provide precise delivery of pro-angiogenic factors while minimizing deleterious immune responses.

Modulating the heparin content of the ternary hydrogel was shown to control the mobility of heparin-affine proteins within hydrogel networks and the release out of the matrices (**Figure 4.18**). The burst release of SDF1 α and VEGF165 could be attenuated through the incorporation of $\sim 1.5 \mu\text{M}$ of heparin ($\leq 1\%$ of the hydrogel polymer content). Besides, the sustained release of growth factors can be achieved for at least over two weeks, which is in line with previous findings [43, 45, 77]. Other than adjusting the heparin content, incorporating heparin with different molecular weight and sulfation patterns may further be applied to tailor the release of heparin-affine proteins from the ternary hydrogel network [6, 38, 43].

The ability to tune the heparin content of ternary hydrogels over a wide range is essential to precisely customize the hydrogel network relevant for particular applications. For example, the hydrogel containing a low amount of heparin is suitable more as a controlled release system of growth factor, whereas those contain a high amount of heparin could rather be applied as cytokine scavenging materials [7]. Furthermore, local as well as overall sulfate density of the hydrogel may also be adjusted to control the binding of cytokines with different properties [78].

Soluble signaling gradient is essential to regulate various physiological processes, including cell migration, homeostasis, angiogenesis, and development [249]. Therefore, various strategies such as source-sink methods have been developed to recapitulate the formation of biomolecular gradients in engineered biomaterials for studying such process *in vitro* [250, 251]. The resulting gradient could be maintained stably for a long period, such as through the covalent immobilization of growth factors or flow applications [252, 253]. However, such approaches could compromise the protein functionalities and may be expensive due to the requirement to continuously perfuse the growth factor feeding solution.

In this study, the glycosaminoglycan-based hydrogel was utilized to generate signaling molecule gradients by harnessing the natural affinity of GAGs to various cationic growth factors. The hydrogel could stably maintain the gradient of heparin-affine proteins but not the non-affine proteins for at least 48 H (**Figure 4.19**). Here, the ternary hydrogels with varied heparin content subsequently allowed for the modulation of the gradient of heparin-affine proteins. Notably, decreasing the heparin content of hydrogel was shown to change the resulting profile of protein gradient from a steep and short-range toward a shallow and long-range (**Figure 4.20**). Besides, computational modeling based on the reaction-diffusion model has also been developed to predict the establishment of growth factor gradient within hydrogels. The parameter of the model, such as the GAG content, affinity of growth factor to GAG building blocks, and the geometry of hydrogel, can be adjusted to allow for the prediction of the growth factor gradient profile under various scenarios.

Finally, the capacity of ternary hydrogel matrices to support 3D cultures of endothelial cells was examined (**Figure 4.21**). The ternary hydrogel was shown to be cytocompatible, as demonstrated here, by the ability to promote endothelial cell morphogenesis. The concentration of heparin within hydrogels needs to be rationally adjusted to maintain high retention and bioactivity of growth factors within the polymer matrix while at the same time could still provide an adequate amount of free factors to stimulate cellular responses. We have shown that the hydrogels containing heparin as low as 5 μM induced a greater extent of vascularization than those with higher heparin concentration or pure PEG hydrogel. The gel matrix's functionalization with 1.5 μM of heparin was sufficient to maintain 80% of growth factor retention within the polymer network for several days. Moreover, as shown in **section 4.2**, the presence of a low concentration of heparin could sufficiently maintain a high concentration of free growth factor within the hydrogel. Therefore, we speculate that the superiority of ternary hydrogel containing 5 μM of heparin could be attributed to the balance of local retention and availability of the free factor, as well as the preservation growth factor activity within the scaffold.

Nevertheless, the ternary gel containing 5 μM of heparin could not support a similar vascularization as much as the binary hydrogel with 500 μM of heparin, despite the elevated free factor concentration. Parameters other than the free factor concentration may play a more critical role in regulating the vascular morphogenesis within the hydrogels. For example, the inclusion of starPEG–Mal in the ternary hydrogel might increase the local physical constraints and decrease the degradability of the polymer network. Besides, biopolymer-derived matrices with known angiogenic properties, such as collagen and fibrin gels, consist of components with a large molecular weight (≥ 70 kDa), allowing the creation of a matrix with a larger mesh size in comparison to our gel system with a smaller PEG (10 kDa) as the major building block [254-257]. Therefore, future studies can potentially be done to investigate the effects of polymer molecular weight on the extent of capillary structure formation within the hydrogel. In particular, systematic approaches using the design of experiment (DOE) to simultaneously analyze different combinations of ternary hydrogel network parameters [258, 259], might be utilized to identify matrix conditions that promote the formation of endothelial vascular structures.

In conclusion, we have developed the ternary hydrogel system, which is tunable for the mechanical properties over a broad-range of heparin content. The modulation of the gel's heparin content was shown to be superior for controlling the administration of heparin-affine pro-angiogenic growth factors. Combining rational design strategies to tune the hydrogel network and mathematical modeling for predicting the transport of signaling molecules, we could potentially apply the resulting materials as versatile tissue engineering matrices and advanced 3D cell culture platforms.

5. General discussion

5.1 Summary and conclusion

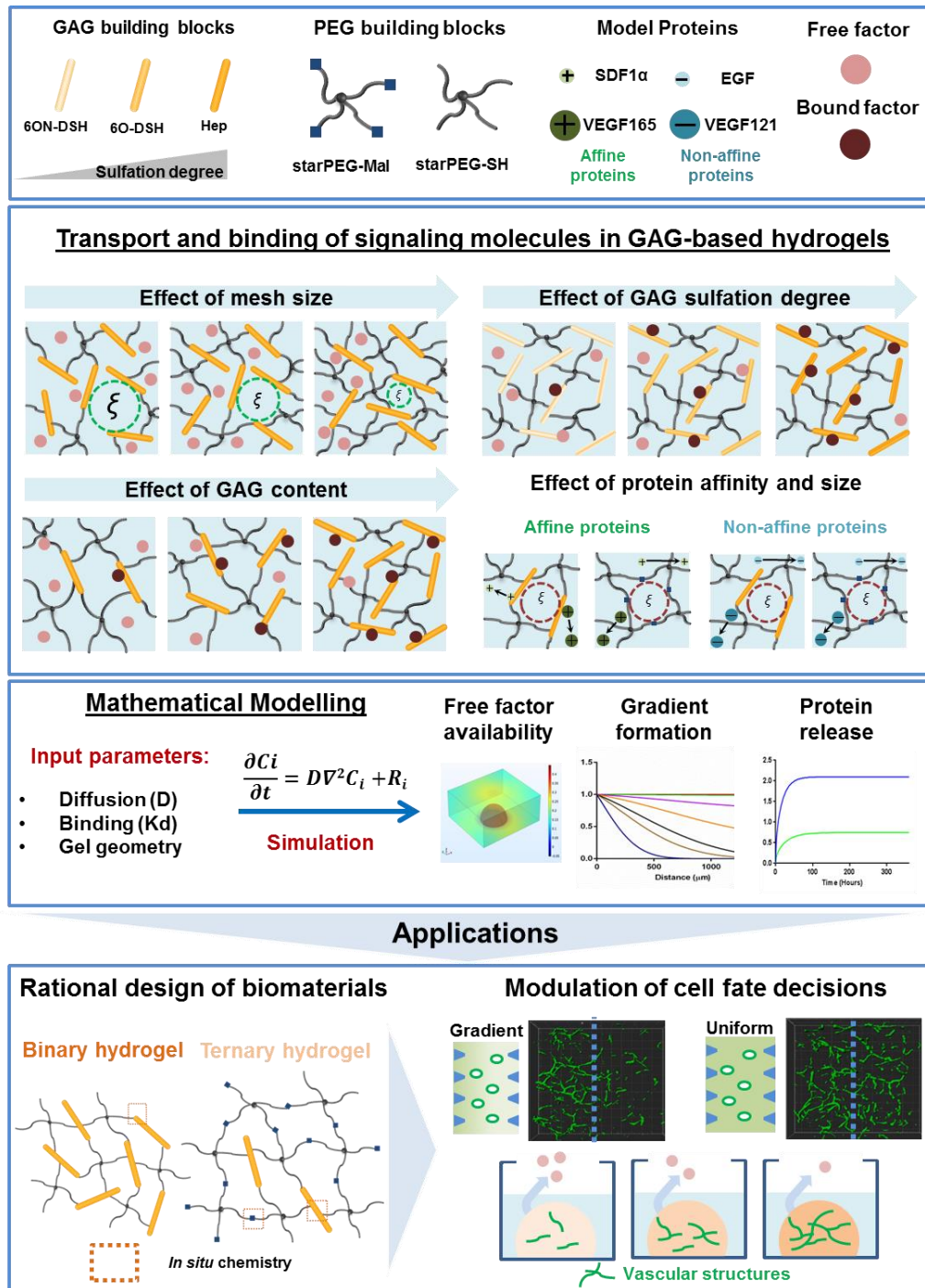


Figure 5.1. A systematic study of the mobility of signaling molecules and the mathematical modeling rationally guide the design of GAG-based biomaterials to precisely modulate the cell fate decisions.

This thesis aimed to systematically investigate molecular transport and binding of signaling molecules with different properties in a binary starPEG-GAG hydrogel system [47], by combining mathematical modeling and experimental approaches. The fundamental principles underlying the transport properties of the signaling molecules were then applied to modulate the morphogenesis of endothelial cells into vascular structures within the hydrogel and rationally design a set of GAG-based materials with tunable network properties that could significantly enhance the current state of the art for the modulation of the hydrogel-based administration of pro-angiogenic growth factors.

5.1.1 Molecular transport and binding in the starPEG-GAG hydrogels

Understanding the molecular transport and binding of various signaling molecules within the starPEG-GAG hydrogels is essential for the rational design of the material to control the formation of cell-instructive gradients and the local morphogen concentration (**Figure 5.1**). Many studies have investigated the impact of GAG hydrogel network parameters, including the mesh size, GAG content, and the GAG sulfation on the mobility of growth factors relevant for particular applications [4-6, 43]. However, none of them has systematically investigated the influence of each parameter on the mobility of the signaling molecules of different properties.

To address these issues, we first investigated the impact of mesh size, GAG-content, and the sulfation pattern of GAG building block of the binary starPEG-GAG hydrogels on the mobility of representative signaling molecules that differ in their molecular weight and GAG-affinity including the VEGF165 (MW 38.2 kDa, pI 8.3), VEGF121 (MW 28 kDa, pI 6.4), SDF1 α (MW 8 kDa, pI 10), and EGF (MW 6.2 kDa, pI of 4.6) (**Section 4.1**). Rational design strategies for polymer networks have enabled the decoupling of mechanical properties (stiffness, mesh size) from bimolecular characteristics (GAG content and the GAG sulfation pattern) of the hydrogel, allowing for the investigation of the influence of each hydrogel network parameter on the mobility of the signaling molecules independently. *Molecular diffusion studies revealed that the mobility of GAG-affine proteins is primarily controlled by the GAG content and of GAG*

sulfation pattern, whereas the mobility of non-affine proteins is governed by the mesh size of the hydrogel. Together, this part of the thesis study significantly improved our current understanding of different ways of modulating the mobility of signaling molecules with different properties within the GAG-based biohybrid hydrogels.

To precisely customize the transport of the different signaling molecules within the GAG-based materials, we developed a mathematical model that describes the binding and diffusion process of the molecules within the hydrogel network. Previously, the reaction-diffusion model has been applied to design GAG-based materials with desired growth factor transport properties [32, 33, 53, 55]. The *in vitro* and *in vivo* applications of the model have been demonstrated. However, there was no reported experimental validation on the accuracy of the model to describe the transport characteristics of signaling molecules within the materials. Moreover, most of the models also developed for the biopolymer derived matrix [33, 53, 57], which was shown to have an inherent affinity toward a broad spectrum of the signaling molecules [181] — therefore adding up more complexities on establishing a reliable mathematical model

In this study, for the first time, the reaction-diffusion model was developed to predict the transport of signaling molecules within fully synthetic starPEG-GAG hydrogels. *Experimental release studies of the GAG-affine proteins (VEGF165 or SFD1 α) confirmed the applicability and accuracy of the model prediction for the overall release profile of the proteins from hydrogels displaying completely different geometries* (i.e., a hydrogel loaded at the bottom of the microcentrifuge tube or a free-standing droplet of hydrogel). *Similarly, theoretical modeling could also capture the spatial and temporal dynamics of signaling molecule gradients within the starPEG-GAG hydrogel* that have been established using microfluidic techniques. Thus, the applicability of the mathematical model that we have developed here to predict the molecular transport within the GAG hydrogel could be validated with the experimental results, rationalizing its further usage for the prediction of transport of signaling molecules for more advanced *in vitro* or *in vivo* applications.

Overall, systematic studies on the mobility of the signaling molecules within the GAG-based hydrogels allow for the determination of various GAG hydrogel network parameters that govern the signaling molecules' mobility. In combination with the mathematical modeling, the results allow for the customization of transport of soluble signaling molecules within GAG-based biohybrid hydrogels for a broader context in the field of tissue engineering and regenerative medicines.

5.1.2 Modulation of the activity of pro-angiogenic growth factor within the starPEG-GAG hydrogels

The ability to precisely modulate the spatiotemporal activity of signaling molecules within cell-instructive polymer networks is critically important for the resulting application in tissue engineering. In particular, VEGF is known to be the major pro-angiogenic growth factor that regulates the early process of angiogenesis. Therefore, controlling the extracellular availability within the polymer network could have a tremendous effect on the extent of vascular morphogenesis within the matrices. The effect of GAG content and the GAG sulfation pattern of GAG-based matrices on the released VEGF bioactivity has been previously investigated [4-6, 77]. However, the influence of both parameters on the bioactivity of VEGF to control the cellular fate within the cell-instructive polymer network has not been systematically studied.

To unravel this, the mathematical model that we developed in the first part of the thesis was utilized to predict the effect of the GAG content and the GAG sulfation pattern on the availability of free VEGF within the hydrogel (**Section 4.2**). *Simulation results going along with endothelial vascular morphogenesis studies within the hydrogel with varied GAG content and GAG sulfation pattern concordantly revealed the dependency of the vascular network formation on the concentration of free VEGF within the system.* Interestingly, despite a significantly higher concentration of the free factor within the hydrogel containing 6O-DSH or 6ON-DSH, the hydrogel crosslinked with 6O-DSH building blocks supports a more extensive branching and a larger area of endothelial vasculatures compared to the hydrogel containing 6ON-DSH building block. This indicates *the critical role of the N-sulfate group of the GAG in mediating the formation of the*

endothelial capillary network within the hydrogel, such as their thermal stabilizing effect on the growth factors [227]. Moreover, in line with the simulation prediction on the spatial distribution of free VEGF, *the presentation of VEGF as a gradient promotes a local formation of endothelial vasculatures and significantly induce more directed cell migration toward the source of the growth factor*.

Taken together, the accuracy of the model prediction on the local availability of the signaling molecules, as well as their spatial distribution within the polymer network, could provide relevant information on the resulting pattern of cellular fate within the scaffold. In particular, within the context of the study, the simulation results on the growth factor transport and availability within the GAG-based hydrogels significantly improved our current understanding of how the GAG-content and the GAG sulfation pattern modulate the cellular responses within the three-dimensional matrices.

5.1.3 Cell-instructive ternary hydrogels with variable GAG content

Our detailed analysis of the influence of each GAG hydrogel network parameter on the subsequent release kinetics of VEGF from the hydrogel matrices revealed that adjusting the GAG content of the materials is the most efficient way of modulating the release kinetics from the polymer matrices. While utilization of selectively desulfated GAG derivatives such as 6O-DSH, N-DSH, or 6ON-DSH could modulate the binding and the release of signaling molecules from the polymer matrices [6, 38], the incorporation of fully-sulfated heparin is known to be more beneficial due to the capacity to protect and stabilize a plethora of signaling molecules [26, 227].

Accordingly, in the last part of the thesis study, ternary hydrogels with variable GAG content were developed by extending the currently established synthesis protocol of the binary GAG-based hydrogel system [47] (**Section 4.3**). Specifically, *the ternary hydrogel incorporates the thiol-functionalized starPEG, maleimide-functionalized starPEG, as well as maleimide-functionalized heparin to freely vary the heparin content of the hydrogel over a broad range of concentrations*. As such, hydrogels with variable heparin content in the range

from 1.5-1500 μM have been synthesized while maintaining *a comparable stiffness and volumetric swelling*. Besides, the hydrogel's stiffness can further be controlled by modulating the overall solid content of hydrogels.

The ternary hydrogel system with variable GAG content is tunable for its transport properties. Molecular diffusion, as well as release studies utilizing the pro-angiogenic growth factors (VEGF165 and SDF1 α), demonstrated the strong correlation of their in-gel mobility as well as their release behavior on the heparin content of the particular hydrogels. Moreover, *the gradient of the heparin affine-proteins* (VEGF165 and SDF1 α) established within the hydrogel *could also be modulated by varying the overall heparin content* of the hydrogel, whereas the gradient of non-affine proteins (EGF) was not affected by the presence of heparin.

Subsequent analysis of the endothelial cells embedded within hydrogels with variable heparin and constant VEGF content revealed the matrix's suitability to support 3D endothelial cell morphogenesis and a heparin content-dependent cell response. The hydrogel with a low heparin content (5 μM) promoted a higher vascularization than the hydrogel containing no heparin (pure PEG/PEG gel) or a higher heparin content. The superiority of the hydrogel containing 5 μM of GAG could probably be attributed to the subtle balance between retention, protection, and the enhancement of VEGF availability within the matrices.

Overall, the ternary hydrogels with variable heparin content could serve as a versatile platform to enhance the current state of the art of modulating the transport of pro-angiogenic growth factors. The cytocompatibility and tunability of the hydrogel's network properties allow its potential applications as an advanced three-dimensional scaffold for precision medicine and tissue engineering applications.

5.2 Future perspectives

5.2.1 Advanced modeling transport and binding of protein within the starPEG-GAG hydrogels

The prediction of the transport and the local concentration of signaling molecules within polymer networks are essential for the rational design of GAG-based materials that precisely modulate cell fate decisions. Additional parameters can be considered within the reaction-diffusion model developed and applied in this thesis to improve the accuracy of predicting the transport of signaling molecules within polymeric hydrogel materials.

Protein binding sites

The number of binding sites of protein at the GAG is crucial for predicting the protein's transport within the GAG-based hydrogels. In many cases, the 1:1 binding ratio between the protein and the heparin is only an assumption and might not be valid since for FGF-2 as an example, depending on the molecular weight, each molecule of heparin can have more than two binding sites [40]. *Therefore, further studies should aim to quantify the binding sites of particular signalings molecule to different GAG molecules.* In this context, the generation of ternary hydrogels with strongly varying GAG content might allow for quantifying the number of protein binding sites within the hydrogel as the most relevant parameter. As such, a ternary hydrogel containing a low amount of heparin can be titrated with a series of solutions containing a different concentration of protein. The protein concentration at the maximum binding can be used to determine the protein binding sites' concentration in the hydrogel, allowing the estimation of the number of protein binding sites per GAG molecules.

Competitive binding

Heparin binds to a large variety of positively charged proteins. Notably, for applications of the heparin-based hydrogels *in vivo*, the presence of serum proteins with known affinity for the heparin, such as apolipoproteins and thrombospondins, might interfere with the binding of signaling molecules to the hydrogel matrix [58]. The competitive binding of the serum proteins to the

heparin building block could influence the binding of signaling molecules to- and their release from the hydrogel matrices. As such, *future experiments to measure the affinity constants of signaling molecules to GAGs could be done in the presence of serum* in order to enhance the accuracy of model simulations and the resulting biological performance of the materials *in vivo*.

Binding in 3D matrices

The majority of the available binding data for the signaling molecules to GAGs originates from analyses of individual molecules. However, GAG-protein interactions within charged, hydrated polymer networks typically is dependent on the spatial distribution of charges/ affinity centers that might also influence specific (spatially matching) electrostatic interactions between the GAG and proteins. The crosslinking degree of the hydrogel may influence the signaling molecule diffusion away from the GAG building blocks, therefore increases the probability of the molecules for re-binding to the GAGs. Similarly, the high density of the negative charge within the hydrogel could cooperatively enhance the overall binding capacity of the gel matrix to the signaling molecules, i.e., providing an unspecific contribution to the binding. In contrast, the crosslinking/ covalent modification of the GAG with the synthetic polymer can mask the protein binding sites. All these variables increase the complexities of studying the binding interaction between the protein and GAG within the hydrogels. *Therefore, a direct assay to estimate the binding affinity between the protein and the GAGs crosslinked within the hydrogel could be instrumental in obtaining more realistic binding data.* This can be done, for example, by comparing the actual amount of proteins that bind to the hydrogel (as analytically determined by the ELISA) with the mathematical model for the protein binding [260].

5.2.2 Signaling molecule gradients

On-demand switch of the gradient profile

In this study, gradients of soluble signaling molecules have been created using a microfluidic device. The resulting gradients have been successfully demonstrated to control endothelial cell vascular morphogenesis and chemotaxis. However,

many cellular processes, such as immune cell migration in response to chemokine gradients, occur within a short time scale [261]. ***Therefore, the ability to rapidly alter the gradient profile of the signaling molecules within our GAG-based hydrogel system is instrumental in expanding the system's applicability to recapitulate such process in vitro.*** The high content of the heparin in our gel system is valuable in maintaining a stable long-term gradient of the growth factors. However, the currently established protocol only allowed for the formation of short-range and steep gradient of the heparin-affine proteins, including chemokines such as SDF1 α within the hydrogel after several days. As a result, the technique is limited by the inability to systematically analyze the short term behavior of many cells within the hydrogel. To overcome this, the signaling molecule may be mixed with anionic polyelectrolytes such as soluble heparin during the establishment of the gradient in the microfluidic device. ***The competitive binding between the soluble heparin and the heparin crosslinked within the hydrogel will enhance the growth factors diffusion into the hydrogel and speed up the formation of long-range growth factors gradients.*** Parameters such as the concentration of soluble heparin, the application of flow, and the affinity of the gel matrix to growth factors may be adjusted to provide the on-demand switch of gradient profile.

Localized signaling molecules gradient

Advances in the development of tissue models and organoids are essential for their therapeutic applications or to study the developmental process *in vitro* [262, 263]. In particular, the gradient of soluble signaling molecules plays a significant role in mediating various biological processes, including the neural tube axis specification of vertebrates and the wing disk formation of drosophila [264-267]. The mechanism of gradient generation *in vivo* involves clustering of cells, named signaling center, that secret of morphogens that diffuse away and creates a spatial profile of concentration, the gradient [250]. Based on that, the generation of a localized and short-range gradient of morphogens within engineered biomaterials can be applied to investigate such a process *in vitro*. While gradients of the signaling molecules within bulk hydrogels have been successfully applied and developed here, ***the usage of GAG-based microparticles can further be applied***

to provide a sustained and localized release of morphogens. The ability to tune the GAG content as well the mathematical model that we developed here can then be applied to optimize the gradient profile from the microparticles *to pattern the spatial organization of organoids*, e.g., organoid models such as kidney or neural, allowing the generation of robust organ and disease model *in vitro*.

5.2.3 Network properties and applications of ternary hydrogels

Finally, rational design strategies have been applied to develop ternary hydrogels with variable heparin content. Accordingly, hydrogels with varied heparin content of comparable stiffness can be produced by maintaining similarity in the solid content. However, the individual polymer component, and the ratio between reactive groups of the hydrogel precursors, need to be parametrized to understand their impact on the overall network properties such as hydrogel swelling and stiffness. *To address this issue, empirical equations that allow for predicting and tuning the hydrogel network properties based on the solid content, thiol concentration, and the maleimide to thiol ratio may be obtained using a design of experiment (DOE) approach* [258, 259]. This strategy might not only improve the understanding of existing GAG-based material properties but also help to expand the hydrogel platform towards a fully synthetic sulfonated system. Together, this information will be essential to provide an optimized hydrogel network for a broad range of applications in the tissue engineering field.

The ternary hydrogel with varied heparin content was shown to be cytocompatible and support the endothelial cell morphogenesis. The system *can be applied further as an in vitro model for tissues that naturally display variations in their GAG content*. In particular, the articular cartilage consists of layered structures from the superficial to the calcified zone, which is characterized by an increase in the GAG content and compressive strength [188]. Therefore, a ternary hydrogel with tunable GAG content and physical properties may be used to engineer the articular cartilage *in vitro*. Moreover, in combination with the recently published approaches to print in situ crosslinked hydrogels system, the zonal variation in the cartilage structures may be recapitulated in a high-resolution manner [268].

In conclusion, the systematic study on the mobility of signaling molecules within GAG-based hydrogels revealed fundamental principles that govern the transport of such key mediators within the ECM-mimicking material. Besides, the mathematical model that has been developed here for the prediction of transport processes and the local concentration of signaling molecules within the polymer matrices further enhanced the design concept of customizing the GAG-based hydrogel network that could precisely modulate cell fate decisions. Furthermore, the proposed experiments could lead to further development and application of the mathematical model and the advancement of the GAG-based biohybrid materials for translation in tissue engineering and regenerative medicine.

6. Appendix

6.1 Supplementary materials and methods

6.1.1 Determination of protein binding affinity to GAG and GAG derivatives

Microscale thermophoresis (MST) was used to quantify the strength of interactions between the proteins and GAG or GAG derivatives, as previously described [182, 269]. In this method, the model proteins were labeled with a reactive dye, NT-647, using Monolith NT Protein labeling kit RED-NHS according to the manufacturer's instructions (NanoTemper Technologies). Briefly, proteins were dissolved in a labeling buffer and mixed with the fluorescent dyes at a 1:1 molar ratio with a final concentration in the range of 2-20 μ M. The mixture was then incubated at room temperature for 30 min in the dark. The protein was purified from the unreacted dye using gel filtration columns (Sephadex G25, GE Healthcare). The protein concentration and purity were monitored using NanoDrop™ 1000 Spectrophotometer (Thermo Fisher Scientific, Germany) by measuring the absorption at 280 nm and 650 nm for proteins and the dye, respectively.

Afterward, GAG or GAG derivatives were titrated from 15.25 nM to 1000 μ M in PBS containing 0.05% Tween 20 and 0.1% BSA and mixed with 4-8 nM of labeled proteins in a 1:1 volume ratio. The mixture was then briefly centrifuged for 5 min at 15000 g and 4 °C. Next, the sample mixture was loaded into hydrophobic capillaries (NanoTemper Technologies), and the thermophoresis measurement was carried out at 22 °C in the Monolith NT.115 Pico instrument (NanoTemper Technologies) using excitation and MST power of 20% and 40%, respectively. Four independent measurements were carried out for each GAG-protein pair, and the data were pooled and analyzed using MO. Affinity Analysis software v2.2.4 (NanoTemper Technologies) to determine the protein-GAG binding constant. For all the analysis, only interactions that produce a binding curve with a signal to noise ratio of > 2 were considered to have an affinity.

6.1.2 Estimation of biomolecule sizes

The hydrodynamic radius r_h of fluorescein isothiocyanate–dextran (FITC-dextran) with varied molecular weights (FD10, FD20, FD70, FD150, and FD2000) (Sigma-Aldrich, Germany), was estimated from a previously reported empirical relation [270, 271].

$$r_h = 0.015(M_w)^{0.53 \pm 0.02} \quad (15)$$

where the molecular weight M_w is expressed in g/mol and r_h in nm.

On the other hand, the protein size is estimated using a zeta sizer software v.7.11 (Malvern Instruments Ltd., UK) using the molecular weight of protein as an input and the globular protein size as an output.

6.1.3 Estimation hydrogel mesh sizes

The mesh size of hydrogels was analyzed based on the rubber-elasticity theory considering a full recovery of elastic hydrogels upon a relatively small deformation ($< 20\%$) [272]. This theory correlates the number of possible covalent cross-links with an average mesh size of the hydrogel networks assuming an equal contribution of all polymer chains while neglecting the influence of hydrogel network defects. Based on these assumptions, the theoretical hydrogel mesh size, ξ is estimated using the following equation:

$$\xi = \left(\frac{G' N_A}{RT} \right)^{-\frac{1}{3}} \quad (16)$$

where G' is the storage modulus, N_A is the Avogadro constant, R is the molar gas constant, and T is the measurement temperature.

6.1.4 The diffusion of signaling proteins within an affinity-based system

The mobility of signaling proteins within an affinity-based system with reversible binding properties, such as a GAG-based hydrogel system, can be described by their effective diffusion coefficient, D_{eff} [166, 184].

$$D_{eff} = D_f(1 + N_T/K_D)^{-1} \quad (17)$$

where D_f is the free diffusion coefficient of the protein in the gel (which is lower than the free diffusion constant of molecules in a buffer because of the steric interaction with the gel network), N_T is the total number of protein binding sites in the system, and K_D (equilibrium dissociation constant) is the strength of affinity interaction between the protein and binding ligand. Assuming each GAG molecule can bind only to a single molecule of protein, the value of N_T is proportional to the GAG concentration within the system. In other words, the overall charge density per unit volume of the hydrogel determines the binding capacity of the system to given signaling molecules. This equation is valid under several assumptions:

1. The protein binds and dissociates from the GAG quickly, allowing the equilibration between the free and bound protein-GAG complex at a given point.
2. The complex between the GAG and protein is immobile, which is applicable as the GAG is covalently crosslinked within the polymer network [47].
3. Binding sites do not reach a saturation point. In our system, the GAG was added (at μM range) in a concentration that is much larger than the typical growth factor loading concentration for the cellular stimulations (at a pM-nM range) [7].
4. The binding of the protein to the gel does not interfere with the integrity of polymer networks.

6.1.5 Mathematical model assumptions

Several assumptions related to the mathematical model that we used in our hydrogel systems:

1. The polymer network of hydrogel only occupied a small fraction of the hydrogel volume. This assumption is particularly valid as the polymer content of all hydrogels prepared was within the range of ~2-4%.
2. The hydrogels remain stable during the experiments as our hydrogels system is based on a covalently crosslinked network. For the characterization of protein release and gradient experiments, non-MMP cleavable starPEG-SH was used, so we did not expect to see a hydrogel degradation. Besides, all the hydrogel samples were monitored regularly, and no significant changes in their morphology were observed.
3. Protein transport only happened because of the diffusion, and there is no mixing or convective flow in the system.
4. The free protein, bound, and unbound GAG concentrations are at equilibrium at the beginning of each experiment ($t=0$ H).
5. 1:1 binding of the protein to GAG. Single GAG molecule contains only one binding site for each protein
6. There was no resistance in the mass transfer of protein in the release medium, and the medium behaved as a sink with unlimited capacity. The volume of release media for the release experiment is 40 times of the hydrogel volume satisfying Crank's assumptions for an infinite open system with nearly zero solute concentration in the release medium [166].

6.1.6 COMSOL modeling

6.1.6.1 Protein release from hydrogels loaded within a conical tube.

Protein release experiments were performed in a 0.5 mL protein low binding microcentrifuge tube (Eppendorf Tubes, Germany). The geometry of the tube, as provided by the manufacturer, was built in the COMSOL software to simulate the release as close as possible to the experimental conditions (**Figure 6.1**). Due to the symmetrical shape of the geometry, a 2D axisymmetric cylindrical coordinate system (r, z) was also used. Here, r is the radial distance from the rotational axis, and the z is the distance measured from the base of the tube.

For the quantification of effective diffusion constant of proteins from the release experiment (**Figure 4.5**), the COMSOL numerical simulation was also used except that the binding affinity of the GAG to protein (K_D) was set to 1 M (no affinity), and the amount of protein release at the end of the release study (360 H) was considered to be the maximum release. The effective diffusion coefficient measured from the FRAP was used as a starting point for the simulation, and the best fit to the experimental data was obtained using the least-square method by systematic variation of D_{gel} . Here, as no protein binding/ interaction to the gel matrix was assumed, the transport of proteins is controlled only by Fickian diffusion. The standard bulk release experiment is the most commonly used method to determine the apparent diffusion coefficients of biomolecules within the biomaterials. The main reasons for this are primarily for comparing the transport properties of different systems where there is no standard method for determining the diffusivity [189].

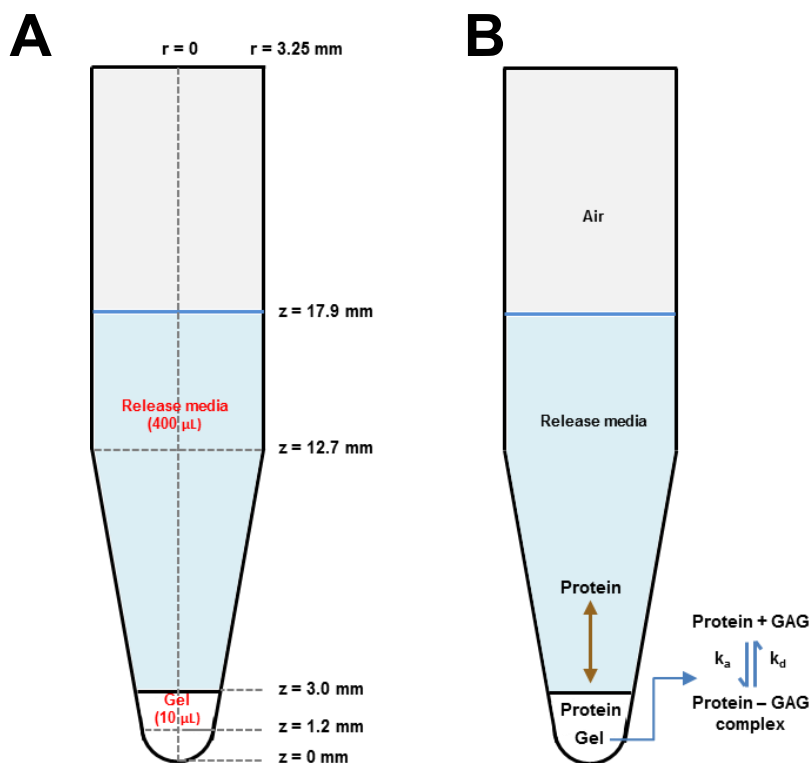


Figure 6.1. Schematic diagram of the protein release from GAG hydrogels within a microcentrifuge tube. (A) The geometry of the release experiment set-up. 10 μ L of hydrogel precursors were loaded at the base of the tube, and after the gel polymerization, 400 μ L of the medium was added to it to initiate the protein release. The hydrogel spans from the $z = 0$ mm to $z = 3.0$ mm, and the buffer spans from $z = 3.0$ mm to the $z = 17.9$ mm. (B) The mass transport dynamic within the system. Protein can reversibly bind to the GAG within the hydrogel to form immobile protein-GAG complexes. Some of the freely diffusing proteins will be released into the medium or rebind to the hydrogel matrix. Z is the height from the base of the gel, and r is the radius measured from the vertical axis of the tube.

In order to solve the reaction-diffusion equations applied for this geometry, the model was divided into two domains: the gel domain and the medium domain. Within the gel domain, the initial free protein, free GAG, and the protein-GAG complex concentration were determined using set equations as described before (**Equation 7-10**). On the other hand, the initial concentration of free protein, GAG, and the complex in the release media is set to zero. Finite element analysis built in the software with a custom physics-controlled, extra fine, and a free triangular mesh was then used to solve the equations. The amount of free protein release into the medium domain at each time points specified in **section 3.5** was

integrated and divided by the initial loading amount to obtain the cumulative protein release.

6.1.6.2 Free and bound protein fraction within a droplet of hydrogels

The reaction-diffusion model was used to estimate the concentration of free VEGF and GAG-bound VEGF, as described in **section 3.9**. The free VEGF concentration in the hydrogel containing different GAG content and GAG-sulfation pattern (various affinities to the factor) with different initial protein loading concentrations was estimated for three days. The details regarding the gel geometry and release media are shown in **Figure 6.2**. Here, the 3D geometry model was built in the COMSOL Multiphysics software. For the simulation, a parametric sweep module was applied, and the diffusion coefficient of VEGF in hydrogels and solution as determined using the FRAP was used for the input parameters. The dissociation rate constant of VEGF from the heparin, as obtained by the bio-layer interferometry experiments, was set to 0.0018 s^{-1} . Moreover, the K_D derived from the curve fitting of the reaction-diffusion model to the experimental release was utilized for the simulation (**Figure 4.9**). The **Equations 11-14** were then solved using the finite element model with a custom physics-controlled, finer mesh in the hydrogel domain, normal mesh in the medium, and free triangular mesh with extra refinement at the gel-buffer interface (maximum element size is $100\text{ }\mu\text{m}$). Surface plot of the free factor concentration with a custom manual color and data range from XY plane passing through the middle of the gel (at $1000\text{ }\mu\text{m}$ above the gel base) was used to visualize the free factor distribution within the system.

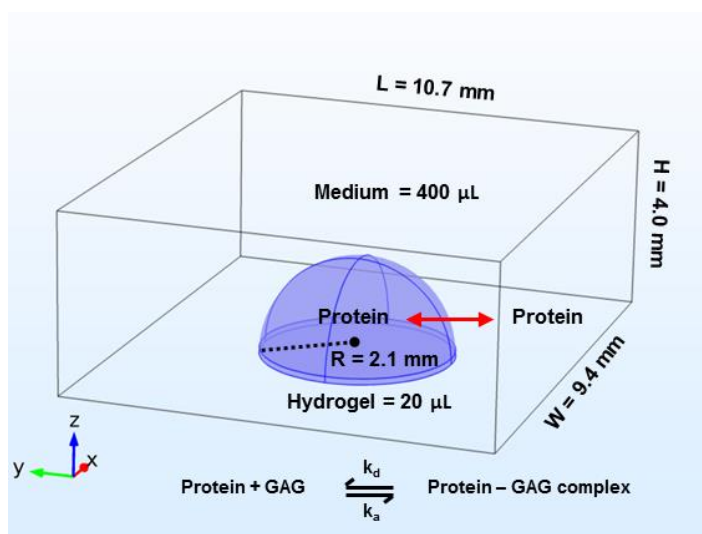


Figure 6.2. A schematic of the protein transport dynamic in a droplet of GAG hydrogel. 20 μL of the hydrogel was cast on a hydrophobic glass slide, and subsequently, 400 μL of the release medium was added into the surrounding of the hydrogel. The hydrogel was modeled as a hemisphere with a radius (R) of 2.1 mm, and the medium was confined within a block of cell culture chamber with the length (L), width (W), and height (H) of 10.7, 9.4, and 4.0 mm, respectively. The concentration of free protein and the GAG-bound protein within the hydrogel matrix is governed by the ratio of dissociation and association rate constant of the protein to the GAG (K_D). Freely diffusing protein can also diffuse in the 3D space within the hydrogel matrix as well as the release media.

6.1.6.3 Protein gradient formation in hydrogels

To understand the formation of protein gradient in the gels confined within the microfluidic chip described in **section 3.3.3**, simulation based on the reaction-diffusion model was applied as described above, implementing one space dimension (1D) model of COMSOL software (**Figure 6.3**). This argument is supported by the fact that the hydrogel channel and the nearby growth factor and sink channels were designed to be in parallel and have the same height. Therefore, we do not expect to see the protein concentration variation across the hydrogel matrix's height. As such, the hydrogel region, and the medium (growth factor) channels flanking the gel channel, were modeled as a line with a width of 1.3 mm, and 0.5 mm, respectively.

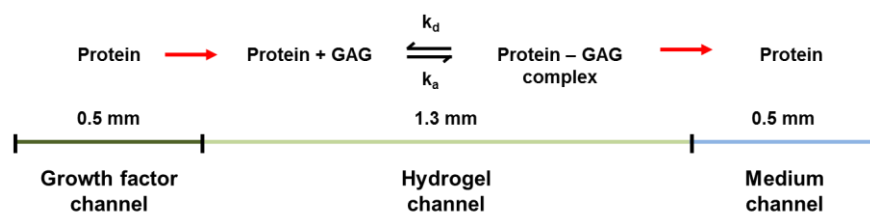


Figure 6.3. Schematic diagram of the protein diffusion through the hydrogel integrated within a microfluidic device. The protein transport is modeled utilizing one space dimension model of the COMSOL software. The width of the growth factor, hydrogel, and medium channel are 0.5, 1.3, and 0.5 mm, respectively. As the protein diffuses into the hydrogel, it binds to the immobilize GAG forming the protein-GAG complex, which persists depending on the strength of affinity interactions between protein and the GAG and the volume density of GAG within the 3D polymer matrix. The net protein diffusion occurs from the growth factor channel into the medium channel creating a biomolecular gradient within the hydrogel.

For the simulation, the diffusion constant of proteins in hydrogels and the pure buffer was determined using the FRAP as previously described. Similarly, the initial free protein, GAG, and protein-GAG complex concentration were determined using the equations described in **section 3.9**. Besides, the dissociation rate constant of the model proteins was fixed to 0.0018/s while the K_D was obtained from the curve fitting of the experimental release to the reaction-diffusion model (**Table 4.1**). The rate constant value was rationally chosen according to the literature values for typical protein-GAG interactions. Furthermore, it was also demonstrated in a peptide-based affinity controlled release system that the values of rate constant (k_a & k_d) at a given K_D did not affect the release of protein from the system as long as physically relevant values were chosen [52]. Afterward, the finite element analysis built in the COMSOL software was used to solve the **Equations 11-14**, utilizing a user-controlled mesh with a maximum element size of 1 μm and free triangular shape. Finally, the protein concentration across the hydrogel width was determined at various GAG concentrations for up to 72 H.

For the simulation of non-GAG affine protein gradients, the protein affinity to GAG was assumed to be negligible, and thereby, we set the K_D value to 1 M. In such condition, the only independent variable was D_{gel} , which was experimentally

6. APPENDIX

determined using FRAP. To compare the simulated gradient profiles with experimental data, the concentration of protein along the width of hydrogels at every time point was normalized to the highest protein concentration (at the interface between the gel and growth factor source).

Table 6.1. Model parameters for each simulation.

Simulation	k_a ($\mu\text{M}^{-1}\text{s}^{-1}$)	k_d (s^{-1})	K_D (μM)	D_{gel} ($\mu\text{m}^2/\text{s}$)	D_{med} ($\mu\text{m}^2/\text{s}$)	C_{P_Total} (μM)	C_{G_Total} (μM)	Geometry
Figure 4.6 (VEGF165-Hep)	8.45×10^{-4}	1.8×10^{-3}	2.13	20	64	2.50	1350	Conical
Figure 4.6 (VEGF165-6ON-DSH)	2.69×10^{-4}	1.8×10^{-3}	6.67	20	64	2.50	1350	Conical
Figure 4.6 (SDF1 α -Hep)	8.14×10^{-4}	1.8×10^{-3}	2.21	81	122	2.50	1350	Conical
Figure 4.6 (SDF1 α -6ON-DSH)	3.28×10^{-4}	1.8×10^{-3}	5.48	81	122	2.50	1350	Conical
Figure 4.7A	1×10^{-3}	1.8×10^{-3}	1.8	20	64	1.5, 15, 150, 1500	1500, 15	Conical
Figure 4.7B	$8.45 \times 10^{-4}, 4.23 \times 10^{-4}, 2.11 \times 10^{-4}, 8.45 \times 10^{-5}$	1.8×10^{-3}	2.13, 4.26, 8.52, 21.3	20	64	2.50	1500, 15	Conical
Figure 4.7C	$8.45 \times 10^{-10}, 8.45 \times 10^{-6}, 8.45 \times 10^{-5}, 8.45 \times 10^{-4}, 8.45 \times 10^{-3}$	$1.8 \times 10^{-9}, 1.8 \times 10^{-5}, 1.8 \times 10^{-4}, 1.8 \times 10^{-3}, 1.8 \times 10^{-2}$	2.13	20	64	2.50	1500, 15	Conical
Figure 4.7D	8.45×10^{-4}	1.8×10^{-3}	2.13	20	64	2.50	1500, 150, 15, 1.5	Conical
Figure 4.9A	1.8×10^{-9}	1.8×10^{-3}	1000000	20	64	1.31	0	droplet
Figure 4.9B	$3.28 \times 10^{-3}, 2.59 \times 10^{-3}, 3.31 \times 10^{-3}$	1.8×10^{-3}	0.548, 0.695, 0.543	20	64	1.31	450, 800, 1000	droplet
Figure 4.9C	$3 \times 10^{-3}, 1.5 \times 10^{-3}, 7.82 \times 10^{-4}$	1.8×10^{-3}	0.6, 1.2, 2.3	20	64	1.31	1000	droplet
Figure 4.14B	1.5×10^{-3}	1.8×10^{-3}	1.2	20		0.25	450	Line
Figure 4.19B-SDF1 α	8.14×10^{-4}	1.8×10^{-3}	2.21	81	122	0.25	1000	Line
Figure 4.19B-VEGF165	1.5×10^{-3}	1.8×10^{-3}	1.2	20	64	0.25	1000	Line
Figure 4.19B-EGF	1.8×10^{-9}	1.8×10^{-3}	1000000	68	133	0.25	1000	Line
Figure 4.19B-VEGF121	1.8×10^{-9}	1.8×10^{-3}	1000000	20	68	0.25	1000	Line
Figure 4.20B-SDF1 α	8.14×10^{-4}	1.8×10^{-3}	2.21	81	122	0.25	0,15,150, 1500	Line
Figure 4.20B-VEGF165	1.5×10^{-3}	1.8×10^{-3}	1.2	20	64	0.25	0,15,150, 1500	Line

6.1.7 Vascular network analysis

Table 6.2. Creation parameters. Parameters used for the Imaris - filament tracer module to analyze 3D confocal images of vasculature.

Algorithm	
Name	Threshold (loops)
Track (overtime)	false
Preprocessing	
Channel Index	2 (Phalloidin)
Enable Preprocessing	false
Approximate Diameter	14.0 μm
Preserve Edges	false
Segmentation	
Fill Cavities	true
Connected BaseLine	true
Threshold Low	2500
Threshold High	15000
Graph Compilation	
Branch Length Ratio	3
Find Dendrite Beginning Point	false
Finish	
Build all Time Points	true
Delete Working Channel	true

6.1.8 Metabolic activity assays

The metabolic activity of HUVECs was evaluated using the PrestoBlue assay following the manufacturer's instructions. Briefly, a PrestoBlue Reagent (ThermoFisher Scientific) was mixed with warm media at 1: 10 dilution. Following the addition of 400 μL of the mixture, the hydrogel samples were incubated at 37°C for 1 H. Subsequently, 150 μL of the solution was transferred in duplicate into a black 96 well plate (Greiner) for the fluorescence measurement using a Tecan Genios plate reader (Tecan Deutschland GmbH). The excitation and emission wavelength were set to 560 and 590 nm, respectively.

6.1.9 Bioactivity of VEGF

To evaluate the bioactivity of VEGF, 10,000 HUVECs/ well were seeded in 96 wells plate for 24 hours. Subsequently, the cells were treated with 1, 10, and 100 ng/mL of freshly prepared VEGF or VEGF pre-incubated for 1-3 days at 37 °C. After three days of treatment, cells' metabolic activity was evaluated with PrestoBlue assay as described above, except that the total volume of medium and PrestoBlue added onto each well was set to 200 μ L. VEGF's bioactivity was then reported as the fluorescence intensity relative to control without the VEGF or GAGs treatment.

6.2 Supplementary data

6.2.1 Protein binding to GAGs or- GAG-derivatives

In this study, four proteins were used as molecular probes representing different signaling molecules with varying molecular sizes and heparin affinity. The epidermal growth factor (**EGF**) was selected to represent a relatively small (6.2 kDa) and (under physiological conditions) negatively charged protein (pI 4.6) [273], thus showing no affinity to heparin. The Stromal cell-derived factor 1 α (**SDF1 α**), with a specific heparin-binding site and cationic excess charge (pI of 10, the molecular weight of 8 kDa), was used as a structurally similar heparin-affine factor [78]. The comparison was extended by growth factors of higher molecular weight (larger size and hydrodynamic radius) to study the influence of molecule size on the diffusion of the weak-heparin binding and weakly acidic **VEGF121** (28 kDa, pI 6.4) [274] as well as the heparin-binding, cationic **VEGF165** (38.2 kDa, pI 8.3) [274].

MicroScale Thermophoresis (MST) is a sophisticated technique to quantify a large variety of biomolecular interactions [120]. The method measures the movement of molecules along a temperature gradient (thermophoresis), which strongly depends on the size, charge, and conformation of molecules [120, 182]. Thus, this technique is quite sensitive to detect the changes in the molecular mobility of protein upon binding to a ligand along the temperature gradient. Here, MST was used to characterize the binding of heparin or desulfated heparin derivatives to the EGF, SDF-1 α , VEGF121, and VEGF165 after their functionalization with the maleimide moiety (**Figure 6.4**). Although the VEGF165 and SDF1 α were already known for their specific binding to heparin [167, 190, 193], with the reported K_D values of 80-1228 nM [167, 275] and 60 nM [275], respectively, the maleimide modifications might alter the structural feature of heparin that influences its recognition by the heparin-binding domain of these proteins. Therefore, this step is critical to ensure that the binding of heparin affine proteins to heparin is preserved.

The 6O and N sulfate group of heparin can be selectively removed to modulate the affinity of heparin to signaling molecules [38]. In general, the binding analysis

using MST showed that the sulfation pattern of GAGs regulates the binding affinity for heparin-binding proteins (SDF1 α & VEGF165). As shown here, decreasing the sulfate content of heparin by removing 6O sulfate decreases the binding affinity of SDF1 α from 1.2 μ M to 16.7 μ M (**Figure 6.4A&E**). However, we could not detect the binding SDF1 α to the 6ON-DSH heparin. Similarly, removing 6O sulfate from the heparin decreased the affinity of heparin to VEGF165 by a factor of four with the strength of interaction (K_D) of 0.9 and 4.2 μ M, for Hep and 6O-DSH, respectively. Also, subsequent removal of N sulfate from 6O-DSH to generate 6ON-DSH almost ablate its affinity for the VEGF165 (K_D = 33.3 μ M) (**Figure 6.4B&E**).

Interestingly, in contrast to the smaller affine protein model, the VEGF165 displayed some weak affinity for the PEG (as shown by the binding curve of VEGF165 to the PEG; the binding responses were observed when the PEG concentration is 10 μ M or higher). Although PEG is considered to be biologically inert [213], the functionalization of polymer with the maleimide group could probably introduce additional hydrophobic interaction, which is more pronounced for a larger protein compared to the smaller ones. Furthermore, as predicted, heparin or its derivatives exhibit no affinity to the non-affine proteins (VEGF121 and EGF), irrespective of their sulfation pattern (**Figure 6.4C-E**).

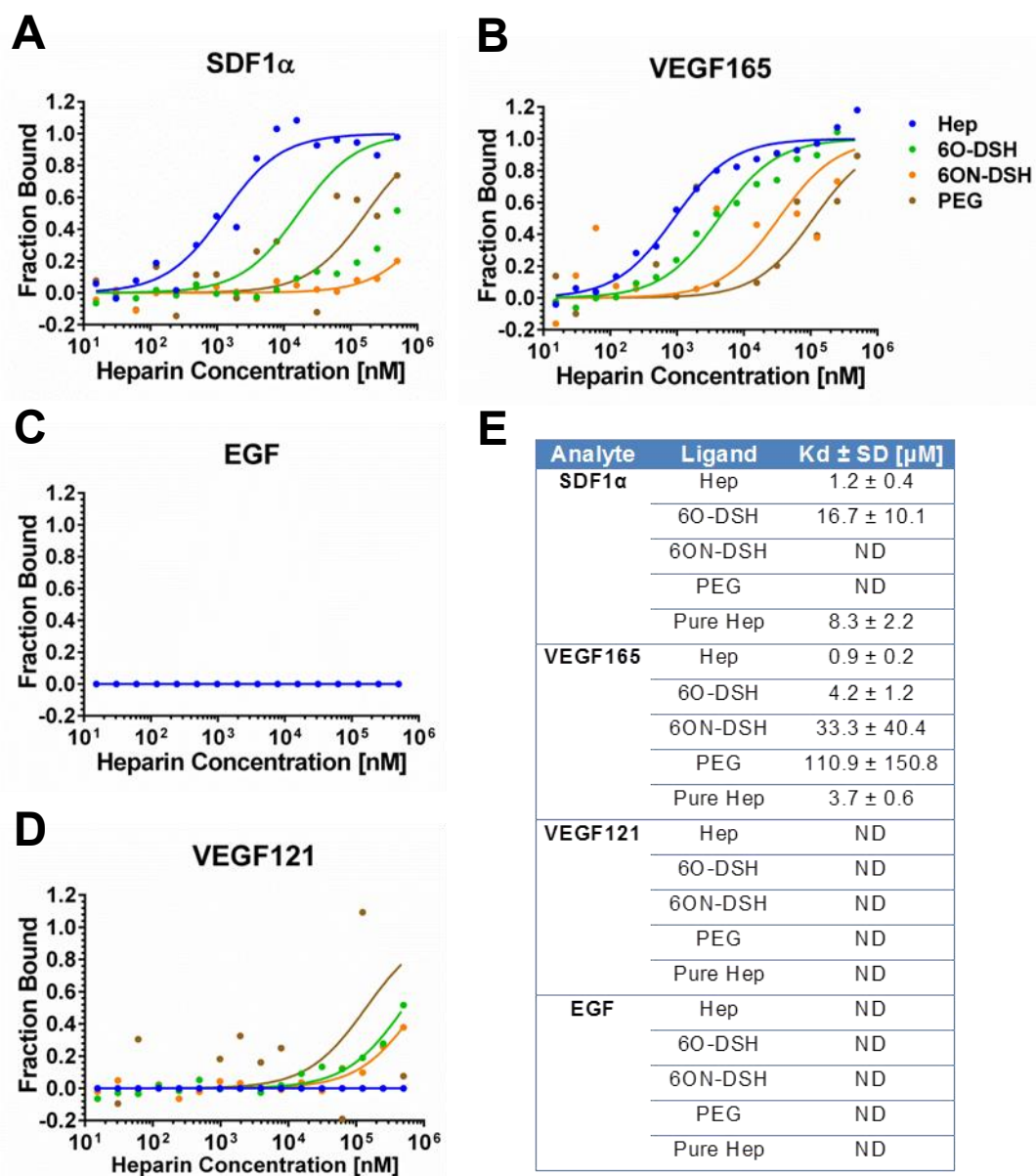


Figure 6.4. Binding analysis of model proteins to maleimide functionalized-Hep or Hep derivatives as determined by microscale thermophoresis (MST). Binding curve of (A) SDF1 α , (B) VEGF165, (C) EGF, and (D) VEGF121 to Hep, 6O-DSH, 6ON-DSH, and PEG. The Hep/ Hep derivatives concentration was titrated in the range of 15.25 to 500000 nM, whereas the concentration of NT647-labeled proteins was kept constant (\sim 2.5 nM). All the measurements were carried out using 30% MST Power. (E) The binding constants of proteins to the Hep/ Hep derivatives. Data represent mean \pm SD from three independent thermophoresis measurements.

6.2.2 Adaptation of FRAP technique to analyze protein mobility in the hydrogels

Several techniques can be used to monitor the diffusion of biomolecules within living cells or materials, such as single-particle tracking (SPT), fluorescence correlation microscopy (FCS), photoactivation, and fluorescence recovery after photobleaching (FRAP) [276, 277]. Of these approaches, FRAP is the most applicable one to quantify the mobility of molecules within numerous biological systems and biomaterials at a micrometer scale as it does not require specialized instruments and analytical tools [202, 278, 279]. In this study, the technique was adapted to measure the diffusion coefficient of model proteins in pure buffer or GAG-hydrogel matrices (**Figure 6.5**). As the technique is based on fluorescent detection, all the proteins here are labeled with fluorescent using NHS-ester chemistry, which specifically reacts with primary amine groups of lysine residues or N-terminal end of polypeptides (**Figure 6.5A**). The reaction rate depends on the pH of the buffer and reaches a maximum at a basic pH of ~8.3 [280]. One of the key successes of FRAP experiments is choosing the right of fluorescent dyes [281]. It is important to note that the chosen fluorescent dye should not significantly interfere with the diffusion of original molecules or their interaction with other molecules. Besides, the fluorescent probe should also have an intermediate photostability to allow for the photobleaching to occur as well as the acquisition of post-bleach images with sufficient signal to the noise ratio. Green fluorescent probes such as Fluorescein Iso Thio Cyanate (FITC) and the Alexa-488 are the most commonly used for the FRAP measurements.

Nevertheless, here, the Alexa-488 was chosen for the labeling of proteins due to the significant bleaching of FITC during the post-bleach image acquisitions, especially during the diffusion measurement of heparin-affine proteins within affine hydrogel systems (data not shown). In our study, both small and large proteins can be successfully labeled with Alexa 488, with an average labeling degree of 1-2 dyes per protein molecule (**Figure 6.5B**). Such a labeling degree was shown to be sufficient to produce an optimum fluorescent signal, which is essential for the subsequent analysis of the FRAP data to obtain a reliable diffusion coefficient of the proteins.

Several diffusion models, which mainly differ on the geometry of the bleach spot and the diffusion dimensionality, have been developed to extract the diffusion coefficient of proteins within hydrogels or pure buffer from the fluorescence recovery curve. However, a uniform disk model for 2D diffusion in a circular spot, which was initially developed by Soumpasis [162], is one of the most widely used because it does not require a complicated analytical tool/ program for processing the FRAP data. Several assumptions of the uniform disk model need to be satisfied to accurately extract the diffusion coefficient from the FRAP curve include [270]:

1. Uniform distribution of fluorescent molecules within the samples. This assumption was validated by our confocal microscopy analysis, which revealed a uniform distribution of fluorescently labeled proteins across the hydrogel thickness and around the bleach spot (**Figure 6.5C-D**)
2. Isotropic diffusion in an infinite medium. This condition can be satisfied as the bleach spot was chosen in a region far away from the gel boundary. Also, the bleach spot size was approximately less than 10% of the total observational area, so a sufficient amount of fluorescent can still diffuse into the bleached spot to recover the fluorescent intensity (**Figure 6.5D**)
3. 2D diffusion. In our study, a 10X objective with a low NA (0.3) was used. Therefore, it could generate a nearly cylindrical bleach profile, which is uniform over the entire thickness of the hydrogel (~120 μm) (**Figure 6.5E**). The uniform bleach profile that extends along the optical axis ensures that the fluorescent diffusion into the bleached spot effectively occurs only by radial diffusion [278].
4. The diffusion during photobleaching is negligible. In this study, the photobleaching took only ~600 ms, which is sufficiently short to avoid significant fluorescence recovery during the bleaching process [161, 270, 282].

In addition to these assumptions, to accurately determine the diffusion constant, the bleached spot's radius needs to be chosen appropriately. The initial uniform disk model developed by Saumpasis [162] employed uniform laser profiles that produce uniform post-bleach profiles. In contrast, current standard commercial

confocal microscopes scan the samples pixel-by-pixel and line-by-line using laser beams with Gaussian profiles [278], resulting in bleaching light distribution/ radial fluorescence intensity profile across the bleached spot that does not follow a discontinuous step function approximation (A sudden fluorescence intensity drop at the transition between the bleached and unbleached regions). As a result, this model may not be readily applicable to measure the diffusion coefficient of proteins using the standard microscopes. However, when the radius of the bleached spot is much larger than the effective Gaussian resolution, the resulting bleaching illumination profile is equivalent to the stationary beam with a uniform radial and Gaussian axial distribution [270]. The failure to take this into account can lead to underestimation of the diffusion coefficient if the Soumpasis equation (**Equation 4**) is used to analyze confocal FRAP data, especially for fastly diffusing proteins.

For the confocal microscopes, the effective bleaching resolution r_b can be approximated as a factor of 2–4 more than the optical resolution [278]. In our study, the optical resolution of the 10X objective with an NA of 0.3 is approximately $\sim 1\ \mu\text{m}$. From this, the effective bleaching resolution can be approximated to be $\sim 2\text{--}4\ \mu\text{m}$. Therefore, to optimize the size of the bleach spot, we analyzed the bleaching intensity distribution of the bleached spot with a nominal size in the range of 2.5–20 μm (**Figure 6.5 F**). As predicted, the bleached spot profile was becoming more uniform with increasing bleached spot size, justifying the selection of 20 μm bleach spot for further testing measurement utilizing biomolecules with known diffusion coefficients. The Bovine Serum Albumin, FD 20, and FD 2000 were then chosen as the test molecules, and subsequently, the diffusion in PBS was measured utilizing the established FRAP protocol. As expected, the measurement results were shown to be comparable with the values obtained from the literature [270, 283, 284] (**Figure 6.5G**), supporting the selection of 20 μm bleach spot size for the subsequent studies. This value was in good agreement with Braeckmans and co-worker's recommendation for using a nominal bleach spot with a radius of at least five times larger than the effective bleaching resolution (2–4 μm) to accurately approximate the diffusion coefficient of molecules [270, 278].

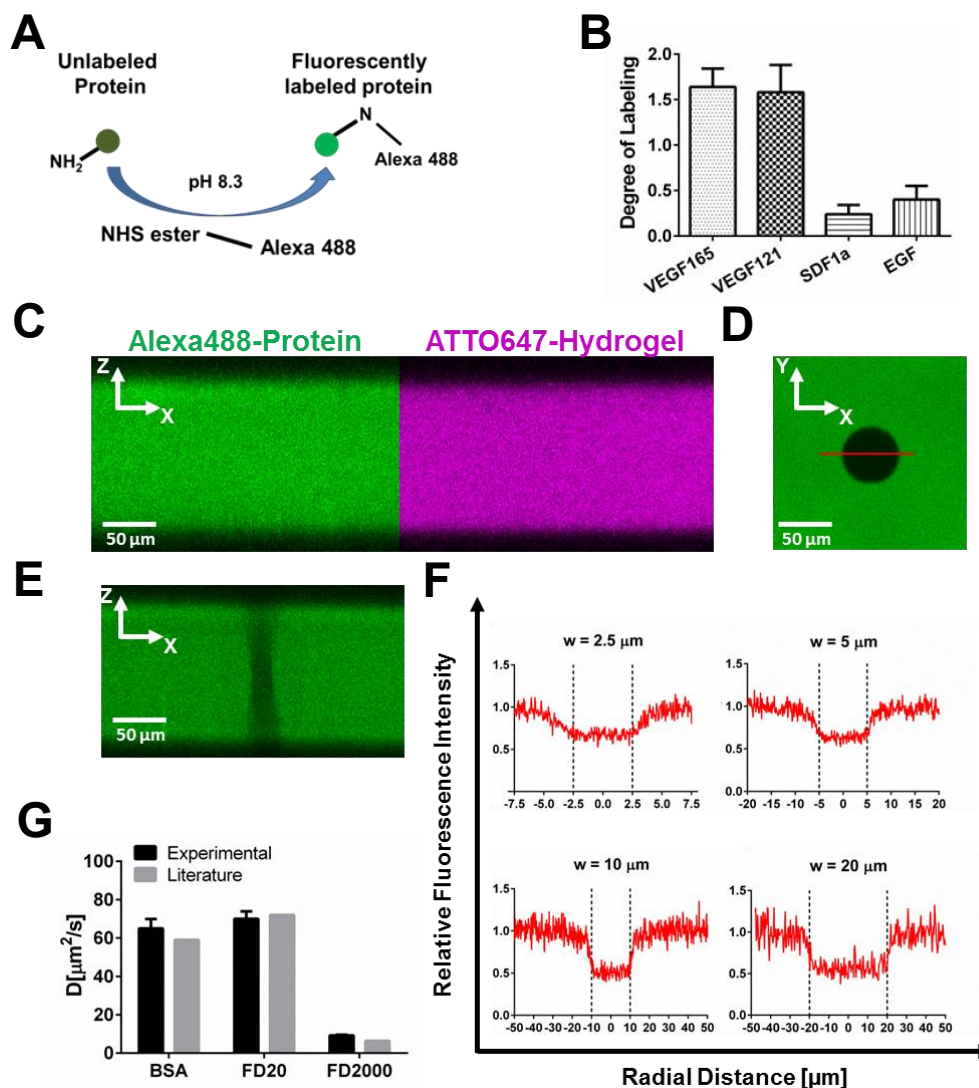


Figure 6.5. Optimization of FRAP experimental parameters for the quantitative analysis of molecular diffusivity using a uniform disk model. (A) Fluorescence labeling of the proteins. Proteins were labeled with fluorescence at their primary amines using NHS ester Alexa-488 at pH 8.3. (B) The degree of fluorescence labeling. The degree of fluorescence labeling was calculated as a molar ratio of dye to protein after the purification step from the unreacted dyes. For each FRAP measurements, proteins were fluorescently labeled with Alexa-488 and encapsulated into the ATTO-647-labeled hydrogel during the gelation process. (C) The XZ section of the FRAP hydrogel sample with a thickness of ~120 μm showing a uniform protein distribution within the hydrogel matrix. (D) A circular bleached spot was generated just after the photobleaching of fluorescently labeled proteins within the middle section of the hydrogel. (E) Uniform bleaching of 20 μm spot was observed across the thickness of a hydrogel sample. (F) Relative bleaching fluorescence intensity distribution of the bleached spot of different sizes was measured immediately after the photobleaching. (G) The diffusion coefficient (D) of the test samples (FITC-BSA, FITC Dextran 20, FITC Dextran 2000) in a solution obtained from the literature and FRAP methods using the optimized parameters. Scale bar 50 μm

6.2.3 Estimation of hydrogel mesh size

The mesh size of hydrogels is known to affect the transport signaling molecules [16] and the survival and functions of encapsulated cells [285]. The mobility of non-charged probe-macromolecules, fluorescently-labeled, FITC-dextran of different molecular sizes (MW: 10-200 kDa) was investigated within a set of hydrogels prepared with different stiffness (~ 0.2 -6.8 kPa) to investigate the potential restriction of the diffusivity of signaling molecules within our GAG hydrogels system (**Figure 6.6A**). The dextran was used as a molecular probe to characterize the mesh size of hydrogels in place of proteins/ growth factors because of its relatively neutral charge at physiological pH. Thereby, we do not expect to see their binding to the hydrogel components. Besides, unlike most growth factors, the dextrans are stable and do not form aggregates over time. Thus, the immobilization of dextrans within the scaffold is caused only by the steric restriction due to the larger molecular size compared to the hydrogel mesh size, but not by the binding or aggregate formation.

While the size of dextrans can be estimated from their molecular weight [270], the mesh size of hydrogels was calculated from the rubber elasticity theory [2]. Based on our estimation, the size of 10-2000 kDa dextran was approximately within the range of ~ 4 -65 nm, while the hydrogels with stiffness ~ 0.2 -6.8 kPa were estimated to have a mesh size of ~ 9 -28 nm, covering all possible mesh sizes of our *in situ* cross-linkable hydrogel system [47]. In general, the fraction of unrecovered fluorescence/ immobile fraction of all type dextrans in solutions is close to zero, indicating a sufficient amount dextran diffused without any restrictions from the unbleached region into the bleached spot (**Figure 6.6B**). Besides, their diffusion within the solutions was shown to be inversely proportional to their molecular size (**Figure 6.6C**). In opposite to that, only the dextran with molecular weight as large as 70 kDa (Size = 11 nm) exhibited no restriction in their mobility within all hydrogels tested. A less than 20% of the dextrans with a molecular weight of 10-70 kD were immobile within the hydrogels. Their diffusivity was also inversely correlated to their molecular size and the gel stiffness.

On the other hand, the mobility of dextran with a molecular weight of 150 kDa or larger was severely reduced beyond a specific hydrogel mesh size. For instance, a significant immobile fraction ($\geq 20\%$) of the dextran with a molecular weight of 150 kDa (size = 17 nm) was found in the hydrogel with a mesh size of 9 nm, whereas that of the 500 kDa dextran (size = 31 nm) was observed in the hydrogel with the mesh size of 11 nm or lower. Moreover, the mobility of 2000 kDa dextran was constrained in all hydrogels type tested, even for the gel with the largest mesh size (28 nm). This finding was in good agreement with previous studies that showed limited mobility for 2000 kDa dextran within PEG-chondroitin-sulfate-hydrogels with a mesh size of ~ 37 nm [286].

Interestingly, the high immobile fractions of the dextran with molecular weight 150 kDa or larger was also accompanied by the lower diffusion constant ($\leq 10 \mu\text{m}^2/\text{s}$). However, we did not see a significant difference in their diffusivity within the hydrogels containing different mesh sizes. This could probably be attributed to their large size that exerts a considerable steric hindrance to the hydrogel network, which hamper their diffusivity even within the hydrogel with the largest mesh size (28 nm).

Altogether, these results supported that the hydrogel mesh size estimated from the rubber elasticity theory corresponds well to the diffusion profile as well as molecular size cut off of the hydrogels for the dextrans of different molecular sizes. All hydrogels allowed dextrans molecules to freely diffuse if the molecular size is smaller than ≤ 70 kDa. In this case, dextran's mobility was primarily governed by the ratio between the molecular size and mesh size of polymer networks. As the molecular weights of all proteins we used in our systematic study were smaller than 70 kDa, any protein immobility within the hydrogels was not expected to be caused by the size filtering of the hydrogel but rather by the protein binding to the hydrogel building blocks or possible protein aggregations.

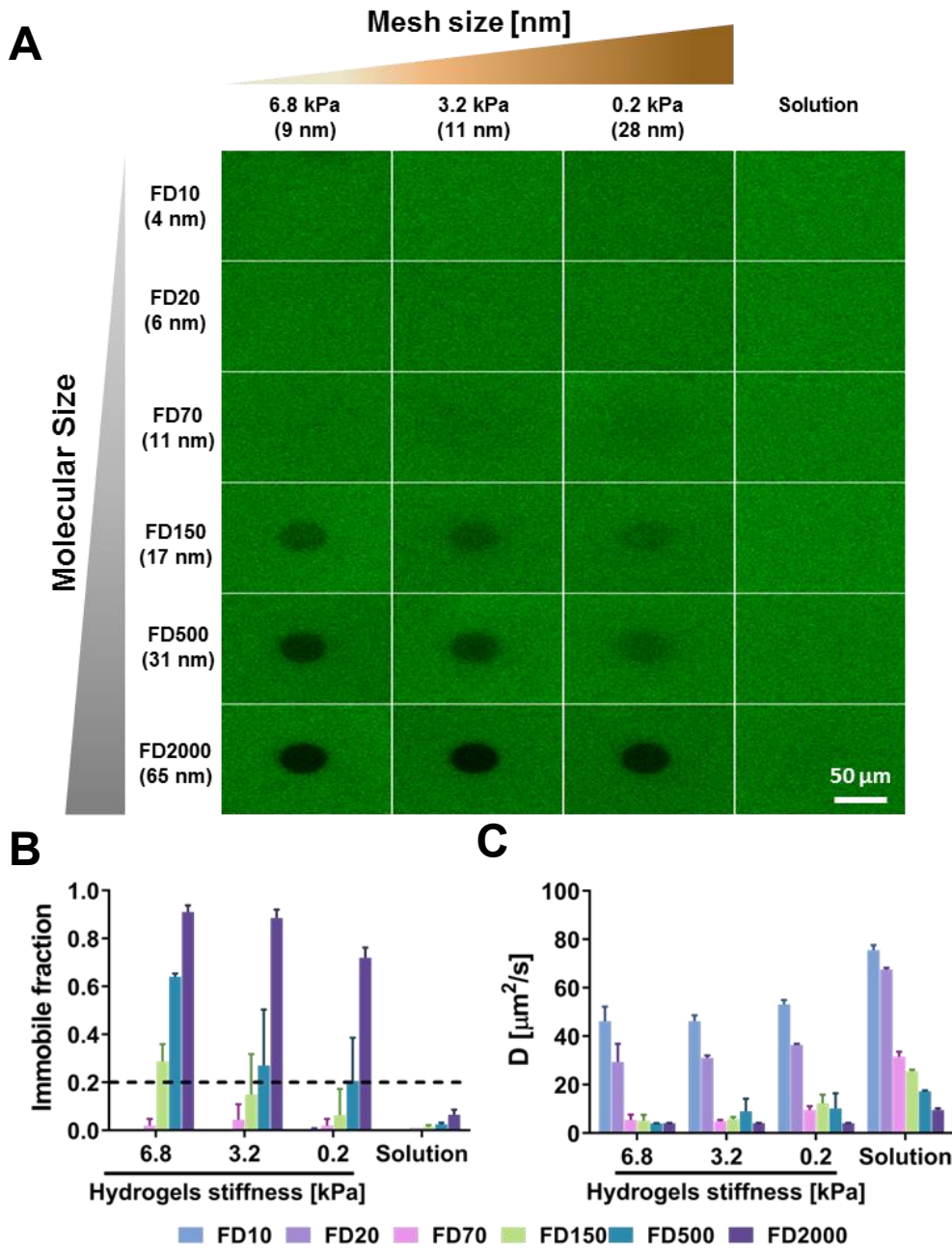


Figure 6.6. The mobility of FITC-dextran with different molecular weights within the GAG hydrogels of various stiffness. The mobility of FITC-dextran with a molecular weight in the range of 10-2000 kDa (FD10-FD2000) was analyzed using fluorescence recovery after photobleaching (FRAP). The hydrogel mesh size was determined using Rubber elasticity theory [2], and the dextran molecular size was estimated as previously described [270]. (A) The post bleach images acquired ~ 120 s after the photobleaching. (B) Quantification of an immobile fraction within hydrogels at ~ 120 s after the bleaching. (C). The diffusion coefficient of dextran within the hydrogels. Data represents mean \pm SD ($n = 3$). Scale bar = 50 μ m.

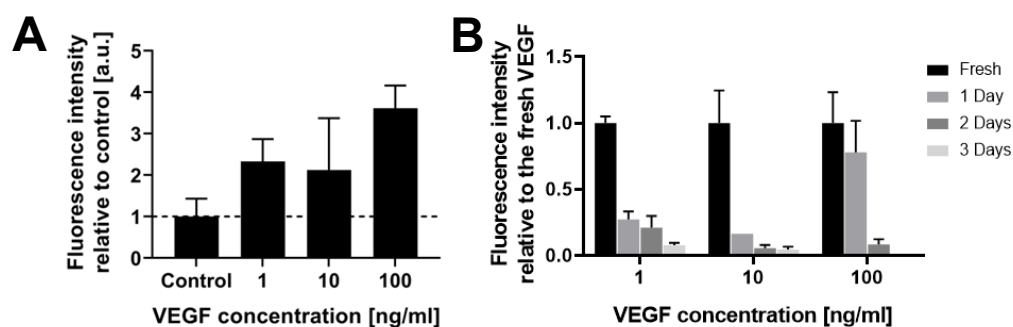


Figure 6.7. Concentration- and time-dependent VEGF-induced cellular metabolic activity. HUVECs on 2D cell culture was incubated with VEGF, and the metabolic activities were assessed via Prestoblue assays. HUVECs were seeded in 96-well plates at 10,000 cells/well in a non-supplemented Basal medium. Results are presented as the relative increase in fluorescence intensity compared to the untreated control. (A) HUVECs treated with various concentrations of VEGF (n=6) showed a dose-dependent stimulatory response. (B) VEGF, which were pre-incubated for 24 h and 48 h at 37°C before added to the cultured cells, exhibited less prominent activity overtime (n=6) to induce HUVEC cellular metabolic activity.

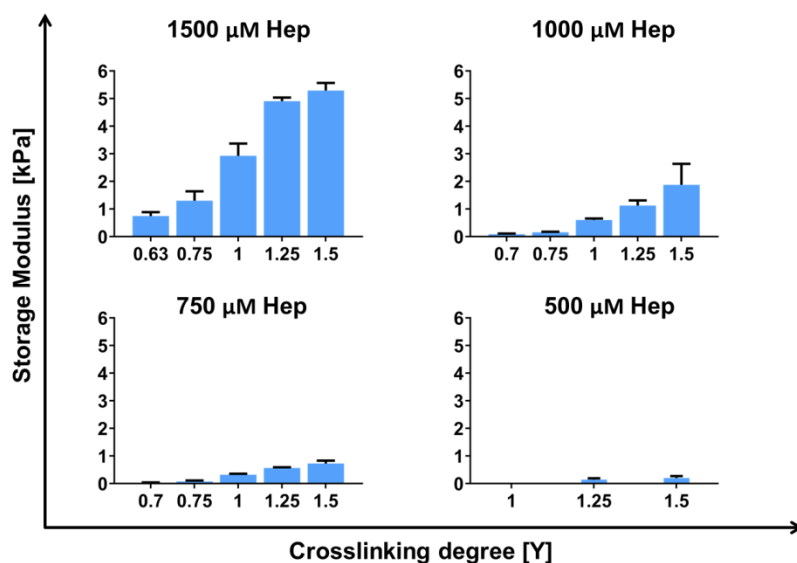


Figure 6.8. The mechanical properties of the binary starPEG-GAG hydrogel containing variable GAG content at different crosslinking degree/ molar ratio of starPEG to heparin (Y)

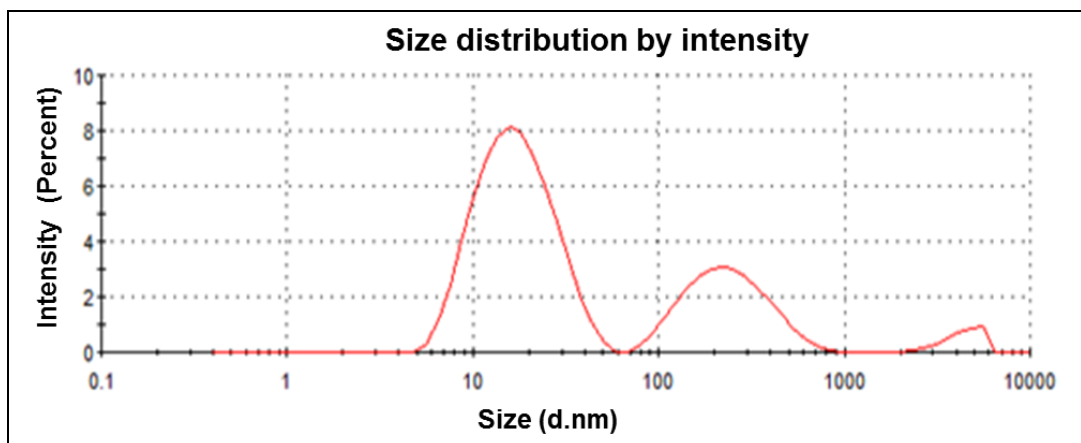


Figure 6.9. Particle size analysis of the VEGF121 dissolved in the PBS (pH 7.4) as determined using a dynamic light scattering method.

Bibliography

- [1] Lee K, Silva EA, Mooney DJ. Growth factor delivery-based tissue engineering: general approaches and a review of recent developments. *Journal of the Royal Society, Interface*. 2011;8:153-70.
- [2] Freudenberg U, Hermann A, Welzel PB, Stirl K, Schwarz SC, Grimmer M, et al. A star-PEG-heparin hydrogel platform to aid cell replacement therapies for neurodegenerative diseases. *Biomaterials*. 2009;30:5049-60.
- [3] Chwalek K, V. Tsurkan M, Freudenberg U, Werner C. Glycosaminoglycan-based hydrogels to modulate heterocellular communication in in vitro angiogenesis models. *Scientific Reports*. 2014;4:4414.
- [4] Zieris A, Prokoph S, Levental KR, Welzel PB, Grimmer M, Freudenberg U, et al. FGF-2 and VEGF functionalization of starPEG-heparin hydrogels to modulate biomolecular and physical cues of angiogenesis. *Biomaterials*. 2010;31:7985-94.
- [5] Zieris A, Chwalek K, Prokoph S, Levental KR, Welzel PB, Freudenberg U, et al. Dual independent delivery of pro-angiogenic growth factors from starPEG-heparin hydrogels. *Journal of controlled release : official journal of the Controlled Release Society*. 2011;156:28-36.
- [6] Freudenberg U, Zieris A, Chwalek K, Tsurkan MV, Maitz MF, Atallah P, et al. Heparin desulfation modulates VEGF release and angiogenesis in diabetic wounds. *Journal of Controlled Release*. 2015;220:79-88.
- [7] Lohmann N, Schirmer L, Atallah P, Wandel E, Ferrer RA, Werner C, et al. Glycosaminoglycan-based hydrogels capture inflammatory chemokines and rescue defective wound healing in mice. *Science translational medicine*. 2017;9.
- [8] Dellacherie MO, Seo BR, Mooney DJ. Macroscale biomaterials strategies for local immunomodulation. *Nature Reviews Materials*. 2019.
- [9] Gelain F, Unsworth LD, Zhang S. Slow and sustained release of active cytokines from self-assembling peptide scaffolds. *Journal of controlled release : official journal of the Controlled Release Society*. 2010;145:231-9.
- [10] Kearney CJ, Mooney DJ. Macroscale delivery systems for molecular and cellular payloads. *Nat Mater*. 2013;12:1004-17.
- [11] Belair DG, Le NN, Murphy WL. Design of growth factor sequestering biomaterials. *Chem Commun (Camb)*. 2014;50:15651-68.
- [12] Belair DG, Miller MJ, Wang S, Darjatmoko SR, Binder BYK, Sheibani N, et al. Differential regulation of angiogenesis using degradable VEGF-binding microspheres. *Biomaterials*. 2016;93:27-37.
- [13] Lee KY, Martin CP, Kenneth WA, Mooney D, J. Controlled growth factor release from synthetic extracellular matrices. *Nature*. 2000;408:998.
- [14] Ito Y. Growth factor engineering for biomaterials. *ACS Biomater Sci Eng*. 2019;5:5597-609.
- [15] Caballero Aguilar LM, Silva SM, Moulton SE. Growth factor delivery: Defining the next generation platforms for tissue engineering. *Journal of Controlled Release*. 2019;306:40-58.

-
- [16] Li J, Mooney DJ. Designing hydrogels for controlled drug delivery. *Nat Rev Mater.* 2016;1.
- [17] Martino MM, Brkic S, Bovo E, Burger M, Schaefer DJ, Wolff T, et al. Extracellular Matrix and Growth Factor Engineering for Controlled Angiogenesis in Regenerative Medicine. *Frontiers in Bioengineering and Biotechnology.* 2015;3.
- [18] Lin CC, Metters AT. Hydrogels in controlled release formulations: network design and mathematical modeling. *Advanced drug delivery reviews.* 2006;58:1379-408.
- [19] Prokoph S, Chavakis E, Levental KR, Zieris A, Freudenberg U, Dimmeler S, et al. Sustained delivery of SDF-1 α from heparin-based hydrogels to attract circulating pro-angiogenic cells. *Biomaterials.* 2012;33:4792-800.
- [20] Subbiah R, Guldborg RE. Materials Science and Design Principles of Growth Factor Delivery Systems in Tissue Engineering and Regenerative Medicine. *Adv Healthc Mater.* 2019;8:e1801000.
- [21] Martino MM, Briquez PS, Guc E, Tortelli F, Kilarski WW, Metzger S, et al. Growth Factors Engineered for Super-Affinity to the Extracellular Matrix Enhance Tissue Healing. *Science.* 2014;343:885-8.
- [22] Anderson SM, Chen TT, Iruela-Arispe ML, Segura T. The Phosphorylation of Vascular Endothelial Growth Factor Receptor-2 (VEGFR-2) by Engineered Surfaces with Electrostatically or Covalently Immobilized VEGF. *Biomaterials.* 2009;30:4618-28.
- [23] Leslie-Barbick JE, Moon JJ, West JL. Covalently-immobilized vascular endothelial growth factor promotes endothelial cell tubulogenesis in poly(ethylene glycol) diacrylate hydrogels. *J Biomater Sci Polym Ed.* 2009;20:1763-79.
- [24] Phelps EA, Headen DM, Taylor WR, Thule PM, Garcia AJ. Vasculogenic bio-synthetic hydrogel for enhancement of pancreatic islet engraftment and function in type 1 diabetes. *Biomaterials.* 2013;34:4602-11.
- [25] Freudenberg U, Liang Y, Kiick KL, Werner C. Glycosaminoglycan-Based Biohybrid Hydrogels: A Sweet and Smart Choice for Multifunctional Biomaterials. *Advanced materials (Deerfield Beach, Fla).* 2016;28:8861-91.
- [26] Schirmer L, Atallah P, Werner C, Freudenberg U. StarPEG-Heparin Hydrogels to Protect and Sustainably Deliver IL-4. *Adv Healthc Mater.* 2016;5:3157-64.
- [27] Chen FM, Wu LA, Zhang M, Zhang R, Sun HH. Homing of endogenous stem/progenitor cells for in situ tissue regeneration: Promises, strategies, and translational perspectives. *Biomaterials.* 2011;32:3189-209.
- [28] Lars J, Johan K, Lars L, Inger E, Lena K, Lena C-W. Heparan Sulfate in trans Potentiates VEGFR-Mediated Angiogenesis. *Developmental Cell.* 2006;10:625-34.
- [29] Teran M, Nugent MA. Synergistic Binding of Vascular Endothelial Growth Factor-A and Its Receptors to Heparin Selectively Modulates Complex Affinity. *The Journal of biological chemistry.* 2015;290:16451-62.
- [30] Hettiaratchi MH, Miller T, Temenoff JS, Guldborg RE, McDevitt TC. Heparin microparticle effects on presentation and bioactivity of bone morphogenetic protein-2. *Biomaterials.* 2014;35:7228-38.
- [31] Baumann L, Prokoph S, Gabriel C, Freudenberg U, Werner C, Beck-Sickinger AG. A novel, biased-like SDF-1 derivative acts synergistically with

starPEG-based heparin hydrogels and improves eEPC migration in vitro. *Journal of controlled release : official journal of the Controlled Release Society*. 2012;162:68-75.

[32] Sakiyama-Elbert SE, Hubbell JA. Controlled release of nerve growth factor from a heparin-containing fibrin-based cell ingrowth matrix. *Journal of controlled release : official journal of the Controlled Release Society*. 2000;69:149-58.

[33] Taylor SJ, McDonald JW, 3rd, Sakiyama-Elbert SE. Controlled release of neurotrophin-3 from fibrin gels for spinal cord injury. *Journal of controlled release : official journal of the Controlled Release Society*. 2004;98:281-94.

[34] Wood MD, Borschel GH, Sakiyama-Elbert SE. Controlled release of glial-derived neurotrophic factor from fibrin matrices containing an affinity-based delivery system. *J Biomed Mater Res A*. 2009;89:909-18.

[35] Watarai A, Schirmer L, Thoenes S, Freudenberg U, Werner C, Simon JC, et al. TGF beta functionalized starPEG-heparin hydrogels modulate human dermal fibroblast growth and differentiation. *Acta biomaterialia*. 2015;25:65-75.

[36] Smith RAA, Murali S, Rai B, Lu X, Lim ZXH, Lee JIL, et al. Minimum structural requirements for BMP-2-binding of heparin oligosaccharides. *Biomaterials*. 2018;184:41-55.

[37] Tellier LE, Miller T, McDevitt TC, Temenoff JS. Hydrolysis and Sulfation Pattern Effects on Release of Bioactive Bone Morphogenetic Protein-2 from Heparin-Based Microparticles. *J Mater Chem B*. 2015;3:8001-9.

[38] Atallah P, Schirmer L, Tsurkan M, Putra Limasale YD, Zimmermann R, Werner C, et al. In situ-forming, cell-instructive hydrogels based on glycosaminoglycans with varied sulfation patterns. *Biomaterials*. 2018;181:227-39.

[39] Zieris A, Dockhorn R, Rohrich A, Zimmermann R, Muller M, Welzel PB, et al. Biohybrid networks of selectively desulfated glycosaminoglycans for tunable growth factor delivery. *Biomacromolecules*. 2014;15:4439-46.

[40] Arakawa T, Wen J, Philo JS. Stoichiometry of heparin binding to basic fibroblast growth factor. *Arch Biochem Biophys*. 1994;308:267-73.

[41] Zhao J, Luo C, Chen Y, Wu D, Shen C, Han W, et al. Preparation, structure and BMP-2 controlled release of heparin-conjugated hyaluronan microgels. *Carbohydrate Polymers*. 2011;86:806-11.

[42] Jha AK, Tharp KM, Ye J, Santiago-Ortiz JL, Jackson WM, Stahl A, et al. Enhanced survival and engraftment of transplanted stem cells using growth factor sequestering hydrogels. *Biomaterials*. 2015;47:1-12.

[43] Jha AK, Mathur A, Svedlund FL, Ye J, Yeghiazarians Y, Healy KE. Molecular Weight and Concentration of Heparin in Hyaluronic Acid-based Matrices Modulates Growth Factor Retention Kinetics and Stem Cell Fate. *Journal of controlled release : official journal of the Controlled Release Society*. 2015;209:308-16.

[44] Chung YI, Tae G, Hong Yuk S. A facile method to prepare heparin-functionalized nanoparticles for controlled release of growth factors. *Biomaterials*. 2006;27:2621-6.

[45] Marchioli G, Luca AD, de Koning E, Engelse M, Van Blitterswijk CA, Karperien M, et al. Hybrid Polycaprolactone/Alginate Scaffolds Functionalized with VEGF to Promote de Novo Vessel Formation for the Transplantation of Islets of Langerhans. *Adv Healthc Mater*. 2016;5:1606-16.

-
- [46] Kim I, Lee SS, Bae S, Lee H, Hwang NS. Heparin Functionalized Injectable Cryogel with Rapid Shape-Recovery Property for Neovascularization. *Biomacromolecules*. 2018;19:2257-69.
- [47] Tsurkan MV, Chwalek K, Prokoph S, Zieris A, Levental KR, Freudenberg U, et al. Defined polymer-peptide conjugates to form cell-instructive starPEG-heparin matrices in situ. *Advanced materials (Deerfield Beach, Fla)*. 2013;25:2606-10.
- [48] Nie T, Baldwin A, Yamaguchi N, Kiick KL. Production of Heparin-Functionalized Hydrogels for the Development of Responsive and Controlled Growth Factor Delivery Systems. *Journal of controlled release : official journal of the Controlled Release Society*. 2007;122:287-96.
- [49] Young ME, Carroad PA, Bell RL. Estimation of diffusion coefficients of proteins *Biotechnology and Bioengineering*. 1980;22:947-55.
- [50] Chwalek K, Levental KR, Tsurkan MV, Zieris A, Freudenberg U, Werner C. Two-tier hydrogel degradation to boost endothelial cell morphogenesis. *Biomaterials*. 2011;32:9649-57.
- [51] Vulic K, Shoichet MS. Affinity-based drug delivery systems for tissue repair and regeneration. *Biomacromolecules*. 2014;15:3867-80.
- [52] Vulic K, Pakulska MM, Sonthalia R, Ramachandran A, Shoichet MS. Mathematical model accurately predicts protein release from an affinity-based delivery system. *Journal of controlled release : official journal of the Controlled Release Society*. 2014;197:69-77.
- [53] Sakiyama-Elbert SE, Hubbell JA. Development of fibrin derivatives for controlled release of heparin-binding growth factors. *Journal of controlled release : official journal of the Controlled Release Society*. 2000;65:389-402.
- [54] Anderson SM, Siegman SN, Segura T. The effect of vascular endothelial growth factor (VEGF) presentation within fibrin matrices on endothelial cell branching. *Biomaterials*. 2011;32:7432-43.
- [55] Hettiaratchi MH, Rouse T, Chou C, Krishnan L, Stevens HY, Li MA, et al. Enhanced in vivo retention of low dose BMP-2 via heparin microparticle delivery does not accelerate bone healing in a critically sized femoral defect. *Acta biomaterialia*. 2017;59:21-32.
- [56] Nih LR, Gojgini S, Carmichael ST, Segura T. Dual-function injectable angiogenic biomaterial for the repair of brain tissue following stroke. *Nat Mater*. 2018;17:642-51.
- [57] Maxwell DJ, Hicks BC, Parsons S, Sakiyama-Elbert SE. Development of rationally designed affinity-based drug delivery systems. *Acta biomaterialia*. 2005;1:101-13.
- [58] Hettiaratchi MH, Chou C, Servies N, Smeekens JM, Cheng A, Esancy C, et al. Competitive Protein Binding Influences Heparin-Based Modulation of Spatial Growth Factor Delivery for Bone Regeneration. *Tissue Eng Part A*. 2017;23:683-95.
- [59] Ansorge M, Rastig N, Steinborn R, Koenig T, Baumann L, Moeller S, et al. Short-range cytokine gradients to mimic paracrine cell interactions in vitro. *Journal of Controlled Release*. 2016;224:59-68.
- [60] Ansorge M, Sapudom J, Chkolnikov M, Wilde M, Anderegg U, Möller S, et al. Mimicking Paracrine TGF β 1 Signals during Myofibroblast Differentiation in 3D Collagen Networks. *Scientific Reports*. 2017;7:1-8.

-
- [61] Willerth SM, Johnson PJ, Maxwell DJ, Parsons SR, Doukas ME, Sakiyama-Elbert SE. Rationally designed peptides for controlled release of nerve growth factor from fibrin matrices. *J Biomed Mater Res A*. 2007;80:13-23.
- [62] Fu J, Wang DA. In Situ Organ-Specific Vascularization in Tissue Engineering. *Trends Biotechnol*. 2018;36:834-49.
- [63] Jain RK, Au P, Tam J, Duda DG, Fukumura D. Engineering vascularized tissue. *Nat Biotechnol United States* 2005. p. 821-3.
- [64] Carmeliet P, Jain RK. Angiogenesis in cancer and other diseases. *Nature*. 2000;407:249-57.
- [65] Tien J. Tissue Engineering of the Microvasculature. *Compr Physiol*. 2019;9:1155-212.
- [66] Trappmann B, Baker BM, Polacheck WJ, Choi CK, Burdick JA, Chen CS. Matrix degradability controls multicellularity of 3D cell migration. *Nature Communications*. 2017;8:371.
- [67] Sieminski AL, Hebbel RP, Gooch KJ. The relative magnitudes of endothelial force generation and matrix stiffness modulate capillary morphogenesis in vitro. *Exp Cell Res*. 2004;297:574-84.
- [68] Sack KD, Teran M, Nugent MA. Extracellular Matrix Stiffness Controls VEGF Signaling and Processing in Endothelial Cells. *J Cell Physiol*. 2016;231:2026-39.
- [69] Ruhrberg C. Growing and shaping the vascular tree: multiple roles for VEGF. *Bioessays*. 2003;25:1052-60.
- [70] Gerhardt H. VEGF and endothelial guidance in angiogenic sprouting. *Organogenesis*. 2008;4:241-6.
- [71] Ferrara N. Role of vascular endothelial growth factor in regulation of physiological angiogenesis. *Am J Physiol Cell Physiol*. 2001;280:C1358-66.
- [72] Wang S, Li X, Parra M, Verdin E, Bassel-Duby R, Olson EN. Control of endothelial cell proliferation and migration by VEGF signaling to histone deacetylase 7. *Proc Natl Acad Sci U S A* 2008. p. 7738-43.
- [73] Uccelli A, Wolff T, Valente P, Maggio ND, Pellegrino M, Gürke L, et al. Vascular endothelial growth factor biology for regenerative angiogenesis. *Swiss Medical Weekly* 2019 149:0304. 2019.
- [74] Ozawa CR, Banfi A, Glazer NL, Thurston G, Springer ML, Kraft PE, et al. Microenvironmental VEGF concentration, not total dose, determines a threshold between normal and aberrant angiogenesis. *J Clin Invest*. 2004;113:516-27.
- [75] Dor Y, Djonov V, Abramovitch R, Itin A, Fishman GI, Carmeliet P, et al. Conditional switching of VEGF provides new insights into adult neovascularization and pro-angiogenic therapy. *Embo j*. 2002;21:1939-47.
- [76] Tafuro S, Ayuso E, Zacchigna S, Zentilin L, Moimas S, Dore F, et al. Inducible adeno-associated virus vectors promote functional angiogenesis in adult organisms via regulated vascular endothelial growth factor expression. *Cardiovasc Res*. 2009;83:663-71.
- [77] Pike DB, Cai S, Pomraning KR, Firpo MA, Fisher RJ, Shu XZ, et al. Heparin-regulated release of growth factors in vitro and angiogenic response in vivo to implanted hyaluronan hydrogels containing VEGF and bFGF. *Biomaterials*. 2006;27:5242-51.

-
- [78] Atallah P, Limasale YDP, Freudenberg U, Werner C. Charge-tuning of glycosaminoglycan-based hydrogels to program cytokine sequestration. *Faraday Discussions*. 2019.
- [79] Freudenberg U, Sommer J-U, Levental KR, Welzel PB, Zieris A, Chwalek K, et al. Using Mean Field Theory to Guide Biofunctional Materials Design. *Advanced functional materials*. 2012;22:1391-8.
- [80] Lu P, Takai K, Weaver VM, Werb Z. Extracellular matrix degradation and remodeling in development and disease. *Cold Spring Harb Perspect Biol*. 2011;3.
- [81] Rozario T, DeSimone DW. The extracellular matrix in development and morphogenesis: a dynamic view. *Dev Biol*. 2010;341:126-40.
- [82] Mouw JK, Ou G, Weaver VM. Extracellular matrix assembly: a multiscale deconstruction. *Nat Rev Mol Cell Biol*. 2014;15:771-85.
- [83] Naba A, Clauser KR, Hoersch S, Liu H, Carr SA, Hynes RO. The matrisome: in silico definition and in vivo characterization by proteomics of normal and tumor extracellular matrices. *Mol Cell Proteomics*. 2012;11:M111.014647.
- [84] Bonnans C, Chou J, Werb Z. Remodelling the extracellular matrix in development and disease. *Nat Rev Mol Cell Biol*. 2014;15:786-801.
- [85] Xue M, Jackson CJ. Extracellular Matrix Reorganization During Wound Healing and Its Impact on Abnormal Scarring. *Adv Wound Care (New Rochelle)*2015. p. 119-36.
- [86] Ricard-Blum S, Ruggiero F. The collagen superfamily: from the extracellular matrix to the cell membrane. *Pathol Biol (Paris)*. 2005;53:430-42.
- [87] Urry LA, Cain ML, Wasserman SA, Minorsky PV, Reece JB. *Campbell Biology*2016.
- [88] Bishop JR, Schuksz M, Esko JD. Heparan sulphate proteoglycans fine-tune mammalian physiology. *Nature*. 2007;446:1030-7.
- [89] Varki A, Cummings RD, Esko JD, Freeze HH, Stanley P, Bertozzi CR, et al. *Essentials of Glycobiology*. 2009.
- [90] Wade A, McKinney A, Phillips JJ. Matrix regulators in neural stem cells functions. *Biochim Biophys Acta*. 2014;1840:2520-5.
- [91] Johnson KG, Ghose A, Epstein E, Lincecum J, O'Connor MB, Van Vactor D. Axonal heparan sulfate proteoglycans regulate the distribution and efficiency of the repellent slit during midline axon guidance. *Curr Biol*. 2004;14:499-504.
- [92] Maeda N, Ishii M, Nishimura K, Kamimura K. Functions of chondroitin sulfate and heparan sulfate in the developing brain. *Neurochem Res*. 2011;36:1228-40.
- [93] Martino MM, Hubbell JA. The 12th-14th type III repeats of fibronectin function as a highly promiscuous growth factor-binding domain. *Faseb j*. 2010;24:4711-21.
- [94] Sarrazy V, Koehler A, Chow ML, Zimina E, Li CX, Kato H, et al. Integrins α v β 5 and α v β 3 promote latent TGF- β 1 activation by human cardiac fibroblast contraction. *Cardiovasc Res*. 2014;102:407-17.
- [95] Humphrey JD, Dufresne ER, Schwartz MA. Mechanotransduction and extracellular matrix homeostasis. *Nat Rev Mol Cell Biol*. 2014;15:802-12.
- [96] Janmey PA, Miller RT. Mechanisms of mechanical signaling in development and disease. *J Cell Sci*. 2011;124:9-18.
- [97] Hussey GS, Dziki JL, Badylak SF. Extracellular matrix-based materials for regenerative medicine. *Nature Reviews Materials*. 2018;3:159-73.

-
- [98] Weiss RJ, Esko JD, Tor Y. Targeting Heparin- and Heparan Sulfate-Protein Interactions. *Org Biomol Chem*. 2017;15:5656-68.
- [99] Yue B. Biology of the extracellular matrix: an overview. *J Glaucoma*. 2014;23:S20-3.
- [100] Davis GE, Senger DR. Endothelial extracellular matrix: biosynthesis, remodeling, and functions during vascular morphogenesis and neovessel stabilization. *Circ Res*. 2005;97:1093-107.
- [101] Veevers-Lowe J, Ball SG, Shuttleworth A, Kielty CM. Mesenchymal stem cell migration is regulated by fibronectin through $\alpha 5 \beta 1$ -integrin-mediated activation of PDGFR- β and potentiation of growth factor signals. *J Cell Sci*. 2011;124:1288-300.
- [102] Sedlak E, Fedunova D, Vesela V, Sedlakova D, Antalík M. Polyanion hydrophobicity and protein basicity affect protein stability in protein-polyanion complexes. *Biomacromolecules*. 2009;10:2533-8.
- [103] Formulation, Characterization, and Stability of Protein Drugs - Case Histories | Rodney Pearlman | Springer: Kluwer Academic Publishers; 2002.
- [104] Capila I, Linhardt RJ. Heparin-protein interactions. *Angew Chem Int Ed Engl*. 2002;41:391-412.
- [105] Zakrzewska M, Wiedlocha A, Szlachcic A, Krowarsch D, Otlewski J, Olsnes S. Increased protein stability of FGF1 can compensate for its reduced affinity for heparin. *The Journal of biological chemistry*. 2009;284:25388-403.
- [106] Briquez PS, Clegg LE, Martino MM, Gabhann FM, Hubbell JA. Design principles for therapeutic angiogenic materials. *Nature Reviews Materials*. 2016;1.
- [107] Vempati P, Popel AS, Mac Gabhann F. Extracellular regulation of VEGF: isoforms, proteolysis, and vascular patterning. *Cytokine Growth Factor Rev*. 2014;25:1-19.
- [108] Park JE, Keller GA, Ferrara N. The vascular endothelial growth factor (VEGF) isoforms: differential deposition into the subepithelial extracellular matrix and bioactivity of extracellular matrix-bound VEGF. *Mol Biol Cell*. 1993;4:1317-26.
- [109] Grunstein J, Masbad JJ, Hickey R, Giordano F, Johnson RS. Isoforms of vascular endothelial growth factor act in a coordinate fashion To recruit and expand tumor vasculature. *Mol Cell Biol*. 2000;20:7282-91.
- [110] Vempati P, Popel AS, Mac Gabhann F. Formation of VEGF isoform-specific spatial distributions governing angiogenesis: computational analysis. *BMC Syst Biol*. 2011;5:59.
- [111] Ruhrberg CG, Holger; Golding, Matthew; Watson, Rose ; Ioannidou, Sofia , Hajime Fujisawa CB, 2 and David T. Shima. Spatially restricted patterning cues provided by heparin-binding VEGF-A control blood vessel branching morphogenesis. 2002.
- [112] Lee S, Jilani SM, Nikolova GV, Carpizo D, Iruela-Arispe ML. Processing of VEGF-A by matrix metalloproteinases regulates bioavailability and vascular patterning in tumors. *J Cell Biol*. 2005;169:681-91.
- [113] Lai J, Jiang P, Gaddes ER, Zhao N, Abune L, Wang Y. Aptamer-functionalized hydrogel for self-programmed protein release via sequential photoreaction and hybridization. *Chem Mater*. 2017;29:5850-7.

-
- [114] Kunisch E, Knauf A-K, Hesse E, Freudenberg U, Werner C, Bothe F, et al. StarPEG/heparin-hydrogel based in vivo engineering of stable bizonal cartilage with a calcified bottom layer. *Biofabrication*. 2019;11.
- [115] Wei C-C, Jensen D, Boyle T, O'Brien LC, Meo CD, Shabestary N, et al. Isothermal Titration Calorimetry and Macromolecular Visualization for the Interaction of Lysozyme and Its Inhibitors. 2015.
- [116] Karlsson R, Larsson A. Affinity measurement using surface plasmon resonance. *Methods Mol Biol*. 2004;248:389-415.
- [117] Shah NB, Duncan TM. Bio-layer Interferometry for Measuring Kinetics of Protein-protein Interactions and Allosteric Ligand Effects. *J Vis Exp*2014.
- [118] Gudim I, Lofstad M, Hammerstad M, Hersleth H-P. Measurement of FNR-NrdI Interaction by Microscale Thermophoresis (MST). *Bio-Protocol*. 2017;7.
- [119] Pakulska MM, Miersch S, Shoichet MS. Designer protein delivery: From natural to engineered affinity-controlled release systems. *Science*. 2016;351:aac4750.
- [120] Jerabek-Willemsen M, André T, Wanner R, Roth HM, Duhr S, Baaske P, et al. MicroScale Thermophoresis: Interaction analysis and beyond. *Journal of Molecular Structure*. 2014;1077:101-13.
- [121] Fortebio. Interactions. 2008.
- [122] Fortebio. Interactions. 2009.
- [123] Vuignier K, Schappler J, Veuthey JL, Carrupt PA, Martel S. Drug-protein binding: a critical review of analytical tools. *Anal Bioanal Chem*. 2010;398:53-66.
- [124] Ladbury JE, Chowdhry BZ. Sensing the heat: the application of isothermal titration calorimetry to thermodynamic studies of biomolecular interactions. *Chem Biol*. 1996;3:791-801.
- [125] Kastiris PL, Bonvin AM. On the binding affinity of macromolecular interactions: daring to ask why proteins interact. *Journal of the Royal Society, Interface*. 2013;10:20120835.
- [126] Verneret M. Surface Plasmon Resonance Molecular Interactions and Ligand Binding Analysis | SGS. 2014.
- [127] Osmond RI, Kett WC, Skett SE, Coombe DR. Protein-heparin interactions measured by BIAcore 2000 are affected by the method of heparin immobilization. *Anal Biochem*. 2002;310:199-207.
- [128] Lin CC, Metters AT. Enhanced protein delivery from photopolymerized hydrogels using a pseudospecific metal chelating ligand. *Pharm Res*. 2006;23:614-22.
- [129] Lin CC, Metters AT. Metal-chelating affinity hydrogels for sustained protein release. *J Biomed Mater Res A*. 2007;83:954-64.
- [130] Pakulska MM, Vulic K, Shoichet MS. Affinity-based release of chondroitinase ABC from a modified methylcellulose hydrogel. *Journal of controlled release : official journal of the Controlled Release Society*. 2013;171:11-6.
- [131] Delplace V, Ortin-Martinez A, Tsai ELS, Amin AN, Wallace V, Shoichet MS. Controlled release strategy designed for intravitreal protein delivery to the retina. *Journal of controlled release : official journal of the Controlled Release Society*. 2019;293:10-20.
- [132] Vulic K, Shoichet MS. Tunable growth factor delivery from injectable hydrogels for tissue engineering. *J Am Chem Soc*. 2012;134:882-5.

-
- [133] Parker J, Mitrousis N, Shoichet MS. Hydrogel for Simultaneous Tunable Growth Factor Delivery and Enhanced Viability of Encapsulated Cells in Vitro. *Biomacromolecules*. 2016;17:476-84.
- [134] Peattie RA, Nayate AP, Firpo MA, Shelby J, Fisher RJ, Prestwich GD. Stimulation of in vivo angiogenesis by cytokine-loaded hyaluronic acid hydrogel implants. *Biomaterials*. 2004;25:2789-98.
- [135] Tae G, Scatena M, Stayton PS, Hoffman AS. PEG-cross-linked heparin is an affinity hydrogel for sustained release of vascular endothelial growth factor. *J Biomater Sci Polym Ed*. 2006;17:187-97.
- [136] Fujita M, Ishihara M, Simizu M, Obara K, Ishizuka T, Saito Y, et al. Vascularization in vivo caused by the controlled release of fibroblast growth factor-2 from an injectable chitosan/non-anticoagulant heparin hydrogel. *Biomaterials*. 2004;25:699-706.
- [137] Peattie RA, Pike DB, Yu B, Cai S, Shu XZ, Prestwich GD, et al. Effect of gelatin on heparin regulation of cytokine release from hyaluronan-based hydrogels. *Drug Deliv*. 2008;15:389-97.
- [138] Peattie RA, Rieke ER, Hewett EM, Fisher RJ, Shu XZ, Prestwich GD. Dual growth factor-induced angiogenesis in vivo using hyaluronan hydrogel implants. *Biomaterials*. 2006;27:1868-75.
- [139] Ogle ME, Krieger JR, Tellier LE, McFaline-Figueroa J, Temenoff JS, Botchwey EA. Dual Affinity Heparin-Based Hydrogels Achieve Pro-Regenerative Immunomodulation and Microvascular Remodeling. *ACS Biomater Sci Eng*. 2018;4:1241-50.
- [140] Singh RK, Seliktar D, Putnam AJ. Capillary morphogenesis in PEG-collagen hydrogels. *Biomaterials*. 2013;34:9331-40.
- [141] Silva CR, Babo PS, Gulino M, Costa L, Oliveira JM, Silva-Correia J, et al. Injectable and tunable hyaluronic acid hydrogels releasing chemotactic and angiogenic growth factors for endodontic regeneration. *Acta biomaterialia*. 2018;77:155-71.
- [142] Seidlits SK, Drinnan CT, Petersen RR, Shear JB, Suggs LJ, Schmidt CE. Fibronectin-hyaluronic acid composite hydrogels for three-dimensional endothelial cell culture. *Acta biomaterialia*. 2011;7:2401-9.
- [143] Hanjaya-Putra D, Bose V, Shen YI, Yee J, Khetan S, Fox-Talbot K, et al. Controlled activation of morphogenesis to generate a functional human microvasculature in a synthetic matrix. *Blood*. 2011;118:804-15.
- [144] Natividad-Diaz SL, Browne S, Jha AK, Ma Z, Hossainy S, Kurokawa YK, et al. A combined hiPSC-derived endothelial cell and in vitro microfluidic platform for assessing biomaterial-based angiogenesis. *Biomaterials*. 2019;194:73-83.
- [145] Jha AK, Tharp KM, Browne S, Ye J, Stahl A, Yeghiazarians Y, et al. Matrix metalloproteinase-13 mediated degradation of hyaluronic acid-based matrices orchestrates stem cell engraftment through vascular integration. *Biomaterials*. 2016;89:136-47.
- [146] Li S, Nih LR, Bachman H, Fei P, Li Y, Nam E, et al. Hydrogels with precisely controlled integrin activation dictate vascular patterning and permeability. *Nat Mater*. 2017;16:953-61.
- [147] Yan D, Lin X. Shaping morphogen gradients by proteoglycans. *Cold Spring Harb Perspect Biol*. 2009;1:a002493.

-
- [148] Hacker U, Nybakken K, Perrimon N. Heparan sulphate proteoglycans: the sweet side of development. *Nat Rev Mol Cell Biol*. 2005;6:530-41.
- [149] Lau LW, Cua R, Keough MB, Haylock-Jacobs S, Yong VW. Pathophysiology of the brain extracellular matrix: a new target for remyelination. *Nat Rev Neurosci*. 2013;14:722-9.
- [150] Parish CR. The role of heparan sulphate in inflammation. *Nature reviews Immunology*. 2006;6:633-43.
- [151] Afratis N, Gialeli C, Nikitovic D, Tsegenidis T, Karousou E, Theocharis AD, et al. Glycosaminoglycans: key players in cancer cell biology and treatment. *Febs j*. 2012;279:1177-97.
- [152] Scott RA, Panitch A. Glycosaminoglycans in Biomedicine. *Wiley Interdiscip Rev Nanomed Nanobiotechnol*. 2013;5:388-98.
- [153] Bray LJ, Binner M, Holzheu A, Friedrichs J, Freudenberg U, Hutmacher DW, et al. Multi-parametric hydrogels support 3D in vitro bioengineered microenvironment models of tumour angiogenesis. *Biomaterials*. 2015;53:609-20.
- [154] Weber HM, Tsurkan MV, Magno V, Freudenberg U, Werner C. Heparin-based hydrogels induce human renal tubulogenesis in vitro. *Acta biomaterialia*. 2017;57:59-69.
- [155] Gvaramia D, Muller E, Muller K, Atallah P, Tsurkan M, Freudenberg U, et al. Combined influence of biophysical and biochemical cues on maintenance and proliferation of hematopoietic stem cells. *Biomaterials*. 2017;138:108-17.
- [156] Ferdowsian HR, Gluck JP. The ethical challenges of animal research. *Camb Q Healthc Ethics*. 2015;24:391-406.
- [157] Schurig K, Zieris A, Herman A, Freudenberg U, Heidel S, Grimmer M, et al. Neurotropic growth factors and glycosaminoglycan based matrices to induce dopaminergic tissue formation. *Biomaterials*. 2015;67:205-13.
- [158] Newland B, Welzel PB, Newland H, Renneberg C, Kolar P, Tsurkan M, et al. Tackling cell transplantation anoikis: an injectable, shape memory cryogel microcarrier platform material for stem cell and neuronal cell growth. *Small*. 2015;11:5047-53.
- [159] Tsurkan MV, Hauser PV, Zieris A, Carvalhosa R, Bussolati B, Freudenberg U, et al. Growth factor delivery from hydrogel particle aggregates to promote tubular regeneration after acute kidney injury. *Journal of controlled release : official journal of the Controlled Release Society*. 2013;167:248-55.
- [160] Chemistry and Biology of Heparin and Heparan Sulfate: Elsevier B.V.; 2005.
- [161] Brandl F, Kastner F, Gschwind RM, Blunk T, Teßmar J, Göpferich A. Hydrogel-based drug delivery systems: Comparison of drug diffusivity and release kinetics. *Journal of Controlled Release*. 2010;142:221-8.
- [162] Soumpasis DM. Theoretical analysis of fluorescence photobleaching recovery experiments. *Biophys J*. 1983;41:95-7.
- [163] Zervantonakis IK, Hughes-Alford SK, Charest JL, Condeelis JS, Gertler FB, Kamm RD. Three-dimensional microfluidic model for tumor cell intravasation and endothelial barrier function. *Proc Natl Acad Sci U S A*. 2012;109:13515-20.
- [164] Weis JR, Sun B, Rodgers GM. Improved method of human umbilical arterial endothelial cell culture. *Thromb Res*. 1991;61:171-3.

-
- [165] Zengel P, Nguyen-Hoang A, Schildhammer C, Zantl R, Kahl V, Horn E. μ -Slide Chemotaxis: A new chamber for long-term chemotaxis studies. *BMC Cell Biol* 2011. p. 21.
- [166] Crank J. *The Mathematics of Diffusion*. 2 Edition: Oxford University Press; 1975.
- [167] Zhao W, McCallum SA, Xiao Z, Zhang F, Linhardt RJ. Binding affinities of vascular endothelial growth factor (VEGF) for heparin-derived oligosaccharides. *Bioscience reports*. 2012;32:71-81.
- [168] Lienemann PS, Devaud YR, Reuten R, Simona BR, Karlsson M, Weber W, et al. Locally controlling mesenchymal stem cell morphogenesis by 3D PDGF-BB gradients towards the establishment of an in vitro perivascular niche. *Integr Biol (Camb)*. 2015;7:101-11.
- [169] Herzog S, Reth M, Jumaa H. Regulation of B-cell proliferation and differentiation by pre-B-cell receptor signalling. *Nature reviews Immunology*. 2009;9:195-205.
- [170] Darnell M, Mooney DJ. Leveraging advances in biology to design biomaterials. *Nat Mater*. 2017;16:1178-85.
- [171] Nguyen EH, Schwartz MP, Murphy WL. Biomimetic approaches to control soluble concentration gradients in biomaterials. *Macromol Biosci*. 2011;11:483-92.
- [172] Parlato M, Murphy W. Chapter 1. Soluble Molecule Transport Within Synthetic Hydrogels in Comparison to the Native Extracellular Matrix. 2014:1-30.
- [173] Papadimitriou C, Celikkaya H, Cosacak MI, Mashkaryan V, Bray L, Bhattarai P, et al. 3D Culture Method for Alzheimer's Disease Modeling Reveals Interleukin-4 Rescues A β 42-Induced Loss of Human Neural Stem Cell Plasticity. *Dev Cell*. 2018;46:85-101.e8.
- [174] Fisher SA, Anandakumaran PN, Owen SC, Shoichet MS. Tuning the Microenvironment: Click-Crosslinked Hyaluronic Acid-Based Hydrogels Provide a Platform for Studying Breast Cancer Cell Invasion. *Advanced functional materials*. 2015;25: 7163-72.
- [175] Lin CC, Anseth KS. Controlling Affinity Binding with Peptide-Functionalized Poly(ethylene glycol) Hydrogels. *Advanced functional materials*. 2009;19:2325.
- [176] Koehler KC, Anseth KS, Bowman CN. Diels-Alder mediated controlled release from a poly(ethylene glycol) based hydrogel. *Biomacromolecules*. 2013;14:538-47.
- [177] Belair DG, Khalil AS, Miller MJ, Murphy WL. Serum-dependence of affinity-mediated VEGF release from biomimetic microspheres. *Biomacromolecules*. 2014;15:2038-48.
- [178] Wood MD, Sakiyama-Elbert SE. Release rate controls biological activity of nerve growth factor released from fibrin matrices containing affinity-based delivery systems. *J Biomed Mater Res A*. 2008;84:300-12.
- [179] Shaikh FM, Callanan A, Kavanagh EG, Burke PE, Grace PA, McGloughlin TM. Fibrin: A Natural Biodegradable Scaffold in Vascular Tissue Engineering. *Cells Tissues Organs*. 2019;188:333-46.
- [180] Ishihara J, Ishihara A, Fukunaga K, Sasaki K, White MJV, Briquez PS, et al. Laminin heparin-binding peptides bind to several growth factors and enhance diabetic wound healing. *Nat Commun*. 2018;9:2163.

-
- [181] Martino MM, Briquez PS, Ranga A, Lutolf MP, Hubbell JA. Heparin-binding domain of fibrin(ogen) binds growth factors and promotes tissue repair when incorporated within a synthetic matrix. *Proc Natl Acad Sci U S A*. 2013;110:4563-8.
- [182] Seidel SA, Dijkman PM, Lea WA, van den Bogaart G, Jerabek-Willemsen M, Lazic A, et al. Microscale Thermophoresis Quantifies Biomolecular Interactions under Previously Challenging Conditions. *Methods*. 2013;59:301-15.
- [183] Deschout H, Raemdonck K, Demeester J, De Smedt SC, Braeckmans K. FRAP in pharmaceutical research: practical guidelines and applications in drug delivery. *Pharm Res*. 2014;31:255-70.
- [184] Witten J, Ribbeck K. The particle in the spider's web: transport through biological hydrogels. *Nanoscale*. 2017;9:8080-95.
- [185] Manton KJ, Leong DF, Cool SM, Nurcombe V. Disruption of heparan and chondroitin sulfate signaling enhances mesenchymal stem cell-derived osteogenic differentiation via bone morphogenetic protein signaling pathways. *Stem cells (Dayton, Ohio)*. 2007;25:2845-54.
- [186] Seib FP, Franke M, Jing D, Werner C, Bornhauser M. Endogenous bone morphogenetic proteins in human bone marrow-derived multipotent mesenchymal stromal cells. *European journal of cell biology*. 2009;88:257-71.
- [187] Singh S, Wu BM, Dunn JC. The enhancement of VEGF-mediated angiogenesis by polycaprolactone scaffolds with surface cross-linked heparin. *Biomaterials*. 2011;32:2059-69.
- [188] Ayerst BI, Merry CLR, Day AJ. The Good the Bad and the Ugly of Glycosaminoglycans in Tissue Engineering Applications. *Pharmaceuticals (Basel, Switzerland)*. 2017;10.
- [189] Koutsopoulos S, Unsworth LD, Nagai Y, Zhang S. Controlled release of functional proteins through designer self-assembling peptide nanofiber hydrogel scaffold. *Proc Natl Acad Sci U S A* 2009. p. 4623-8.
- [190] Sadir R, Baleux F, Grosdidier A, Imberty A, Lortat-Jacob H. Characterization of the stromal cell-derived factor-1 α -heparin complex. *The Journal of biological chemistry*. 2001;276:8288-96.
- [191] Roy S, Lai H, Zouaoui R, Duffner J, Zhou H, L PJ, et al. Bioactivity screening of partially desulfated low-molecular-weight heparins: a structure/activity relationship study. *Glycobiology*. 2011;21:1194-205.
- [192] Loo BM, Kreuger J, Jalkanen M, Lindahl U, Salmivirta M. Binding of heparin/heparan sulfate to fibroblast growth factor receptor 4. *The Journal of biological chemistry*. 2001;276:16868-76.
- [193] Ono K, Hattori H, Takeshita S, Kurita A, Ishihara M. Structural features in heparin that interact with VEGF165 and modulate its biological activity. *Glycobiology*. 1999;9:705-11.
- [194] Mitchell AC, Briquez PS, Hubbell JA, Cochran JR. Engineering growth factors for regenerative medicine applications. *Acta biomaterialia*. 2016;30:1-12.
- [195] Niu Y, Li Q, Ding Y, Dong L, Wang C. Engineered delivery strategies for enhanced control of growth factor activities in wound healing. *Advanced drug delivery reviews*. 2018.
- [196] Cao E, Chen Y, Cui Z, Foster PR. Effect of freezing and thawing rates on denaturation of proteins in aqueous solutions. *Biotechnol Bioeng*. 2003;82:684-90.

-
- [197] Demeule B, Gurny R, Arvinte T. Detection and characterization of protein aggregates by fluorescence microscopy. *Int J Pharm.* 2007;329:37-45.
- [198] Branco MC, Pochan DJ, Wagner NJ, Schneider JP. Macromolecular diffusion and release from self-assembled β -hairpin peptide hydrogels. *Biomaterials.* 2009;30:1339-47.
- [199] Van Tomme SR, De Geest BG, Braeckmans K, De Smedt SC, Siepmann F, Siepmann J, et al. Mobility of model proteins in hydrogels composed of oppositely charged dextran microspheres studied by protein release and fluorescence recovery after photobleaching. *Journal of controlled release : official journal of the Controlled Release Society.* 2005;110:67-78.
- [200] Weinbreck F, Rollema HS, Tromp RH, de Kruif CG. Diffusivity of whey protein and gum arabic in their coacervates. *Langmuir.* 2004;20:6389-95.
- [201] Kuijpers AJ, Engbers GHM, Meyvis TKL, De Smedt S, Demeester J, Zaat SAJ, et al. Combined gelatin-chondroitin sulfate hydrogels for controlled release of cationic antibacterial proteins. *Macromolecules.* 2000.
- [202] Kang M, Day CA, Kenworthy AK, DiBenedetto E. Simplified equation to extract diffusion coefficients from confocal FRAP data. *Traffic.* 2012;13:1589-600.
- [203] Thoenes S, Rother S, Wippold T, Blaszkiewicz J, Balamurugan K, Moeller S, et al. Hyaluronan/collagen hydrogels containing sulfated hyaluronan improve wound healing by sustained release of heparin -binding EGF-like growth factor. *Acta biomaterialia.* 2019;86:135-47.
- [204] Moon JJ, Saik JE, Poche RA, Leslie-Barbick JE, Lee SH, Smith AA, et al. Biomimetic hydrogels with pro-angiogenic properties. *Biomaterials.* 2010;31:3840-7.
- [205] Critser P, Kreger S, Voytik-Harbin S, Yoder M. Collagen matrix physical properties modulate endothelial colony forming cell derived vessels in vivo. *Microvasc Res.* 2010;80:23-30.
- [206] Culver JC, Hoffmann JC, Poché RA, Slater JH, West JL, Dickinson ME. Three-Dimensional Biomimetic Patterning in Hydrogels to Guide Cellular Organization. *Advanced materials (Deerfield Beach, Fla).* 2012;24:2344-8.
- [207] Chen TT, Luque A, Lee S, Anderson SM, Segura T, Iruela-Arispe ML. Anchorage of VEGF to the extracellular matrix conveys differential signaling responses to endothelial cells. *J Cell Biol.* 2010;188:595-609.
- [208] Reginato S, Gianni-Barrera R, Banfi A. Taming of the wild vessel: promoting vessel stabilization for safe therapeutic angiogenesis. *Biochem Soc Trans.* 2011;39:1654-8.
- [209] Apte RS, Chen DS, Ferrara N. VEGF in Signaling and Disease: Beyond Discovery and Development. *Cell.* 2019;176:1248-64.
- [210] Pauty J, Usuba R, Cheng IG, Hespel L, Takahashi H, Kato K, et al. A Vascular Endothelial Growth Factor-Dependent Sprouting Angiogenesis Assay Based on an In Vitro Human Blood Vessel Model for the Study of Anti-Angiogenic Drugs. *EBioMedicine.* 2018;27:225-36.
- [211] Hanjaya-Putra D, Yee J, Ceci D, Truitt R, Yee D, Gerecht S. Vascular endothelial growth factor and substrate mechanics regulate in vitro tubulogenesis of endothelial progenitor cells. *J Cell Mol Med.* 2010;14:2436-47.

-
- [212] Tsurkan MV, Chwalek K, Levental KR, Freudenberg U, Werner C. Modular StarPEG-Heparin Gels with Bifunctional Peptide Linkers. *Macromol Rapid Commun.* 2010;31:1529-33.
- [213] Zhu JM. Bioactive modification of poly(ethylene glycol) hydrogels for tissue engineering. *Biomaterials.* 2010;31:4639-56.
- [214] Gerhardt H, Golding M, Fruttiger M, Ruhrberg C, Lundkvist A, Abramsson A, et al. VEGF guides angiogenic sprouting utilizing endothelial tip cell filopodia. *J Cell Biol.* 2003;161:1163-77.
- [215] Dyer DP, Salanga CL, Volkman BF, Kawamura T, Handel TM. The dependence of chemokine-glycosaminoglycan interactions on chemokine oligomerization. *Glycobiology.* 2016;26:312-26.
- [216] Handel TM, Johnson Z, Crown SE, Lau EK, Proudfoot AE. Regulation of protein function by glycosaminoglycans--as exemplified by chemokines. *Annu Rev Biochem.* 2005;74:385-410.
- [217] Risau W. Mechanisms of angiogenesis. *Nature.* 1997;386:671-4.
- [218] Rousseau S, Houle F, Kotanides H, Witte L, Waltenberger J, Landry J, et al. Vascular endothelial growth factor (VEGF)-driven actin-based motility is mediated by VEGFR2 and requires concerted activation of stress-activated protein kinase 2 (SAPK2/p38) and geldanamycin-sensitive phosphorylation of focal adhesion kinase. *The Journal of biological chemistry.* 2000;275:10661-72.
- [219] Chiu LL, Radisic M. Scaffolds with covalently immobilized VEGF and Angiopoietin-1 for vascularization of engineered tissues. *Biomaterials.* 2010;31:226-41.
- [220] Moulisova V, Gonzalez-Garcia C, Cantini M, Rodrigo-Navarro A, Weaver J, Costell M, et al. Engineered microenvironments for synergistic VEGF - Integrin signalling during vascularization. *Biomaterials.* 2017;126:61-74.
- [221] Wijelath E, Namekata M, Murray J, Furuyashiki M, Zhang S, Coan D, et al. Multiple mechanisms for exogenous heparin modulation of vascular endothelial growth factor activity. *J Cell Biochem.* 2010;111:461-8.
- [222] Roudsari LC, Jeffs SE, Witt AS, Gill BJ, West JL. A 3D Poly(ethylene glycol)-based Tumor Angiogenesis Model to Study the Influence of Vascular Cells on Lung Tumor Cell Behavior. *Sci Rep.* 2016;6:32726.
- [223] Joyce MH, Lu C, James ER, Hegab R, Allen SC, Suggs LJ, et al. Phenotypic Basis for Matrix Stiffness-Dependent Chemoresistance of Breast Cancer Cells to Doxorubicin. *Front Oncol.* 2018;8.
- [224] HF EL-S, Hawkins DM, Stevenson D, Reddy SM. Determination of protein binding affinities within hydrogel-based molecularly imprinted polymers (HydroMIPs). *Phys Chem Chem Phys.* 2014;16:15483-9.
- [225] Goodwin AM. In vitro assays of angiogenesis for assessment of angiogenic and anti-angiogenic agents. *Microvasc Res.* 2007;74:172-83.
- [226] Galanternik MV, Kramer KL, Piotrowski T. Heparan Sulfate Proteoglycans regulate Fgf signaling and cell polarity during collective cell migration. *Cell Rep.*
- [227] Seto SP, Miller T, Temenoff JS. Effect of selective heparin desulfation on preservation of bone morphogenetic protein-2 bioactivity after thermal stress. *Bioconjug Chem.* 2015;26:286-93.
- [228] Jeong GS, Han S, Shin Y, Kwon GH, Kamm RD, Lee SH, et al. Sprouting angiogenesis under a chemical gradient regulated by interactions with an endothelial monolayer in a microfluidic platform. *Anal Chem.* 2011;83:8454-9.

-
- [229] Whisler JA, Chen MB, Kamm RD. Control of perfusable microvascular network morphology using a multiculture microfluidic system. *Tissue Eng Part C Methods*. 2014;20:543-52.
- [230] Hanjaya-Putra D, Wong KT, Hirotsu K, Khetan S, Burdick JA, Gerecht S. Spatial Control of Cell-Mediated Degradation to Regulate Vasculogenesis and Angiogenesis in Hyaluronan Hydrogels. *Biomaterials*. 2012;33:6123-31.
- [231] Farrukh A, Paez JI, del Campo A. 4D Biomaterials for Light-Guided Angiogenesis. *Advanced functional materials*. 2018;29.
- [232] Rouwkema J, Khademhosseini A. Vascularization and Angiogenesis in Tissue Engineering: Beyond Creating Static Networks. *Trends Biotechnol*. 2016;34:733-45.
- [233] Choi WI, Kim M, Tae G, Kim YH. Sustained release of human growth hormone from heparin-based hydrogel. *Biomacromolecules*. 2008;9:1698-704.
- [234] Tae G, Kim YJ, Choi WI, Kim M, Stayton PS, Hoffman AS. Formation of a novel heparin-based hydrogel in the presence of heparin-binding biomolecules. *Biomacromolecules*. 2007;8:1979-86.
- [235] Place ES, Evans ND, Stevens MM. Complexity in biomaterials for tissue engineering. *Nat Mater*. 2009;8:457-70.
- [236] van Duinen V, Zhu D, Ramakers C, van Zonneveld AJ, Vulto P, Hankemeier T. Perfused 3D angiogenic sprouting in a high-throughput in vitro platform. *Angiogenesis*. 2019;22:157-65.
- [237] Chandra P, Atala A. Engineering blood vessels and vascularized tissues: technology trends and potential clinical applications. *Clin Sci (Lond)*. 2019;133:1115-35.
- [238] Hu X, Neoh KG, Zhang J, Kang E-T, Wang W. Immobilization strategy for optimizing VEGF's concurrent bioactivity towards endothelial cells and osteoblasts on implant surfaces. *Biomaterials*. 2012;33:8082-93.
- [239] Bai Y, Bai L, Zhou J, Chen H, Zhang L. Sequential delivery of VEGF, FGF-2 and PDGF from the polymeric system enhance HUVECs angiogenesis in vitro and CAM angiogenesis. *Cell Immunol*. 2018;323:19-32.
- [240] Tengood JE, Kovach KM, Vescovi PE, Russell AJ, Little SR. Sequential delivery of vascular endothelial growth factor and sphingosine 1-phosphate for angiogenesis. *Biomaterials*. 2010;31:7805-12.
- [241] Koide HD, Yoshimatsu K, Hoshino Y, Ariizumi S, Okishima A, Ide T, et al. Sequestering and inhibiting a vascular endothelial growth factor in vivo by systemic administration of a synthetic polymer nanoparticle. *Journal of Controlled Release*. 2019;295:13-20.
- [242] Wu J, Ye J, Zhu J, Xiao Z, He C, Shi H, et al. Heparin-Based Coacervate of FGF2 Improves Dermal Regeneration by Asserting a Synergistic Role with Cell Proliferation and Endogenous Facilitated VEGF for Cutaneous Wound Healing. *Biomacromolecules*. 2016;17:2168-77.
- [243] Welzel PB, Prokoph S, Zieris A, Grimmer M, Zschoche S, Freudenberg U, et al. Modulating Biofunctional starPEG Heparin Hydrogels by Varying Size and Ratio of the Constituents. *Polymers*. 2011;3:602-20.
- [244] Nie T, Akins RE, Jr., Kiick KL. Production of heparin-containing hydrogels for modulating cell responses. *Acta biomaterialia*. 2009;5:865-75.

-
- [245] Tae G, Scatena M, Stayton PS, Hoffman AS. PEG-cross-linked heparin is an affinity hydrogel for sustained release of vascular endothelial growth factor. *Journal of Biomaterials Science, Polymer Edition*. 2012;17:187-97.
- [246] Jeon O, Powell C, Solorio LD, Krebs MD, Alsberg E. Affinity-based growth factor delivery using biodegradable, photocrosslinked heparin-alginate hydrogels. *Journal of controlled release : official journal of the Controlled Release Society*. 2011;154:258-66.
- [247] Engler AJ, Sen S, Sweeney HL, Discher DE. Matrix elasticity directs stem cell lineage specification. *Cell*. 2006;126:677-89.
- [248] Webber MJ, Khan OF, Sydlik SA, Tang BC, Langer R. A Perspective on the Clinical Translation of Scaffolds for Tissue Engineering. *Ann Biomed Eng*. 2015;43:641-56.
- [249] Lin B, Levchenko A. Spatial manipulation with microfluidics. *Front Bioeng Biotechnol*. 2015;3:39.
- [250] Manfrin A, Tabata Y, Paquet ER, Vuaridel AR, Rivest FR, Naef F, et al. Engineered signaling centers for the spatially controlled patterning of human pluripotent stem cells. *Nature Methods*. 2019;16:640.
- [251] Uzel SG, Amadi OC, Pearl TM, Lee RT, So PT, Kamm RD. Simultaneous or Sequential Orthogonal Gradient Formation in a 3D Cell Culture Microfluidic Platform. *Small*. 2016;12:612-22.
- [252] O'Grady B, Balikov DA, Wang JX, Neal EK, Ou Y-C, Bardhan R, et al. Spatiotemporal control and modeling of morphogen delivery to induce gradient patterning of stem cell differentiation using fluidic channels. 2019.
- [253] Odedra D, Chiu LL, Shoichet M, Radisic M. Endothelial cells guided by immobilized gradients of vascular endothelial growth factor on porous collagen scaffolds. *Acta biomaterialia*. 2011;7:3027-35.
- [254] Raeber GP, Lutolf MP, Hubbell JA. Molecularly Engineered PEG Hydrogels: A Novel Model System for Proteolytically Mediated Cell Migration. *Biophys J* 2005. p. 1374-88.
- [255] Beamish JA, Juliar BA, Cleveland DS, Busch ME, Nimmagadda L, Putnam AJ. Deciphering the relative roles of matrix metalloproteinase- and plasmin-mediated matrix degradation during capillary morphogenesis using engineered hydrogels. *J Biomed Mater Res B Appl Biomater*. 2019.
- [256] Hettiaratchi MH, Schudel A, Rouse T, Garcia AJ, Thomas SN, Guldberg RE, et al. A rapid method for determining protein diffusion through hydrogels for regenerative medicine applications. *APL Bioeng*. 2018;2:026110.
- [257] Wallace DG, Rosenblatt J. Collagen gel systems for sustained delivery and tissue engineering. *Advanced drug delivery reviews*. 2003;55:1631-49.
- [258] Pakulska MM, Vulic K, Tam RY, Shoichet MS. Hybrid Crosslinked Methylcellulose Hydrogel: A Predictable and Tunable Platform for Local Drug Delivery. *Advanced materials (Deerfield Beach, Fla)*. 2015;27:5002-8.
- [259] Moshayedi P, Nih LR, Llorente IL, Berg AR, Cinkornpumin J, Lowry WE, et al. Systematic optimization of an engineered hydrogel allows for selective control of human neural stem cell survival and differentiation after transplantation in the stroke brain. *Biomaterials*. 2016;105:145-55.
- [260] EL-Sharif HF, Hawkins DM, Stevenson D, Reddy SM. Determination of protein binding affinities within hydrogel-based molecularly imprinted polymers (HydroMIPs). *Phys Chem Chem Phys*. 2014;16:15483-9.

-
- [261] Haessler U, Pisano M, Wu M, Swartz MA. Dendritic cell chemotaxis in 3D under defined chemokine gradients reveals differential response to ligands CCL21 and CCL19. 2011.
- [262] McLelland BT, Lin B, Mathur A, Aramant RB, Thomas BB, Nistor G, et al. Transplanted hESC-Derived Retina Organoid Sheets Differentiate, Integrate, and Improve Visual Function in Retinal Degenerate Rats. *Invest Ophthalmol Vis Sci*. 2018;59:2586-603.
- [263] Kratochvil MJ, Seymour AJ, Li TL, Paşca SP, Kuo CJ, Heilshorn SC. Engineered materials for organoid systems. *Nature Reviews Materials*. 2019:1-17.
- [264] Jessell TM. Neuronal specification in the spinal cord: inductive signals and transcriptional codes. *Nat Rev Genet*. 2000;1:20-9.
- [265] Zecca M, Basler K, Struhl G. Direct and long-range action of a wingless morphogen gradient. *Cell*. 1996;87:833-44.
- [266] Demers CJ, Soundararajan P, Chennampally P, Cox GA, Briscoe J, Collins SD, et al. Development-on-chip: in vitro neural tube patterning with a microfluidic device. *Development*. 2016;143:1884-92.
- [267] Briscoe J, Chen Y, Jessell TM, Struhl G. A hedgehog-insensitive form of patched provides evidence for direct long-range morphogen activity of sonic hedgehog in the neural tube. *Mol Cell*. 2001;7:1279-91.
- [268] Zimmermann R, Hentschel C, Schron F, Moedder D, Buttner T, Atallah P, et al. High resolution bioprinting of multi-component hydrogels. *Biofabrication*. 2019.
- [269] Wienken CJ, Baaske P, Rothbauer U, Braun D, Duhr S. Protein-binding assays in biological liquids using microscale thermophoresis. *Nature Communications*. 2010;1:100.
- [270] Braeckmans K, Peeters L, Sanders NN, De Smedt SC, Demeester J. Three-Dimensional Fluorescence Recovery after Photobleaching with the Confocal Scanning Laser Microscope. *Biophys J*. 2003;85:2240-52.
- [271] De Smedt SC, Lauwers A, Demeester J, Engelborghs Y, De Mey G, Du M. Structural information on hyaluronic acid solutions as studied by probe diffusion experiments | *Macromolecules*. *Macromolecules*. 1994;27:141-6.
- [272] Rubinstein M, Colby RH. *Polymer Physics*: OUPAcademic; 2003.
- [273] Thorne RG, Hrabetova S, Nicholson C. Diffusion of epidermal growth factor in rat brain extracellular space measured by integrative optical imaging. *J Neurophysiol*. 2004;92:3471-81.
- [274] Kaur H, Yung LY. Probing high affinity sequences of DNA aptamer against VEGF165. *PLoS One*. 2012;7:e31196.
- [275] Freeman I, Kedem A, Cohen S. The effect of sulfation of alginate hydrogels on the specific binding and controlled release of heparin-binding proteins. *Biomaterials*. 2008;29:3260-8.
- [276] Miyawaki A. Proteins on the move: insights gained from fluorescent protein technologies. *Nat Rev Mol Cell Biol*. 2011;12:656-68.
- [277] Zustiak SP, Boukari H, Leach JB. Solute diffusion and interactions in cross-linked poly(ethylene glycol) hydrogels studied by Fluorescence Correlation Spectroscopy. *Soft Matter*. 2010;6.
- [278] Loren N, Hagman J, Jonasson JK, Deschout H, Bernin D, Cella-Zanacchi F, et al. Fluorescence recovery after photobleaching in material and life sciences: putting theory into practice. *Quarterly reviews of biophysics*. 2015;48:323-87.

-
- [279] Koulouras G, Panagopoulos A, Rapsomaniki MA, Giakoumakis NN, Taraviras S, Lygerou Z. EasyFRAP-web: a web-based tool for the analysis of fluorescence recovery after photobleaching data. *Nucleic Acids Res* 2018. p. W467-72.
- [280] Lang K, Chin JW. Bioorthogonal reactions for labeling proteins. *ACS Chem Biol*. 2014;9:16-20.
- [281] Cheng Y, Prud'homme RK, Thomas JL. Diffusion of Mesoscopic Probes in Aqueous Polymer Solutions Measured by Fluorescence Recovery after Photobleaching. 2002.
- [282] Meyvis TK, De Smedt SC, Van Oostveldt P, Demeester J. Fluorescence recovery after photobleaching: a versatile tool for mobility and interaction measurements in pharmaceutical research. *Pharm Res*. 1999;16:1153-62.
- [283] Putnam FW. *The Plasma Proteins: Structure, Function and Genetic Control*. 2 Edition New York: Academic Press; 1975.
- [284] Braga J, Desterro JM, Carmo-Fonseca M. Intracellular Macromolecular Mobility Measured by Fluorescence Recovery after Photobleaching with Confocal Laser Scanning Microscopes. *Mol Biol Cell*. 2004;15:4749-60.
- [285] Weber LM, Lopez CG, Anseth KS. The effects of PEG hydrogel crosslinking density on protein diffusion and encapsulated islet survival and function. *J Biomed Mater Res A*. 2009;90:720-9.
- [286] Anjum F, Lienemann PS, Metzger S, Biernaskie J, Kallos MS, Ehrbar M. Enzyme responsive GAG-based natural-synthetic hybrid hydrogel for tunable growth factor delivery and stem cell differentiation. *Biomaterials*. 2016;87:104-17.

List of figures

Figure 1.1. Different strategies to modulate the transport of signaling molecules within GAG-based materials.....	4
Figure 2.1. The extracellular matrix (ECM)	12
Figure 2.2. Cells respond to biophysical and biomolecular signals from the ECM and actively remodel their microenvironment	14
Figure 2.3. GAG regulates the activity of soluble signaling molecules.....	16
Figure 2.4. Affinity-based growth factor delivery system	19
Figure 2.5. The application of GAG-based material to control the activity of pro-angiogenic growth factors	24
Figure 2.6. Modular starPEG-GAG biohybrid hydrogels.....	27
Figure 3.1. FRAP experiment set-up.....	33
Figure 3.2. Generation of a biomolecular gradient within a microfluidic device .	35
Figure 3.3. Schematic of μ -Slide Chemotaxis design for HUVECs chemotaxis assay	39
Figure 4.1. Effect of protein physical size and affinity to GAG on the mobility of proteins.....	47
Figure 4.2. Effects of hydrogel mesh size on the mobility of proteins.	49
Figure 4.3. Effect of GAG concentration on the mobility of proteins.	51
Figure 4.4. Effect of GAG sulfation pattern on the mobility of proteins.....	53
Figure 4.5. The release characteristics of model proteins from binary GAG hydrogels containing different GAG sulfation patterns.	56
Figure 4.6. Experimental release (data points) and the resulting least-squares best fits of the data using the reaction-diffusion model (solid line) of VEGF165 and SDF1 α from GAG hydrogels with variable sulfation	57
Figure 4.7. COMSOL simulations of the VEGF165 release from GAG hydrogel systems.....	61
Figure 4.8. The formation and physical properties of the GAG-based hydrogel with adjustable local and overall sulfate density.....	74
Figure 4.9. GAG content and GAG sulfation patterns modulate the release of VEGF from hydrogels.....	77

Figure 4.10. Schematic view of <i>in vitro</i> assay of endothelial morphogenesis within the hydrogel.....	78
Figure 4.11. COMSOL simulation of the free VEGF concentration in hydrogel droplets with varied GAG content and the GAG sulfation..	80
Figure 4.12. Effect of heparin content of the hydrogel on the endothelial cell capillary morphogenesis at various VEGF loading	82
Figure 4.13. Effect of GAG sulfation pattern of the hydrogel on the endothelial cell capillary morphogenesis at various VEGF loading..	83
Figure 4.14. The gradient of VEGF modulates the spatial organization of endothelial cell vascular structures within the hydrogel	86
Figure 4.15. Endothelial cell chemotaxis in response to the VEGF gradient.....	88
Figure 4.16. Ternary GAG hydrogel systems with tunable GAG content and mechanical properties	97
Figure 4.17. The physical properties of ternary hydrogels with variable GAG content	99
Figure 4.18. The GAG content of ternary hydrogels modulates the in-gel mobility and release of GAG-affine proteins.....	101
Figure 4.19. The gradient of signaling molecules with different molecular sizes and affinity to the GAG	104
Figure 4.20. The GAG content of ternary hydrogels modulates the gradient of GAG-affine proteins	105
Figure 4.21. The ternary hydrogel system supports endothelial cell vascular morphogenesis.....	107
Figure 5.1. A systematic study of the mobility of signaling molecules and the mathematical modeling rationally guide the design of GAG-based biomaterials to precisely modulate the cell fate decisions.	112
Figure 6.1. Schematic diagram of the protein release from GAG hydrogels within a microcentrifuge tube	128
Figure 6.2. A schematic of the protein transport dynamic in a droplet of GAG hydrogel.....	130
Figure 6.3. Schematic diagram of the protein diffusion through the hydrogel integrated within a microfluidic device..	131

Figure 6.4. Binding analysis of the model proteins to maleimide functionalized-GAG or GAG derivatives as determined by microscale thermophoresis (MST).	137
Figure 6.5. Optimization of FRAP experimental parameters for the quantitative analysis of molecular diffusivity using a uniform disk model.....	141
Figure 6.6. The mobility of FITC-dextran with different molecular weights within the GAG hydrogels of various stiffness.....	144
Figure 6.7. Concentration- and time-dependent VEGF-induced cellular metabolic activity.....	145
Figure 6.8. The mechanical properties of the binary starPEG-GAG hydrogel containing variable GAG content at different crosslinking degree/ molar ratio of starPEG to heparin (Y).....	145
Figure 6.9. Particle size analysis of the VEGF121 dissolved within the PBS (pH 7.4) as determined using a dynamic light scattering method.	146

List of tables

Table 2.1. Different methods used to quantify binding interactions	18
Table 4.1. Affinity constants of the VEGF165 and SDF1 α to the heparin or heparin derivatives as determined by microscale thermophoresis (MST) and the release simulation (sim) based on the reaction-diffusion model from the GAG hydrogels with variable sulfation	58
Table 6.1. Model parameters for each simulation	132
Table 6.2. Creation parameters.....	133

Nomenclature

• 6O-DSH	• 6-O-desulfated heparin
• 6ON-DSH	• 6-O-N- desulfated N-acetylated heparin
• ANOVA	• Analysis of variance
• BDNF	• Brain-derived neurotrophic factor
• BLI	• Bio-layer interferometry
• BSA	• Bovine serum albumin
• BMP-2	• Bone Morphogenetic Protein 2
• CS	• Chondroitin sulfate
• CNTF	• Ciliary neurotrophic factor
• DLS	• Dynamic light scattering
• DMEM	• Dulbecco's modified eagle medium
• DMSO	• Dimethyl sulfoxide
• DS	• Dermatan sulfate
• DSF	• Differential scanning fluorimetry
• ECM	• Extracellular matrix
• EDC	• 1-Ethyl-3-(3-dimethylaminopropyl) carbodiimide
• eEPC	• Early Endothelial Progenitor Cell
• ELISA	• Enzyme-linked immunosorbent assay
• FBS	• Fetal bovine serum
• FD	• FITC-dextran
• FGF-2	• Fibroblast growth factor-2
• FGFR	• Fibroblast growth factor receptors
• FITC	• Fluorescein isothiocyanate
• FMI	• Forward migration index
• FRAP	• Fluorescence recovery after photobleaching
• GAG	• Glycosaminoglycan
• GDNF	• Glial cell-derived neurotrophic factor

• HA	• Hyaluronic acid
• Hep	• Heparin
• Hep Mal	• Heparin maleimide conjugate
• HS	• Heparan sulfate
• HUVECs	• Human umbilical vein endothelial cells
• IGF-1	• Insulin-like growth factor-1
• IL-4	• Interleukin 4
• ITC	• Isothermal titration calorimetry
• k_a	• association rate constant
• k_d	• dissociation rate constant
• K_D	• Equilibrium dissociation constant
• KGF	• Keratinocyte growth factor
• KS	• Keratan sulfate
• MMP	• Matrix metalloproteinase
• MSC	• Mesenchymal stem cell
• MST	• Microscale thermophoresis
• N-DSH	• N- desulfated N-acetylated heparin
• NGF	• Nerve growth factor
• NT-3	• Neurotrophic factor-3
• NMR	• Nuclear magnetic resonance
• PDGF-bb	• Platelet-derived growth factor-BB
• SDF1 α	• Stromal cell-derived factor α
• sHA	• Sulfated hyaluronic acids
• S-NHS	• N-Hydroxysulfosuccinimide
• SPR	• Surface plasmon resonance
• starPEG	• 4 arm star-shaped
• TGF- β	• Transforming growth factor-beta
• VEGF165	• Vascular endothelial growth factor 165
• VEGF121	• Vascular endothelial growth factor 121
• VEGF189	• Vascular endothelial growth factor 189
• γ	• starPEG to heparin ratio

Erklärung entsprechend §5.5 der Promotionsordnung

Hiermit versichere ich, dass ich die vorliegende Arbeit ohne unzulässige Hilfe Dritter und ohne Benutzung anderer als der angegebenen Hilfsmittel angefertigt habe; die aus fremden Quellen direkt oder indirekt übernommenen Gedanken sind als solche kenntlich gemacht. Die Arbeit wurde bisher weder im Inland noch im Ausland in gleicher oder ähnlicher Form einer anderen Prüfungsbehörde vorgelegt.

Die Dissertation wurde im Zeitraum vom 01 September 2015 bis 31 August 2019 verfasst und von Prof. Dr. rer. nat. Carsten Werner, Fakultät Chemie, Leibniz Institut für Polymerforschung betreut.

Meine Person betreffend erkläre ich hiermit, dass keine früheren erfolglosen Promotionsverfahren stattgefunden haben.

Ich erkenne die Promotionsordnung der Fakultät für Mathematik und Naturwissenschaften, Technische Universität Dresden an.

Date, Yanuar Dwi Putra Limasale